

February, 2009.

Thesis for degree of Ph. D.

A study on the metabolic pathway change by the proteomic analysis

Graduate school of Chosun University

Department of Chemical Engineering

Jin, Li-Hua

A study on the metabolic pathway change by the proteomic analysis

단백질체 분석을 통한 metabolic pathway 변화에 대한 연구

February, 25th, 2009

Graduate school of Chosun University

Department of Chemical Engineering

Jin, Li-Hua

A study on the metabolic pathway change by the proteomic analysis

Professor Lee, Jung-Heon






October, 2008

Graduate school of Chosun University

Department of Chemical Engineering

Jin, Li-Hua

Accepted in Jin, Li-Hua' s thesis for
Doctor Degree of Philosophy

Chairman	Chosun Univ.	<u>Prof. Cha, Wol-Suk</u>	
Committee Member	Chosun Univ.	<u>Prof. Kim, Sun-Il</u>	
Committee Member	Chosun Univ.	<u>Prof. Kim, Jung-Kyu</u>	
Committee Member	Chungbuk Univ.	<u>Prof. Kim, Yang-Hoon</u>	
Committee Member	Chosun Univ.	<u>Prof. Lee, Jung-Heon</u>	

December, 2008

Graduate school of Chosun University

Contents

ABSTRACT	x
국문 요약.....	xiii
Chapter 1	1
Introduction	1
Chapter 2.....	6
Proteomic analysis of curdlan-producing <i>Agrobacterium</i> sp. in response to pH downshift	6
2.1. Introduction	6
2.2. Materials and Methods	10
2.2.1. Bacterial strain and culture conditions	10
2.2.2. Cell mass, curdlan, and beta-1,3-glucan synthase assay	11
2.2.3. UTP, and UDP-glucose assay	12
2.2.4. Sample preparation for two-dimensional electrophoresis	13
2.2.5. Two-dimensional gel electrophoresis	14
2.2.6. MALDI-TOF mass spectrometric analysis and database search	16

2.3. Results and discussion	18
2.3.1. Proteomic response of <i>Agrobacterium</i> sp. ATCC 31750 batch culture to pH downshift.....	18
2.3.2. Estimation of curdlan overproduction metabolism after pH downshift	25
2.3.3. Lipopolysaccharide, peptidoglycan, and isoprenoid biosynthesis	36
2.3.4. Amino acid biosynthesis	37
2.3.5. Stress–induced proteins.....	38
2.4. Conclusion	40
Chapter 3.....	41
Effect of Uracil Addition on Proteomic Profiles and 1,3–beta–Glucan Production in <i>Agrobacterium</i> sp.	41
3.1. Introduction	41
3.2. Materials and Methods	43
3.2.1. Strain and culture conditions	43
3.2.2. Analytical methods.....	43
3.2.3. Sample preparation	44

3.2.4. 2D SDS–PAGE analysis	44
3.2.5. Detection of key metabolites	45
3.3. Results and discussion	46
3.3.1. Effect of uracil addition at 90h	46
3.3.2. Analysis enzymes expression levels with 2–dimensional electrophoresis	48
3.3.3. Effect of uracil addition on metabolite concentration	55
3.3.4. Change of 1,3– β –glucan synthase activity	55
3.3.5. Change of enzymes expression level	56
3.4. Conclusion	62
Chapter 4	63
The Change in the Proteomic Profiles of Genetically Modified 1,3–Propanediol Producing Recombinant E. coli	
4.1. Introduction	63
4.2. Materials and methods	66
4.2.1. Recombinant strain	66
4.2.2. Protein Preparation	66

4.2.3. 2D Gel Electrophoresis	67
4.2.4. Data Processing and Analysis	68
4.2.5. Analytical Procedure.....	70
4.2.6. High Performance Liquid Chromatography Analysis.....	70
4.3. Result and discussions	72
4.3.1. Effect of controlled glucose level on glycerol, 1,3-PDO, and acetic acid.....	72
4.3.2. Analysis of 1,3-PDO synthesis metabolic pathway	76
4.4. Conclusion	81
Chapter 5.....	82
Conclusion.....	82
Chapter 6.....	82
The other studies during the course work:	85
6.1 Introduction	85
6.2 Materials and Methods.....	88
6.2.1 Materials	88
6.2.2 Methods	88

6.2.2.1. Preparation and characterization of the supporting magnetized nanomaterials.....	88
6.2.2.2. Enzyme immobilization process.....	90
6.2.2.3. Scanning electron microscopy (SEM).....	91
6.2.2.4. Activity measurement.....	91
6.2.2.5. Application of the immobilized enzymes	93
6.3 Results and Discussion	94
6.3.1 SEM images of PANI and PAMP	94
6.3.2 Properties of nanomaterials.....	96
6.3.2.1. BET and BJH of the PANI and PAMP	96
6.3.2.2. Long term stability and characterization.....	100
6.3.3 Application of the immobilized enzymes.....	104
6.3.3.1 Pectin gellation with immobilized laccase	104
6.3.3.2. Immobilized lactase hydrolyze the lactose and can recycle.....	104
6.3.3.3. Immobilized lysing enzyme produce the glucose from carbohydrates.....	105
References.....	112

List of Figures

Figure 2.1. Time-course profiles of cell growth, curdlan production, and sucrose consumption.	23
Figure 2.2. Silver-stained 2-D SDS-PAGE gels.....	24
Figure 2.3. Time-course variations in spot intensity.....	33
Figure 2.4. Interacellular levels of beta-1,3-glucan synthase, UTP and UDP-glucose.....	34
Figure 2.5. Proposed overview of the altered metabolic pathways during the low pH culture of <i>Agrobacterium</i> sp. ATCC 31750.	35
Figure 3.1. Effect of uracil addition(at 90 hrs) on curdlan production with <i>Agrobacterium</i> sp. ATCC 31750.....	47
Figure 3.2. Silver-stained 2-D SDS-PAGE gel at the cell growth phase.....	50
Figure 3.3. Silver-stained 2-D SDS-PAGE gel at the curdlan producing phase without uracil addition.....	51
Figure 3.4. Silver-stained 2-D SDS-PAGE gel at the curdlan producing phase with uracil addition.....	52
Figure 3.5. with and without uracil added samples in spot intensity	53
Figure 3.6. Detection of beta-1,3-glucan synthase activity with fluorescence	

assay.....	58
Figure 3.7. Detection of UTP levels from three difference samples.....	59
Figure 3.8. Detection of UDP–glucose levels from three difference samples.....	60
Figure 3.9. Metabolic pathway and changes in the level of enzyme expression during β –1,3–glucan(curdlan) synthesis.	61
Figure 4.1. Cell growth and 1,3–PDO production with feedback glucose concentration control between 5–10 g/l.....	74
Figure 4.2. 1,3–PDO production metabolic pathway from glucose as a carbon source.....	75
Figure 4.3. Protein images of the mutant <i>E. coli</i> Δ 6 producing 1,3–PDO separated by 2D–PAGE and stained with ammoniacal silver.....	78
Figure 4.4. The change in enzyme expression level in the cell growth phase and 1,3–PDO production phase.....	79
Figure 6.1. SEM images of the four nanonmaterials.	95
Figure 6.2. Changes in the BET and BJH of the two nanomaterials.....	99
Figure 6.3. Adsorption and desorption isotherms of PANI and PAMP.....	101
Figure 6.4. Ferulic acid was converted to radical form by laccase.....	106
Figure 6.5. Pectin was gelated by radical formed ferulic acid.....	107

Figure 6.6. Batch lactose hydrolysis using recycled immobilized lactase.....	108
Figure 6.7. Degradation of polysaccharide with magnetically separable immo- bilized lysing enzyme.....	109
Figure 6.8. Production of glucose using various carbohydrate using PAMP immo- bilized lysing enzyme.....	110
Figure6.9. Effect of immobilized enzyme recycle.....	111

List of Tables

Table 2.1. The 27 proteins of the 797 proteins showing a prolonged significant difference in the intracellular protein level.....	21
Table 3.1. Key metabolic enzymes showing a significant difference in intracellular protein expression level	54
Table 4.1. The identification of the proteins from the <i>E.coli</i> $\Delta 6$ mutant	80
Table 6.1. Properties of PANI and PAMP.....	98
Table 6.2. Catalytic activity of free lactase and immobilized lactases with various supporting nanofibers	102
Table 6.3. Stability of immobilized lactase using various supporting materials.	103

ABSTRACT

A study on the metabolic pathway change by the proteomic analysis

Li-Hua Jin

Advisor: Prof. Jung-Heon Lee Ph.D.

Department of Chemical Engineering,

Graduate School of Chosun University

This paper reports the results of three different proteomic experiments.

In the first series of experiments, comparative proteome analyses of a control (pH 7.0) and low pH culture (pH 5.5) of *Agrobacterium* sp. revealed curdlan overproduction to be accompanied by significant changes in the level of synthesis of the key metabolic enzymes involved in the curdlan biosynthesis and nucleotide biosynthesis pathways. These results suggest that the altered metabolic conversion leading to the accumulation of UTP and UDP-glucose as well as the inhibition of the lipopolysaccharide and peptidoglycan biosynthesis

pathways and key precursors play important roles in producing large amounts of curdlan.

In the second series of results, the intracellular level of enzymes and metabolites were measured at the cell growth phase with or without adding uracil as a UDP-glucose precursor, and used to explain the increase in the rate of 1,3- β -glucan synthase production during *Agrobacterium* sp. fermentation. From proteomic analysis, after uracil addition, all key metabolic enzymes used for the synthesis of 1,3- β -glucan were activated significantly with the exception of UTP-glucose-1-phosphate uridylyltransferase. Moreover, enzymes, such as glucose-1-phosphate adenylyltransferase and glucose-6-phosphate isomerase, which were catalyzed as a side reaction of 1,3- β -glucan synthase, were repressed.

In the third series of experiments, there were changes in the proteomic profiles of 1,3-PDO producing recombinant *E. coli* using 2-D gel electrophoresis. Seven out of 11 enzymes in the 1,3-PDO production metabolism were identified, and their changes in expression from cell growth to 1,3-PDO production were examined. The major enzymes that enhanced the level of 1,3-PDO production, except for alcohol dehydrogenase, were over expressed.

Glycerol, an intermediate compound of 1,3-PDO production, was produced rapidly when the glucose concentration was $> 5 \text{ g/}\ell$ and inhibited 1,3-PDO production. As a result, the amount of 1,3-PDO accumulation increased to $35 \text{ g/}\ell$. The level of 1,3-PDO production increased when the glucose concentration was $< 1 \text{ g/}\ell$, which prevented the overproduction of glycerol. $43 \text{ g/}\ell$ of 1,3-PDO was produced after 60 hrs of fed-batch fermentation.

국문 요약

단백질체 분석을 통한 metabolic pathway 변화에 대한 연구

김 려 화

지도교수: 이 중 현

조선대학교 일반대학원 화학공학과

본 연구는 주로 단백질체 분석을 통하여 균 주로부터 필요한 산물을 생산해 내는 데 직간접적으로 작용하는 효소들을 찾아냄으로써 균 주의 대사경로의 변화를 알아보는 데 초점을 맞추었다. 이는 한층 생산적이고 유익한 균 주를 개발하는 중요한 기초 자료로 활용할 수 있으며 효소화 반응을 통하여 화학물질을 합성하는 등 여러 분야에 대량의 자료를 제공할 수 있는 연구라고 볼 수 있다.

본 연구에서는 주로 세가지 단백질체 분석 결과를 보여주고 있다.

첫째, 우수한 특성을 가진 생체성 고분자인 커들란을 생산하는 균 주인 *Agrobacterium* sp. 의 균 주 성장 단계와 커들란 생산 단계의 단백질체의 분석을 통하여 커들란 합성에 관여하는 주요 효소들을 찾아내고 그 합성 대사 경로의 변화를 알아보았다. pH 7.0 인 균 주 성장 단계와 비교할 때 pH 5.0 인 커들란 생산 단계에서는 커들란 합성 관여 효소와 뉴클레오타이드, 바이오 합성에 관여하는 효소들이 상당한 변화를 보였다. 이러한 결과는 균 주가 환경이 바뀔에 따라 커들란 합성에 필요

한 UTP, UDP-glucose 등을 축적하고 리포다당류, 펩티도글리칸 등 합성 경로를 저해하는 방향으로 효소들을 합성 하고 대사물질들을 축적하고 있음을 제시하고 있다.

둘째, 우라실을 발효과정에 첨가하였을 때 *Agrobacterium* sp. 균주는 더 높은 커들란 생산성을 보인다. 따라서 우라실을 넣기 전, 후의 단백질을 분석을 진행하여 우라실이 커들란 합성에 관여하는 효소들은 활성화 시키고 부가 반응으로 가는 효소들을 차단시키는 작용을 하여 커들란 생산량이 증가하고 있음을 증명하였다.

셋째, 차세대 석유 대체물로 인기가 좋은 1,3-propanediol(PDO)을 생산하는 대장균 재조합 균 주의 단백질을 분석을 진행하였다. 1,3-propanediol 생산단계와 균주 성장 단계를 비교하여 보았을 때 PDO 생산 단계에서 PDO의 전구체인 glycerol 합성에 관여하는 주요 단백질들의 발현이 증가하는 것을 확인하였다. 또한 PDO의 전구체인 글리세롤은 기질중의 글루코즈의 농도가 5 g/l 보다 크면 대량으로 생성되면서 PDO의 생성을 억제하나 글루코즈의 농도를 1 g/l 이하로 유지하는 경우 글루코즈는 100 % PDO로 전환되었다. 여기서 우리는 기질중의 글루코즈의 농도를 조절하여 발효를 진행하면 60 h 발효로 최대 43 g/l 의 1,3-propanediol까지 얻을 수 있었다.

Chapter 1

Introduction

Curdlan is a water-insoluble microbial exo-polysaccharide. Only few strains of bacteria belonging to the *Alcaligenes faecalis* (now reclassified as an *Agrobacterium*) and *Agrobacterium* spp. Species have been reported to produce this linear polysaccharide. Production of curdlan also occurs in a few *Rhizovium* strains and in species of cellulomonas [1]. Curdlan is a homopolymer of D-glucose linked β -(1→3) without side chains (Figure 1.1). The average molecular weight is difficult to estimate as a result of its poor solubility and remains still a challenge [2]. Under alkaline solution (>0.2M), curdlan is completely soluble and exists as random coils. Lee (2000) reported that its molecular weight has been estimated to be in the range of $5.3 \times 10^4 \sim 2.0 \times 10^6$ Da [3].

Curdlan has some specific properties. Curdlan has water-binding properties and when curdlan was suspended in water and heated to over 80°C, an irreversible gel was formed and its particular characteristics have been used for food purposes and binders for small particles. Curdlan was approved as a food material by the FDA (US Food and Drug Administration) in 1996.

There also have a many reports about the biological activity of the bacterial

glucan. Jagodzinski et al. reported that curdlan sulfate having a β -1,3-glucan backbone showed high anti-AIDS virus activity with low side effects [4]. Mikio et al disclosed that a curdlan derivative, modified by reaction with glycidol, developed excellent antiviral activity with extremely low toxicity [5].

As one of its numerous properties described in the literature, curdlan has been reported to favour the growth of *Bifidobacterium* bacteria in rats cecum (prebiotic action). *Bifidobacteria*, known with *Lactobacillus* species to have probiotic property, furnished beneficial physiological effects to the host. By analogy with fructo- and xylooligosaccharides, both described as prebiotics, hypotheses have been made that β -1,3-glucan-oligosaccharides from curdlan could also present prebiotic properties and would therefore be a potentially new ingredient for the nutraceutical market [6, 7]. To further demonstrate the putative prebiotic activity of oligo β -1,3-glucans, it is firstly necessary to produce them in larger quantities. There are many efforts in increasing the products from bacteria. For instance, developing new mutant strains and analyzing the metabolic pathways to find the key enzymes related in product [8–10].

Nowadays, the proteomics is becoming increasingly important because the

expression of a gene has no definitive relationship to the ultimate expression or abundance of its protein product, emphasizing the need to also profile protein expression in order to understand disease at the molecular level [11, 12]. The proteome, unlike the genome, is not a fixed feature of an organism. Instead, it changes with the state of development, the tissue or even the environmental conditions under which an organism finds itself [11]. So proteomic studies are possible to understand the highlight sites for post-translational modifications based on the specific protein sequence motifs that play important roles in the structure, activity and compartmentalization of proteins [13, 14]. In order to separate and quantify of high-resolute protein, enhanced proteomic technologies, liquid chromatography (LC), high performance liquid chromatography (HPLC), capillary electrophoresis and 2D-PAGE are used and developed [15–17].

Proteomic studies involve the generation of very large data sets, which must be organized, stored, and made accessible in logical ways. As sequence databases are growing exponentially from genome sequencing programs, and automation increases our ability to create proteomic information, the demands on bioinformatics are ever increasing. There is currently a critical need to develop additional software tools that can combine biochemical data about an unidentified

peptide from different experiments and search protein sequence, nucleic acid sequence and expressed sequence tag databases to identify the most probable genetic basis [12].

Application of proteomics provides a protein profile of a cell or tissue that can be used to compare a healthy with a diseased state for protein differences in the search for drugs or drug targets [18]. Proteomics has an application as an assay for the potential utility of drug candidates. In additions, a proteomic approach is a highly efficient method to rapidly separate and characterize the differentially expressed proteins by microorganisms grown under different conditions.

This study was divided into two areas. In the first area, the overall protein expression pattern of a curdlan-producing *Agrobacterium* sp. ATCC31750 during batch fermentation was examined. In addition, the level of synthesis and the change in the pattern of many intracellular proteins with time was examined by comparative analysis of the proteomic responses to growth condition tuning by a pH downshift from 7.0 to 5.5 and with and without uracil addition. For some selected proteins, the peptide masses analyzed by MALDI-TOF were matched with the theoretical peptide masses of the *Agrobacterium tumefaciens* database, and their functional characteristics in the cellular metabolisms were examined in

detail.

In the second section, a change in the protein expression levels related to the two natural metabolic pathways (glucose to glycerol and glycerol to 1,3-PDO) were detected. A recombinant *E. coli* was chosen as a model organism for the production of 1,3-PDO, and the utilization of glucose during the production of 1,3-PDO by *E. coli* was investigated.

Chapter 2

Proteomic analysis of curdlan-producing *Agrobacterium* sp. in response to pH downshift

2.1. Introduction

Curdlan is a neutral, essentially linear, water-insoluble biopolysaccharide that is composed exclusively of β -(1 \rightarrow 3)-linked glucose, and is synthesized by *Agrobacterium* species under nitrogen-limiting conditions [19, 20]. The linear structure of curdlan makes it resistant to heat and other external influences, including pH. In addition, the unique rheological and thermal gelling properties of curdlan have been exploited and can be applied advantageously to areas as diverse as admixtures of concrete, edible fibers, immobilizing supports, and new calorie-reduced food products [21–23]. Recently, curdlan has also been applied as a drug delivery polymer for sustained drug and control drug diffusion [24], and curdlan sulfate was developed as an antiviral agent to inhibit human immunodeficiency virus (HIV)-1 infections [25]. In addition, based on its immunomodulating responses [1, 26], it has been proposed that curdlan might find uses in cosmetic formulations and as a protective agent for farmed fish [27].

Therefore, in order to increase the economic attractiveness of curdlan, it is important to increase the productivity and minimize its production costs to allow curdlan to compete with other polysaccharides [28, 29]. Many studies focused mainly on optimizing several of the key factors (i.e. temperature, pH, nutrients, agitation, and aeration) involved in the curdlan fermentation process to increase the yield/productivity [1, 30–34]. The production of curdlan by *Agrobacterium* is strain dependent [1, 34], and is typical of a secondary metabolite in that its biosynthesis occurs in the post-stationary growth phase under conditions of nitrogen-starvation [20, 28, 35] suggested that during batch fermentation processes, the specific cell growth rate was the highest at pH 7.0, and the specific curdlan production rate was highest at pH 5.5. In particular, the pH profiles maximizing curdlan production were changed from pH 7.0 optimal for cell growth to pH 5.5 optimal for curdlan production after nitrogen consumption [33].

Furthermore, change in the intracellular nucleotide levels and their stimulatory effects on the metabolic flux of curdlan synthesis in *Agrobacterium* species were examined under nitrogen-limited and sufficient culture conditions [19]. On the other hand, although previous studies focused on cloning the genes related to the curdlan synthesis metabolism in the *Agrobacterium* sp strain ATCC 31749 and

expressed them in heterologous hosts[36, 37], various molecular studies uncovered entirely new characteristics that are important for the development of industrial strains and the interaction with various environments.

With the completion of *Agrobacterium tumefaciens* genome sequencing [38, 39], a new challenge has been launched by many projects to increase the understanding of the cellular physiology at the global level and accelerate strain and metabolic pathway improvement in *Agrobacterium* strains-based bioprocesses. In particular, physiological and biochemical functions of the open reading frames of *Agrobacterium* species newly discovered by genomic sequencing can be determined at the level of the expressed gene products, the proteome. Although there are some comprehensive reports of the physiological state and responses of the *Agrobacterium tumefaciens* metabolism during some culture stresses (e.g. heat shock, oxidative stress, and mild acid stress) using proteomics tools [40–43], the proteomic approach for building a quantitative dynamic analysis and the metabolic synthetic pathway on *Agrobacterium* species is still in the early stages of development. Nevertheless, with the ever-increasing amount of protein sequencing data in various databases, and the improvements in mass spectrometry technology, proteomics has been proposed

elsewhere as a powerful tool for understanding, predicting, and solving real metabolic problems. This study examined the overall protein expression pattern of a curdlan-producing *Agrobacterium* sp. ATCC 31750 during batch fermentation. In addition, the level of synthesis and the change in the pattern of many intracellular proteins with time was determined through a comparative analysis of the proteomic responses to the growth condition tuning by pH downshift from pH 7.0 to pH 5.5. For some selected proteins, the peptide masses analyzed by automated MALDI peptide mass spectrometry were matched with the theoretical peptide masses of the *Agrobacterium tumefaciens* database. Their functional characteristics in the cellular metabolisms were examined in detail. Comparative proteome analysis showed that the curdlan overproduction resulted from a significant change in the synthesis of important metabolic enzymes involved in curdlan biosynthesis.

2.2. Materials and Methods

2.2.1. Bacterial strain and culture conditions

Agrobacterium sp. ATCC 31750 (formerly *Alcaligenes faecalis* subsp. *myxogenens*) was used as the bacterial strain for proteome analysis. Fermentations were carried out in a 5 ℓ fermentor (Kobiotech, Incheon, Korea) containing 3 ℓ of the nutrition medium (100 g/ℓ sucrose, 4 g/ℓ NH₄Cl, 1 g/ℓ KH₂PO₄, 0.5 g/ℓ MgSO₄ · 7H₂O, and 10 ml/ℓ trace element solution [29]. The fermentor was inoculated with 300 ml of a preculture broth that had been grown to the stationary phase on a nutrition medium. Cultivation was carried out at 37 °C with aeration of 0.5 vvm. During fermentation, the optimal growth pH was controlled to 7.0 using 2 N HCl and 2 N NaOH. At the time of ammonium exhaustion, the culture pH was decreased to 5.5 for optimal curdlan production, as previously reported by Lee et al [20]. Cell growth was monitored by measuring the absorbance of the sampled culture at 600 nm.

2.2.2. Cell mass, curdlan, and β -1,3-glucan synthase assay

The dry cell mass was measured by mixing 10 ml of the sample with 15 ml of a 0.5 N NaOH solution. The supernatant was removed by centrifugation. An aliquot was washed with distilled water twice and the dry cell mass was measured after drying overnight at 80 °C. The sucrose concentration was measured using a slight modification of the dinitrosalicylic acid (DNS) method [28]. One milliliter of the sample was mixed with 20 ml of 3 N HCl, and the mixture was hydrolyzed at 100 °C for 15 min. After cooling the mixture, 3 ml of a DNS solution was added, and the resulting mixture was boiled again at 100 °C for 10 min. The sucrose concentrations of the samples were determined by measuring the absorbance at 570 nm. For an analysis of curdlan, 1 ml of an appropriately diluted sample was mixed with 15 ml of a 3 N NaOH solution. The mixture was then incubated at room temperature for 30 min to dissolve the curdlan. After centrifuging the mixture at 5000×g for 15 min, the curdlan present in the supernatant was precipitated under acidic conditions by adding 15 ml of 3 N HCl. The precipitated curdlan was harvested by centrifuging at 5000×g for 15 min, and washed three times with distilled water to remove the salts. The concentration of curdlan was determined by measuring the dry weight after drying overnight at 80 °C. The

ammonium concentration was determined using the indophenol method [44].

For the detection of β -1,3-glucan synthase, fluorescence assays were carried out using the modified method as described by Shedletzky et al. [45]. Aniline blue was used as a fluorescence dye. The fluorescence was quantified using a Synergy HT Fluorescence Reader (Bio-Tek Instruments, USA). The excitation wavelength was 400 nm/slit width 40 and emission wavelength was 460 nm/slit width 40.

2.2.3. UTP, and UDP-glucose assay

The intracellular nucleotides were extracted by using a slight modification of the method described by Ryll and Wagner [46]. The cells (50 mg dry cell weight) were centrifuged immediately at $5000\times g$ at 4 °C for 5 min. The harvested cell pellet was resuspended in 3 ml of an ice-cooled lysis buffer, and disrupted by sonication (Sonic Dismemberator, Fisher 100model) at 4 °C. Sonication consisted of four 10 sec bursts at the maximum setting. After sonication, the cell debris was finally removed by centrifugation at $10,000\times g$ for 30 min. The clear supernatant was filtered through a 0.2 μ m filter (PVDF, Whatman, England). The samples were stored at 20 °C prior to HPLC analysis. The amount of intra cellular

UTP and UDP-glucose formed were quantified by HPLC [46]. The chromatographic system consisted of two HPLC pumps (LC-10A DVP, Shimadzu, JP), a prominence UV detector (Shimadzu, SPD-20A), and a system controller (SCL-10A VP). The separations were carried out on a reverse-phase YMC-pack pro C18 column (250×4.6 mm i.d., S-5 μ m, 12 mm-particle size, YMC Inc., Wilmington, NC), and a 50 mM phosphate buffer (pH 5.3) solution was used. Sample detection was achieved at 254 nm, and the chromatographic peaks were assigned by a comparison with authentic samples. The injection volumes for HPLC analysis were 20 μ l.

2.2.4. Sample preparation for two-dimensional electrophoresis

The cells are harvested by centrifugation at room temperature at 8000 rpm for 15 min. The cell pellets were washed twice with a Tri-HCl buffer (40 mM, pH 8.0) and resuspended in 500 μ l of a lysis buffer (8 M urea, 4 % w/v CHAPS, 40 mM Tris, protease inhibitor cocktail solution (Roche Diagnostics GmbH, Mannheim, Germany)). After sonication for 2 min on ice, the cell debris was removed by centrifugation at 16000 rpm for 60 min. The protein concentration was determined using a Bio-Rad protein assay kit (Hercules, CA, USA) with

bovine serum albumin as the standard. The supernatants were stored at 80 °C until analyzed by 2-D gel electrophoresis. 45 μ g of the proteins were resuspended in a rehydration solution [8 M urea, 0.5 % w/v Triton X-100, 0.005 % w/v orange-G, 1 % w/v DTT, and 1 % v/v carrier ampholyte, pH 3-10, 1 % v/v carrier ampholyte, pH 4-7]. Urea, 3-[(3-cholamidopropyl) dimethylammonio]-1-propanesulfonate (CHAPS), Tris, dithiothreitol (DTT), bromophenol blue, and sodium dodecyl sulfate (SDS) were purchased from Sigma Chemical Co. (St. Louis, MO, USA).

2.2.5. Two-dimensional gel electrophoresis

The first dimension of 2-DE was carried out on a Bio-Rad PROTEAN IEF cell Electrophoresis System at 20 °C. Linear pH 4-7 immobilized pH gradient (IPG) gel strips (17 cm, ReadyStripTM IPG strips, Bio-Rad Laboratories, CA, USA) were rehydrated overnight by placing the strips gel-side-down in the sample-containing rehydration solution in a strip holder and covering them with mineral oil (Bio-Rad Laboratories, CA, USA). The samples were loaded with an intracellular protein level of 45 μ g for silver-staining. The first dimension was performed for 1 h at 250 V, for 5 h at 10000 V, and until 70000 Vhs at 10000 V for

the analytical and preparative gels that had been prepared for image analysis and spot excision for protein identification, respectively. 30 μ g and 120 μ g of the protein per strip was loaded for the analytical and preparative gels, respectively. The IPG gel strips were then equilibrated for 15 min in an equilibration solution [50 mM Tris-HCl, pH 8.8, 6 M urea, 30 % v/v glycerol, 2 % SDS, bromophenol blue trace] with 1 % DTT for 15 min and then 2.5 % iodoacetamide for 15 min. The equilibrated gel strips were placed on a 12.5 % polyacrylamide gel and the second dimensional separation was carried out using a PROTEAN II xi cell system (Bio-rad, CA, USA) in a cold chamber at 4 °C. SDS-PAGE was carried out at 30 mA/gel for 12 h until the bromophenol blue reached to the bottom of the gel. Silver staining was performed using a modified method, as described elsewhere [47]. The molecular weight of the protein was determined using a broad molecular weight standard marker (Bio-Rad, CA, USA). The stained gels were scanned using EPSON EXPRESSION1680 Pro (EPSON, Korea). Progenesis PG200 v2006 from Nonlinear Dynamics was used to locate protein spots within the gel images and quantify the spot intensity scale on a volume basis (i.e. calculated by integrating the spot optical intensity over the spot area).

2.2.6. MALDI–TOF mass spectrometric analysis and database search

The samples for the matrix–assisted laser desorption ionization–time of flight (MALDI–TOF) mass spectrometry analysis were extracted from the silver stained spots according to a previously reported protocol [48]. Enzymatic digestions were carried out with 10–15 g/ml of sequencing grade modified trypsin (Promega, WI, USA) in 25 mM ammonium bicarbonate (pH 8.0) and were incubated overnight at 37 °C in a stationary incubator. The in–gel–digested peptide fragments were extracted from the gel pieces by adding 5 % v/v trifluoroacetic acid in 50 % v/v acetonitrile followed by vortexing for 1 h. After three times repeated, the solute materials including the peptide fragments were dried by vacuum centrifugation. A Ziptip column (Millipore, Bedford, USA), in which C₁₈ resin is fixed at the end of the tip was used to eliminate the impurities in the samples. The peptide solution was prepared with an equal volume of a saturated cyano–4–hydroxycinnamic acid solution in 50 % ACN/0.1 % TFA on the sample plate of the MALDI–TOF mass spectrometer. Protein analyses were performed using a MALDI–TOF mass spectrometry system (Voyager DE–STR, PE Biosystem, Framingham, MA) with the following parameters: peptide

measuring range of 700–4000 Da and a mass tolerance within 50 ppm to maintain the highest certainty of protein identification. The criteria for unambiguous protein identification required at least five peptides, which represented a minimum of 20 % sequence coverage. The spectra were calibrated using a matrix and tryptic autodigestion ion peaks as the internal standards. The peptide mass fingerprints were analyzed using the MASCOT (http://www.matrixscience.com/cgi/search_form.pl?FORMVER=2&SEARCH=PMF) and Swiss–Prot was selected as the reference database in the MASCOT for protein identification.

2.3. Results and discussion

2.3.1. Proteomic response of *Agrobacterium* sp. ATCC 31750 batch culture to pH downshift

pH control during the cultivation is one of the most important factors because it significantly influences cell growth and the rates of curdlan formation. In batch fermentations for curdlan production, the cell growth rate in the pre-stationary phase is optimal at pH 7.0, whereas curdlan production is optimal at pH 5.5 [1, 20, 33, 34]. As the glucose concentrations is increased, higher nitrogen-concentrations are needed to produce a cell mass thereby maximizing the yields of curdlan in the post-stationary, N-limited production phase [34]. In this study, two-dimensional SDS-polyacrylamide gel electrophoresis (2-DE) was used to analyze the characteristics of overall protein expression along with the growth after pH tuning. Prior to 2-DE analysis, *Agrobacterium* sp. ATCC 31750 was cultivated in a batch bioreactor (5 ℓ), and the culture pH was shifted from 7.0 to 5.5 at the time of ammonium exhaustion (data not shown). As shown in Figure 2.1, the cell growth rate was not diminished after the pH downshift. From both batch cultures (P and C at pH 7.0 and pH 5.5, respectively), the culture broth was sampled at 2, 37, and 72 h after pH downshift, and the total intracellular

proteins from each culture sample were prepared after disrupting the cell pellets. For each protein sample, 2-DE was repeated 8~10 times with silver staining for each 2-DE gel, and then for comparative image analysis, an average gel image was prepared with selected three gels showing a high degree of reproducibility using the Progenesis v2006 software (Nonlinear Dynamics, USA).

Approximately, 800 spots were visualized on every average gel image, and the 2-DE gel images of culture samples at pH 5.5 and pH 7.0 were compared systematically at each time point (2, 37, or 72 h after the pH downshift). The following were observed through quantitative and comparative analysis of the proteomic responses to the pH downshift: (1) the levels of 15 proteins were significantly increased after the pH downshift, and the high levels were maintained during the entire low-pH growth period; and (2) 12 proteins were significantly repressed for a prolonged time after decreasing the pH from pH 7.0 to pH 5.5. These proteins are labeled on the 2-DE gel in Figure 2.2 and 3 (spots A-O and 1-12). The time-course variation in protein synthesis level was relatively estimated relatively by defining the spot intensity of the proteins visualized at the C2 phase as 1 (Table 2.1 and Figure 2.3). Different intensity ratios above 1 indicate the stress-responsive induction of protein expression,

and those below 1 indicate stress-responsive repression of protein expression. Protein identification and the overall metabolic characteristics of *Agrobacterium* sp., strain were estimated using the *Agrobacterium tumefaciens* proteome database. The proteins were identified by MALDI-TOF analysis for each protein spot and subsequent PMF using the *A. tumefaciens* MASCOT database, as summarized in Table 2.1 and Figure 2.3. The proteins identified in the list were related to curdlan biosynthesis, energy metabolism, nucleotide biosynthesis, lipopolysaccharide and peptidoglycan biosynthesis, amino acid synthesis, exopolysaccharide and isoprenoid biosynthetic pathways, stress-induced proteins, and cell processes (Table 2.1)

Table 2.1. The 27 proteins of the 797 proteins showing a prolonged significant difference in the intracellular protein level (i.e., spot intensity) during the entire period of low pH growth in a batch culture.

Spot No.	Gene name	Protein name	pI	MW (kDa)	Accession number ^a	% Sequence Coverage ^b	Protein level ratio (fold change) ^c						Function
							C2/C2	C37/C2	C72/C2	P2/C2	P37/C2	P72/C2	
A	dnaK	Chaperone protein dnaK	4.84	68.15	P50019	63	1	2.21	1.31	3.11	4.17	4.95	Chaperone
B	atpA	ATP synthase subunit alpha	6.51	54.62	Q8UC74	52	1	0.76	0.39	1.09	1.22	1.54	Production ATP from ADP
C	glgC	Glucose-1-phosphate adenylyltransferase	5.24	47.03	P39669	68	1	0.77	0.21	0.98	1.29	0.97	Glycogen biosynthesis
D	ispH	4-hydroxy-3-methylbut-2-enyl diphosphate reductase	5.48	37.54	P58673	63	1	0.13	0.09	1.89	2.12	2.28	Isoprenoid biosynthesis
E	glk	Glucokinase	5.42	36.70	Q8UIV7	75	1	0.31	0.12	1.27	1.31	0.93	Glycolysis
F	exoN	UTP-glucose-1-phosphate uridylyltransferase	5.84	33.74	Q8U8P0	68	1	0.74	0.55	1.18	1.44	1.71	Sucrose metabolism
G	rpiA	Ribose-5-phosphate isomerase A	5.10	24.14	Q8UEZ0	59	1	0.95	0.68	1.38	2.25	1.98	Pentose phosphate pathway
H	pyrF	Orotidine 5-phosphate decarboxylase	5.18	25.05	P58638	46	1	1.41	1.59	2.17	2.99	3.12	UMP biosynthesis
I	tal	Transaldolase	5.29	34.50	Q8U7I5	61	1	0.09	0.03	1.09	1.02	1.08	Pentose phosphate pathway
J	upp	Uracil phosphoribosyltransferase	6.32	23.20	Q8UJ06	72	1	0.71	0.21	1.21	1.05	1.01	Pyrimidine salvage pathway
K	bmell	Exopolysaccharide production protein	5.90	46.50	Q8U6L4	55	1	0.01	0.08	1.37	1.29	1.89	EPS production
L	sucC	Succinyl-CoA synthetase beta chain	4.93	41.90	Q8UC60	65	1	0.51	0.21	1.01	1.35	1.21	Tricarboxylic acid cycle
M	pgm	Phosphoglucosmutase	5.30	57.80	P39671	58	1	0.89	0.18	0.97	1.31	3.11	Synthesis of capsular polysaccharide and lipopolysaccharide
N	pgi	Glucose-6-Phosphate isomerase	5.79	58.71	Q8UI94	67	1	1.41	0.97	0.24	2.79	3.17	Glycolysis
O	crd	Putative beta 1,3 glucan	6.81	73.12	Q9X2V0	65	1	0.77	0.38	0.73	1.21	3.82	Curdlan biosynthesis

synthase catalytic subunit													
1	tig	Trigger factor	4.77	54.15	Q8UEU0	69	1	2.01	1.97	0.66	0.45	0.17	Export and maintain of protein
2	glmU	UDP-N-acetylglucosamine pyrophosphorylase	6.28	47.20	Q2K8G2	57	1	1.61	1.54	1.31	0.39	0.19	Peptidoglycan & Lipopolysaccharide biosynthesis
3	murB	UDP-N-acetylenolpyruvoylglucosamine reductase	5.83	34.83	Q8UDN0	51	1	1.32	1.58	0.63	0.41	0.47	Peptidoglycan biosynthesis
4	trpD	Anthranelate phosphoribosyltransferase	5.60	35.38	Q8UER8	63	1	2.41	2.57	0.97	0.79	0.43	Tryptophan biosynthesis
5	murI	Glutamate racemase	5.22	29.98	Q8UE93	63	1	0.99	1.67	0.54	0.13	0.27	Peptidoglycan biosynthesis
6	trpA	Tryptophan synthase alpha chain	5.31	29.27	Q8UJA9	44	1	2.04	1.99	0.97	0.24	0.18	Tryptophan biosynthesis
7	lpxA	Acyl-[acyl-carrier-protein]-UDP-N-acetylglucosamine O-acyltransferase	6.45	28.38	Q8UFL3	66	1	8.11	9.13	0.91	3.17	3.55	Lipopolysaccharide biosynthesis
8	exoR	Exopolysaccharide production negative regulator	5.46	28.81	Q8UEP0	73	1	1.47	1.12	0.61	0.35	0.15	EPS production
9	hisF	Imidazole glycerol phosphate synthase subunit hisF	4.97	27.27	P58799	67	1	21.34	59.78	1.03	6.12	5.68	Histidine biosynthesis
10	kdsA	2-dehydro-3-deoxyphosphooctonate aldolase	5.59	30.11	Q8UFH3	52	1	1.41	1.47	0.86	0.33	0.31	Lipopolysaccharide biosynthesis
11	hisG	ATP phosphoribosyltransferase	5.61	24.81	Q8UHK1	48	1	1.25	2.19	0.77	0.52	0.29	Histidine biosynthesis
12	mscL	Large-conductance mechanosensitive channel	6.25	15.61	Q8UHY0	58	1	8.17	13.54	1.26	4.25	6.14	Regulation of osmotic pressure

^a Accession code refers to the SWISS-2DPAGE database

^b Mass tolerance in protein identification through PMF experiment was 10 ppm

^c Protein expression level in each growth phases compared with C2 phase. Expression level in C2 phase was set at 1.

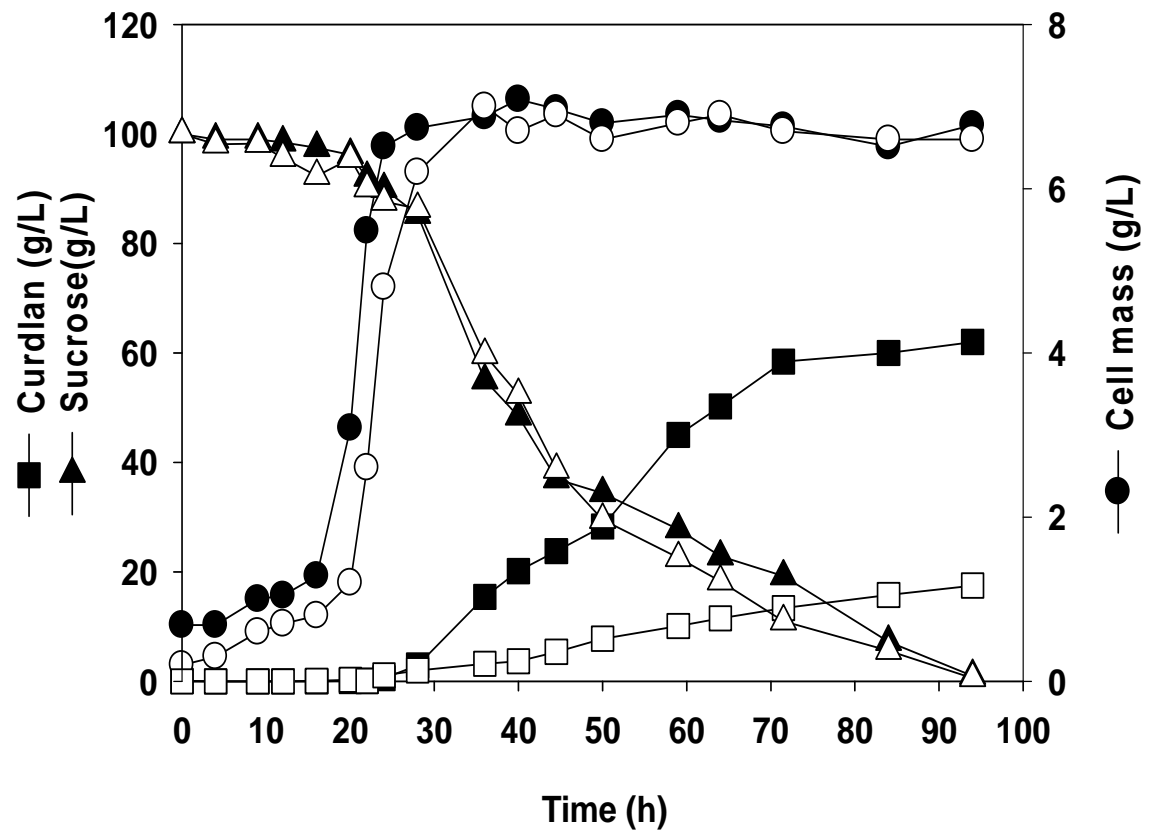


Figure 2.1. Time-course profiles of cell growth, curdlan production, and sucrose consumption.

During batch cultures controlled at pH 7.0 (open circles, rectangles, and triangles) and pH 5.5 (dark circles, rectangles, and triangles). The culture samples were taken from the bioreactor at three different time points (2, 37 and 72 h) after pH downshift. C, control culture (at pH 7.0); P, pH downshift culture (at pH 5.5).

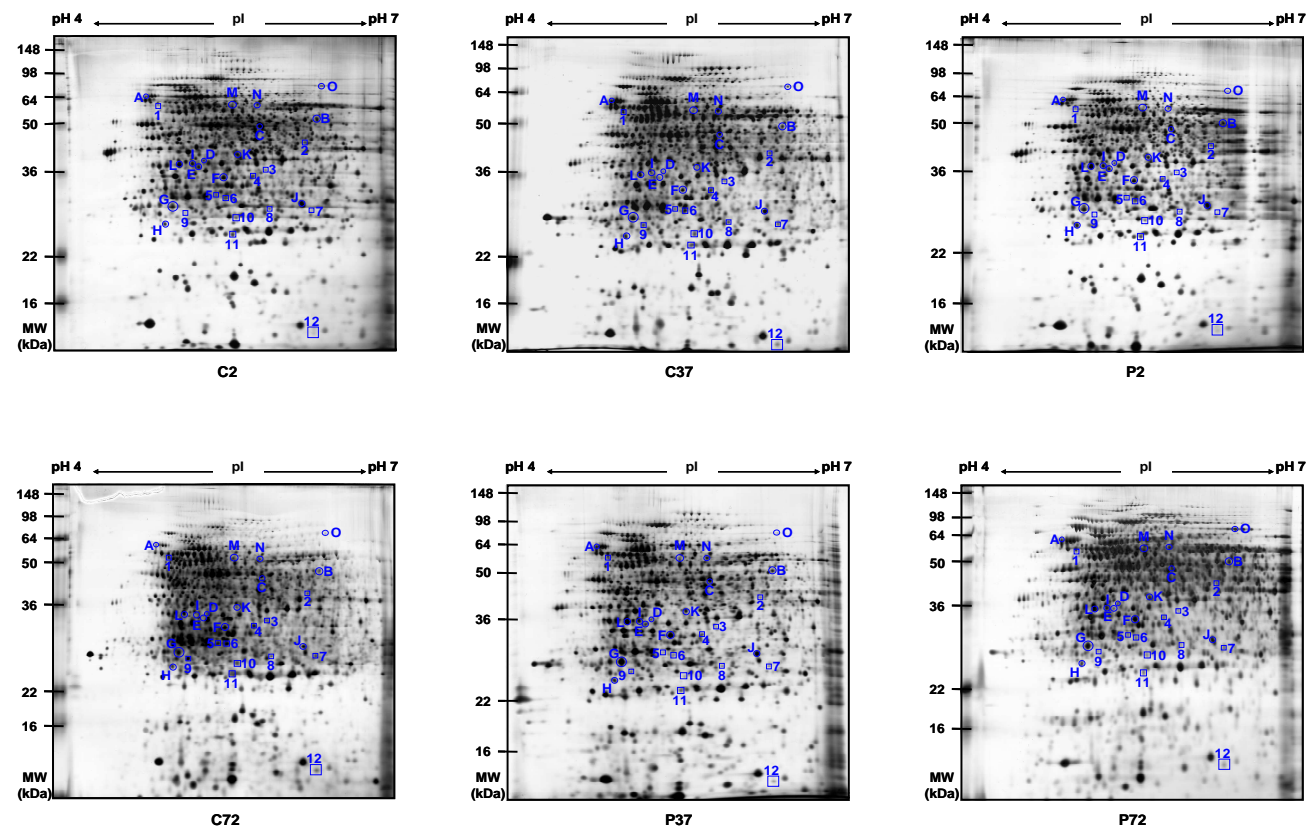


Figure 2.2. Silver-stained 2-D SDS-PAGE gels.

Here showing the 27 protein spots listed in Table 2.1. The protein spots inside the circles indicate the induced proteins after decreasing the pH from pH 7.0 to pH 5.5. The protein spots inside the rectangles indicate the repressed proteins after decreasing the pH from pH 7.0 to pH 5.5.

2.3.2. Estimation of curdlan overproduction metabolism after pH downshift

From comparative proteome analysis, it was possible to observe the differences in metabolic enzyme synthesis related to curdlan biosynthesis and understand how the metabolic flux has been changed after pH downshift on the basis of the differences in the level of the metabolic enzymes that catalyze curdlan synthesis. As shown in Figures 2.2 and 3, several proteins involved in the energy metabolism were induced after the pH downshift. The levels of glucokinase (spot E) glucose-6-phosphate isomerase (spot N), transaldolase (spot I), and succinyl-CoA synthetase beta chain (spot L) synthesis, which are key metabolic enzymes in the glycolysis and tricarboxylic acid (TCA) cycle, were much higher in the low pH culture. In addition, the ATP synthase subunit alpha (spot B), which is involved in ATP-proton motive-force interconversion in the energy metabolism, was also more strongly activated at P72 in the low pH growth than at C72. If the change in the ATP synthase subunit alpha (spot B) is assumed to affect the ATP synthase activity, it may indicate that ATP generation and proton import are simultaneously induced in a low pH environment.

On the other hand, during the biosynthesis of most polysaccharides, sugar nucleotides are used as glycosyl donors. In particular, UDP-glucose, which is a key metabolite in the synthesis of curdlan, serves not only as an activated precursor for glycosyl moieties but also as a precursor in the synthesis of most

polysaccharides [19, 49]. Although cellular nucleotides generally play an important role in the synthesis of sugar nucleotides in the cellular metabolism, little is known regarding the change in the nucleotide levels and their effect on the metabolic fluxes in intracellular metabolism [50].

From Figures 2.2 and 3, three metabolic enzymes (e.g. Ribose-5-phosphate isomerase A (spot G), orotidine 5-phosphate decarboxylase (spot H), and uracil phosphoribosyl transferase (spot J), which are related to the biosynthesis of nucleotides, were significantly oversynthesized to probably expedite the possible conversion of excessively accumulated UMP (Scheme 1). UMP is a key precursor for UTP and UDP-glucose biosynthesis through sequential reactions of nucleotide kinases and UDP-glucose pyrophosphorylase. An increase in the intracellular UMP level caused by nitrogen-limitation enhances curdian biosynthesis by promoting cellular UDP-glucose synthesis [1, 19]. Interestingly, it was observed that the protein level of uracil phosphoribosyl-transferase (spot J) catalyzing the conversion of uracil to UMP was 5 times higher at the P72 phase in the lower pH culture (Figure 2.2 and 3), whereas this protein was significantly repressed in the control culture (pH 7.0). Therefore, it is possible to assume that the addition of uracil to the growth medium may enhance the metabolic flux of UTP synthesis. This is in agreement with previous research on curdian production with *Agrobacterium* sp. [29]. It was previously shown for *Agrobacterium* sp. ATCC 31750 that uracil, which acts as a precursor of UDP-

glucose, served as an activator on the production of curdlan, and uracil addition to a sucrose-containing culture medium at 46 h increased the level of curdlan production compared with the unsupplemented culture after 160 h of growth [29].

Therefore, it is likely that the *Agrobacterium* sp. ATCC 31750 catabolism might be modulated towards increasing the supply of UTP, and hence UDP-glucose, as a means of inducing curdlan synthesis in the low pH culture. At the same time, levels of phosphoglucomutase (spot M) and UTP-glucose-1-phosphate uridylyl transferase (spot F) synthesis were significantly different from that observed in the control culture, i.e., the protein levels of phosphoglucomutase and UTP-glucose-1-phosphate uridylyl transferase were 17.3-fold and 3.3-fold higher at the P72 phase after pH downshift, compared with the level of synthesis in the control at a time point, C72 (Figure 2.3 and Table 2.1).

As shown in scheme 1, it is reasonable to assume that a significant amount of UDP-glucose accumulates in a low pH environment. Therefore, the overall metabolic flow appears to be directed towards the curdlan biosynthetic route. Presumably, a significant amount of the key metabolic precursor related to curdlan biosynthesis might accumulate after the pH downshift, thereby directing the overall metabolic flow toward the curdlan biosynthetic route. As shown in Figure 2.3 and Table 2.1, we evidently observed that the protein level of the β -1,3-glucan synthase catalytic subunit (spot O), which catalyzed the conversion of UDP-glucose into curdlan, was increased during the whole period in the low

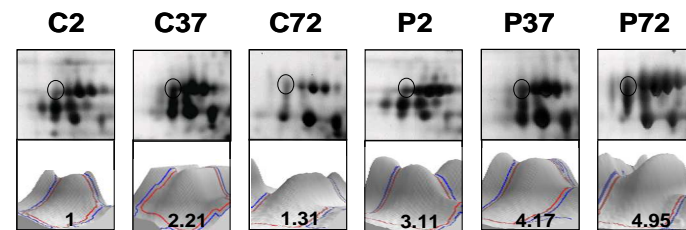
pH environment, i.e., a more than 10-fold increase in the level of β -1,3-glucan synthase catalytic subunit after pH downshift (Figure 2.3, and 2.4). The overexpression of β -1,3-glucan synthase catalytic subunit at the lower pH might explain why curdlan was overproduced by *Agrobacterium* sp. compared with the control culture (Figure 2.1). Additionally, the activity of β -1,3-glucan synthase was investigated using a fluorescence assay. As shown in Figure 2.4a, the activity of β -1,3-glucan synthase was more than 3 times higher at the P72 phase in the low pH culture than in the control at the same time point, C72. This is in line with the comparative proteome analysis as described above.

This study also examined the cellular levels of UTP and the synthesis of UDP-glucose while investigating the biosynthesis metabolism of curdlan. Figure 2.4b and 2.4c shows the intracellular levels of UTP and UDP-glucose. As a result, the initial UTP levels of the control culture (C2) and lower pH culture (P2) were similar at 0.31 and 0.35 mg/ml, respectively. Interestingly, the intracellular UTP levels increased significantly over a prolonged time from 0.35 to 18.4 mg/ml in the lower pH culture, i.e., a 3.3-fold increase in the UTP level after 72 h of pH downshift, compared with the level of synthesis in the control culture at the same time point, C72 (Figure 2.4b).

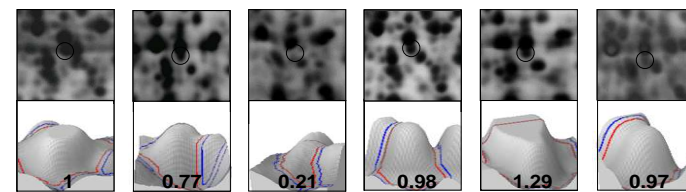
It was also observed that the cellular UDP-glucose level was showed a more than 1.9-fold increase after pH downshift, as shown in Figure 2.4c.

Therefore, the remarkable increase in the cellular metabolic key enzymes

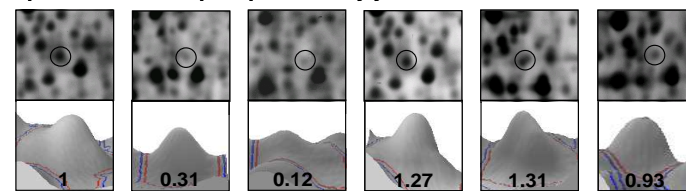
during pH downshift culture enhances the metabolic flux of the key precursor biosynthesis processes, such as UTP and UDP-glucose, resulting in an increase of in curdlan biosynthesis.



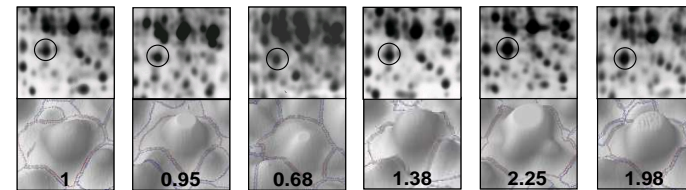
Spot A: Chaperone protein dnaK



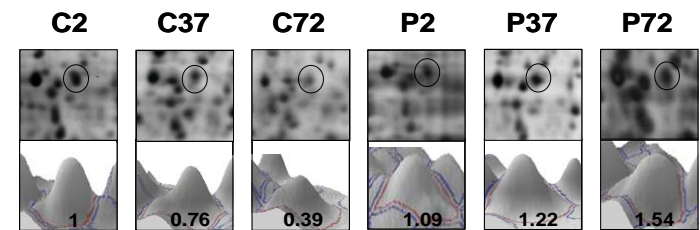
Spot C: Glucose-1-phosphate adenylyltransferase



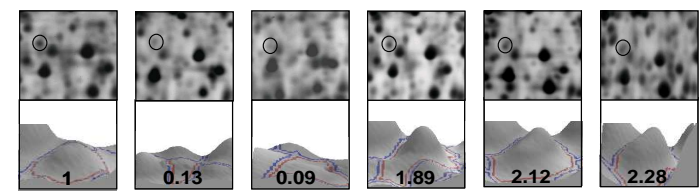
Spot E: Glucokinase



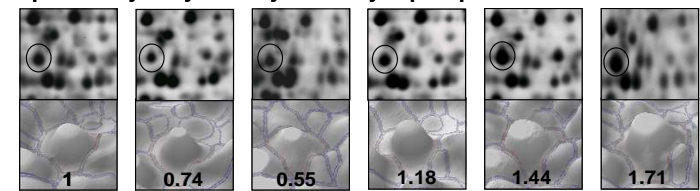
Spot G: Ribose-5-phosphate isomerase A



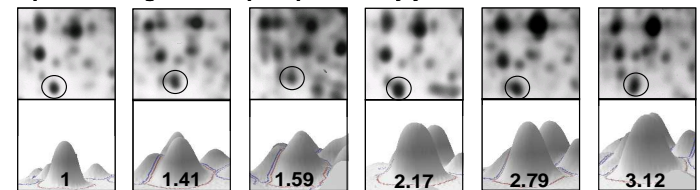
Spot B: ATP synthase subunit alpha



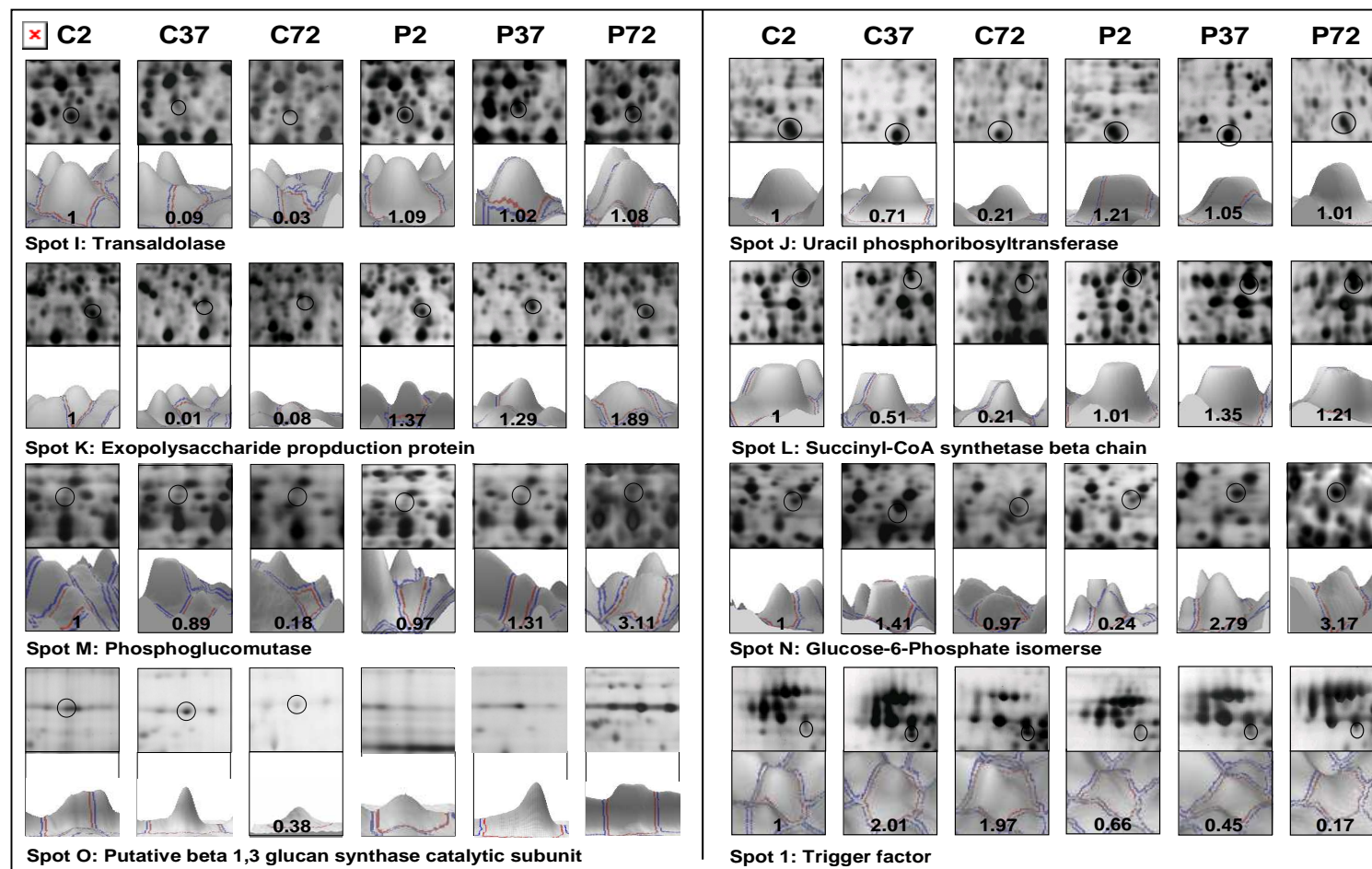
Spot D: 4-hydroxy-3-methylbut-2-enyl diphosphate reductase

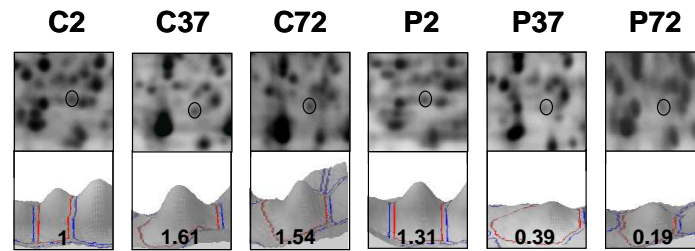


Spot F: UTP-glucose-1-phosphate uridylyltransferase

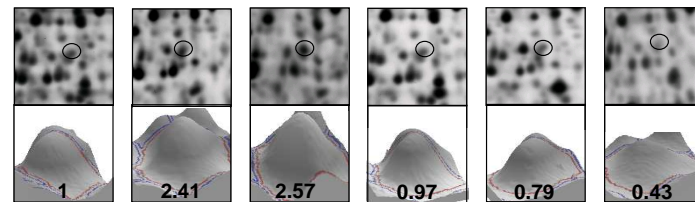


Spot H: Orotidine 5'-phosphate decarboxylase

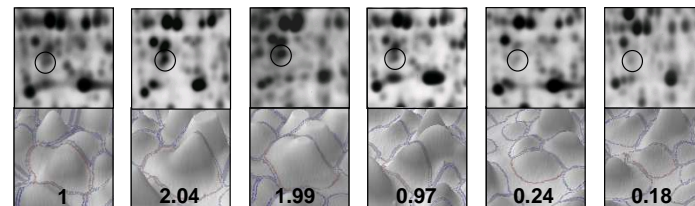




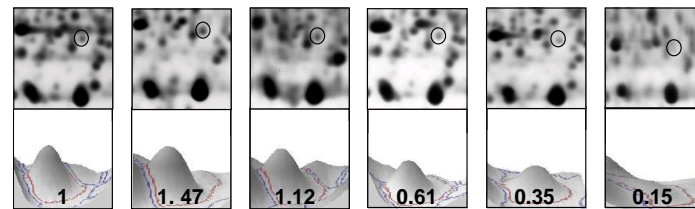
Spot 2: UDP-N-acetylglucosamine pyrophosphorylase



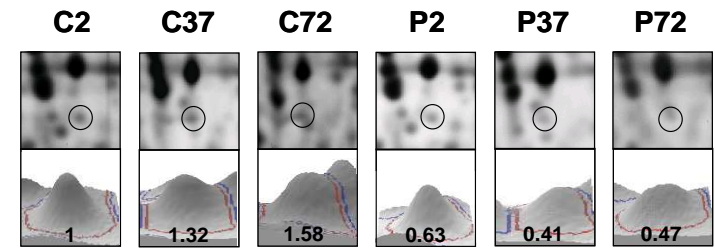
Spot 4: Anthranilate phosphoribosyltransferase



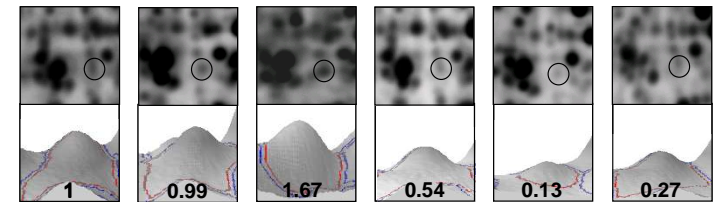
Spot 6: Tryptophan synthase alpha chain



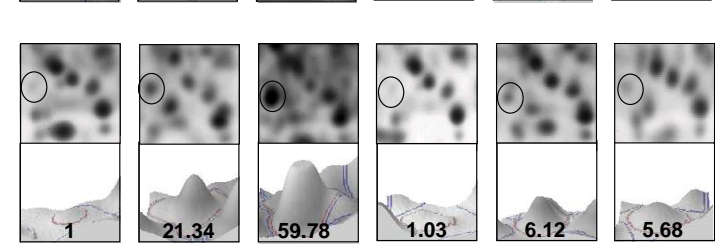
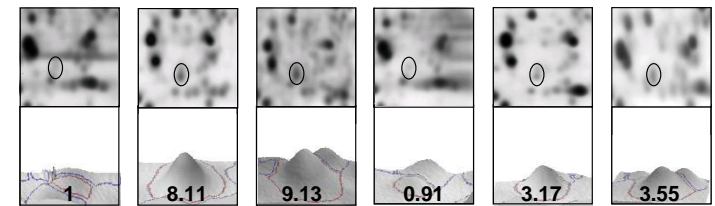
Spot 8: Exopolysaccharide production negative regulator



Spot 3: UDP-N-acetylenolpyruvoylglucosamine reductase



Spot 5: Glutamate racemase



Spot 9: Imidazole glycerol phosphate synthase subunit hisF

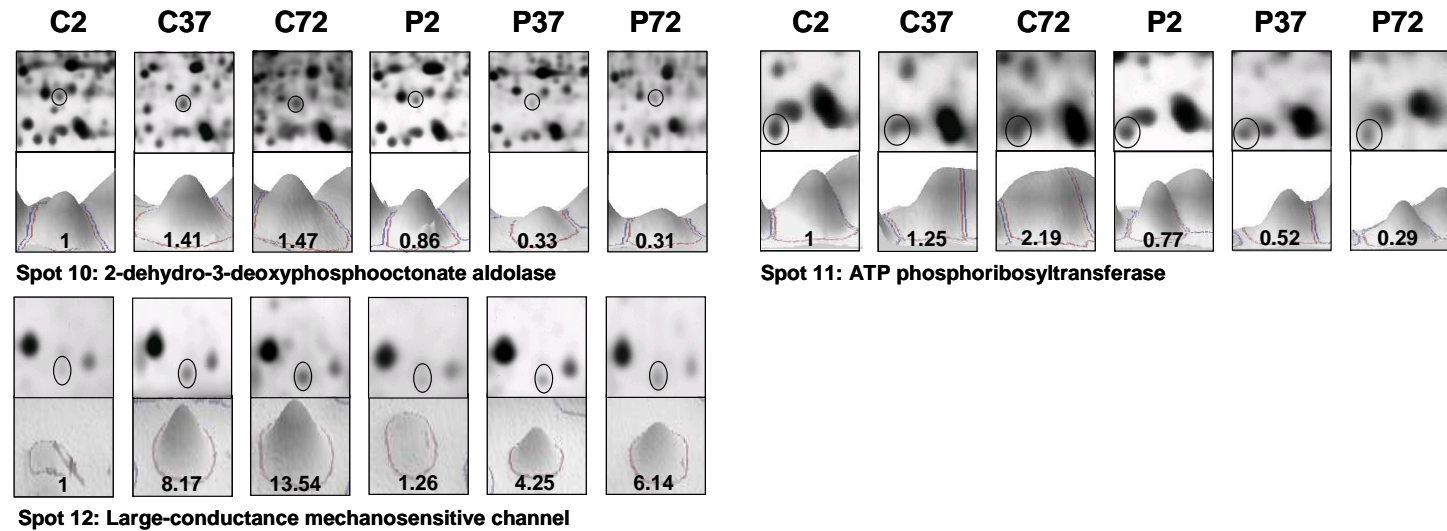


Figure 2.3. Time-course variations in spot intensity.

27 protein spots in the control culture (at pH 7.0); P, lower pH culture (at pH 5.5). (The time-course variation of protein synthesis level was estimated relatively by defining the spot intensity of the proteins visualized at the C2 phase as 1 and 3D image of each protein spots were displayed using Progenesis PG 200).

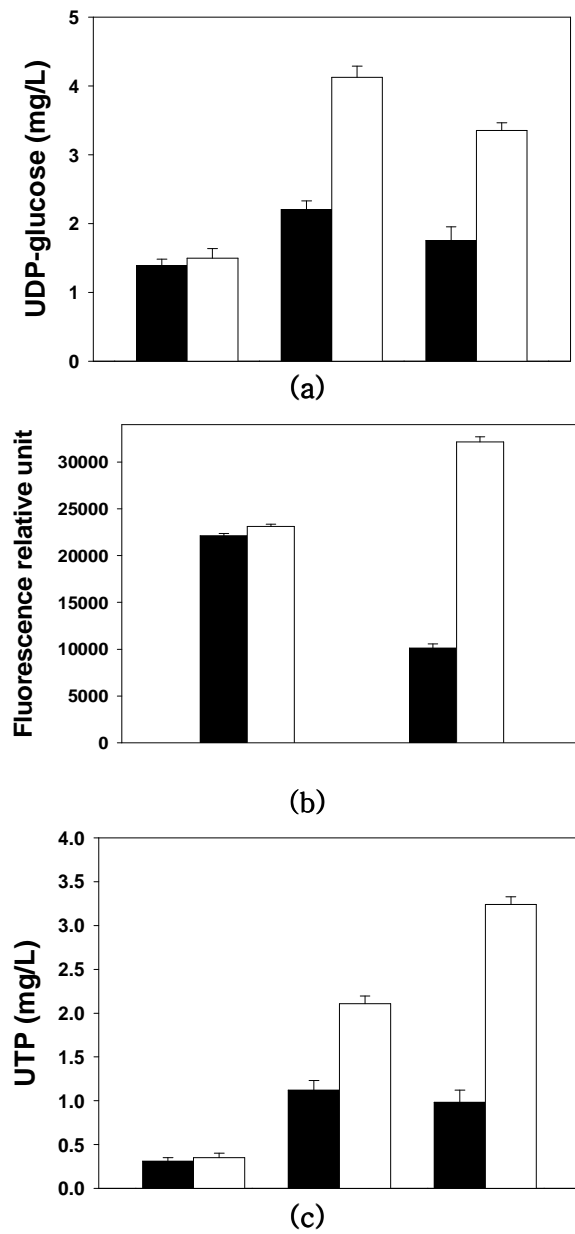


Figure 2.4. Interacellular levels of β -1,3-glucan synthase, UTP and UDP-glucose.

(a) The activity of β -1,3-glucan synthase according to a fluorescence assay. (b) Intracellular levels of UTP. (c) Intracellular levels of UDP-glucose. (Control culture (black columns) and pH downshift culture (white columns)).

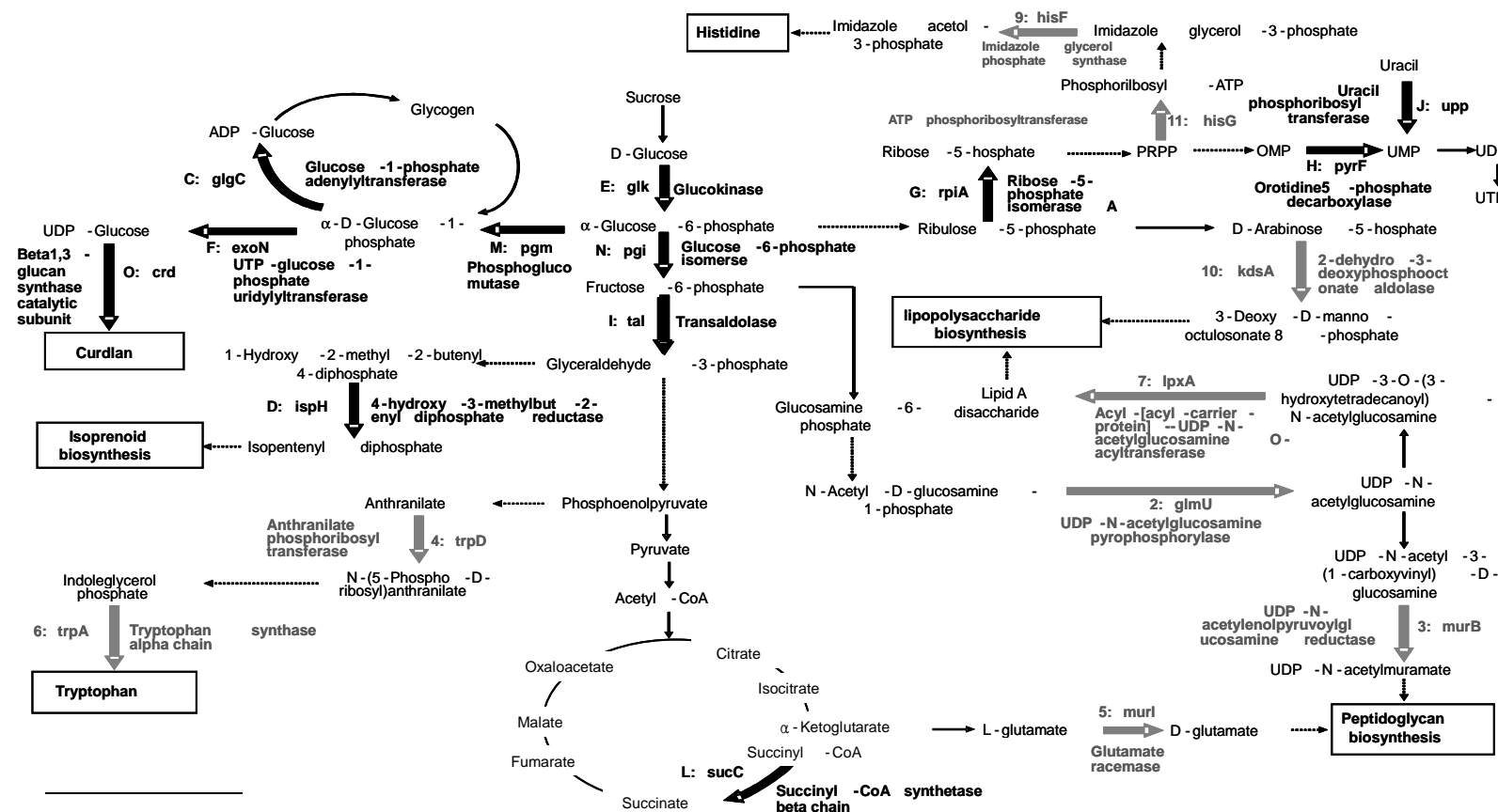


Figure 2.5. Proposed overview of the altered metabolic pathways during the low pH culture of *Agrobacterium* sp. ATCC 31750.

(The thick black arrow show that the metabolic conversion was significantly activated. It is possible that this is due to the increased protein level (i.e. spot intensity) of the corresponding metabolic enzyme. In addition, the thin gray arrow indicates that the metabolic conversion was severely repressed. The cause for this may be a far lower protein level of the corresponding metabolic enzyme)

2.3.3. Lipopolysaccharide, peptidoglycan and isoprenoid biosynthesis

Under nitrogen-limited conditions, polysaccharide synthesis has generally been explained by the roles of carrier lipids [19, 51, 52]. Evidently, a wide variety of proteins were strongly repressed in the low pH culture to maintaining the cellular metabolism related to the biosynthesis of lipopolysaccharide and peptidoglycan. Figures 2.2 and 3 show that the synthesis of UDP-N-acetylglucosamine pyrophosphorylase (spot 2), UDP-N-acetylenolpyruvoylglucosamine reductase (spot 3), Acyl-[acyl-carrier-protein-UDP-N-acetylglucosamine O-acyltransferase (spot 7), and 2-dehydro-3-deoxyphosphooctonate aldolase (spot 10) were significantly lower in pH downshift culture. In addition, another enzyme in the exopolysaccharide production pathway, exopolysaccharide production protein (spot K) was oversynthesized during the low pH condition, as shown in Figure 2.2 and Table 2.1. In contrast, exopolysaccharide production negative regulator protein (spot 8) showed more than 7-fold decrease after 72 h of pH downshift (P72), compared with the level of synthesis in the control culture at the same time point, C72 (Table 2.1). On the other hand, the conversion of 4-hydroxy-3-methyl-2-butenyl diphosphate to isopentenyl diphosphate might be activated by the increased synthesis of 4-hydroxy-3-methyl-2-butenyl diphosphate reductase (spot D), which can further increase the metabolic flux of isoprenoid biosynthesis can further

increase (Figure 2.5). Previous studies reported that polysaccharides are formed through the mediation of isoprenoid lipid intermediates. Moreover, the availability of isoprenoid lipid may provide a means of regulating polysaccharide synthesis [19, 53]. It was also reported that isoprenoid lipid is more available for carrying oligosaccharides under nitrogen-limited conditions instead of cellular lipopolysaccharide and peptidoglycan [1, 19, 53]. As a result, it can be strongly presumed that formation of lipopolysaccharide and peptidoglycan might be inhibited during the low pH culture and isoprenoid plays a key role in producing a large amount of curdlan from *Agrobacterium* sp. ATCC 31750 (Figure 2.5).

2.3.4. Amino acid biosynthesis

Through a comparative proteome analysis of *Agrobacterium* sp. ATCC 31750 batch culture, it was observed that the expression level of the metabolic enzymes involved in the amino acid biosynthesis were changed significantly after a pH downshift, as shown in Table 2.1 and Figure 2.2. The expression of four metabolic enzymes (spots 4, 6, 9, 11) was strongly repressed during the entire period of low pH growth. The level of ATP phosphoribosyltransferase (spot 11) synthesis, which catalyzes the conversion of 5-phosphoribosyl- α -pyrophosphate to phosphoribosyl-ATP, was 7.6-fold lower after 72 h in the lower pH culture than in the control culture (pH 7.0). Furthermore, other key enzymes for the biosynthesis of histidine, i.e., imidazole glycerol phosphate

synthase (spot 9), was also strongly repressed during low pH growth. On the other hand, the synthesis of two key enzymes for tryptophan biosynthesis, namely anthranilate phosphoribosyltransferase (spot 4), and tryptophan synthase alpha chain (spot 6), were significantly repressed.

2.3.5. Stress-induced proteins

In this study, it was observed that an important molecular chaperone, DnaK (spot A), which is a key factor for correct protein folding, was significantly up-regulated in the acid-stress response. Several studies have improved the understanding of the complex stress response in *A. tumefaciens*, using 2-DE [41, 42]. Several heat shock proteins in *A. tumefaciens* were previously identified, which include GroEL, GroES, DnaK, DnaJ, RpoH, and ClpB [41, 54–56]. On the other hand, the RpoH homologue and the CIRCE-HrcA regulatory system were identified as two heat shock control elements in *A. tumefaciens* [57, 58]. In contrast to the gram-positive bacteria, the CIRCE-HrcA system is found only in the *groESL* operon and heat shock transcription of the major chaperone genes is controlled by RpoH [42, 59]. This study showed that the synthesis of the trigger factor (spot 1) was strongly repressed all the way during the entire period of low pH growth. Previous studies showed that the major molecular chaperones in *E. coli* (e.g., DnaK and its cofactors, GroEL and GroES) are not only essential for normal growth at 37 °C but are also heat-shock proteins that

are further induced at higher temperatures and under other harsh conditions that damage the cell proteins. These chaperones can prevent protein aggregation, assist in catalyze protein refolding, and can promote the selective degradation of heat damaged polypeptides [48, 60]. Unlike most molecular chaperones, the trigger factor is not essential for viability at high temperatures and its level increases progressively at low growth temperatures. Although the trigger factor is important for protein folding and might also be important for the cell adaptation at high/low temperatures, the functional complementarities observed between cytosolic molecular chaperones, such as HtpG, ClpB, GroEL/ES, and DnaK/J is during the low pH growth conditions not completely understood.

2.4. Conclusion

2-DE is very useful for understanding the quantitative proteomic responses of curdlan-producing *Agrobacterium* sp. ATCC 31750 to a pH downshift during well-controlled batch fermentation by analyzing the time-course variations in the protein level in detail. Comparative proteome analyses of the control culture (pH 7.0) and low pH culture (pH 5.5) showed that curdlan overproduction accompanied the significant changes in the level of synthesis of the key metabolic enzymes involved in curdlan biosynthesis and the nucleotide biosynthesis pathway. These results strongly suggest that the altered metabolic conversion leading to the accumulation of UTP and UDP-glucose and the inhibition of the lipopolysaccharide and peptidoglycan biosynthesis pathways and key precursors play a key role in producing large amounts of curdlan. For further metabolic engineering of the strain for industrial applications, more complete information on the overall regulation characteristics of curdlan overproduction would be achieved through a detailed analysis of the transcriptomic responses at the gene expression level.

Chapter 3

Effect of Uracil Addition on Proteomic Profiles and β -1,3-Glucan Production in *Agrobacterium* sp.

3.1. Introduction

Because of good properties of curdlan, many efforts were done for improving the productivity of the curdlan. Several optimization strategies have been used to improve the productivity of curdlan. For example, optimization of fermentation pH has been carried out in other studies. However, the productivity in a batch fermentor is as low as 0.5 g/ℓ/hr. In a previous paper, curdlan production was optimized and the final curdlan concentration was increased to 93 g/ℓ after 160 h fermentation with the addition of sucrose and uracil. Uracil was reported to increase the UDP-glucose level and serve not only as an activator of the glycosyl metabolism but also as a precursor in the formation of other monosaccharides[29].

Molecular level studies on curdlan synthesis have identified the curdlan synthesis enzymes. The genes essential for the production of bacterial β -1,3-glucan were transferred to *Agrobacterium* sp. ATCC31749[36]. Additional curdlan related genes whose protein products occur in the cell envelope were

identified by Karnezis *et al.*(2002), and the transposon *TnphoA* was used as a specific genetic probe[61]. Despite these efforts, the mutants did not improve the productivity of curdlan. Another method, called transcriptional profiling, was introduced. It is relatively quick and easy, but the mRNA abundance is not always a reliable indicator of the corresponding protein abundance [62–64].

This study examined the proteomic profile changes as a function of uracil (a precursor of UDP–glucose) addition. Particular focus was on the enzymes related to glucan synthesis metabolism that contribute to the synthesis of UDP glucose. The proteomic profiles both with and without uracil addition were analyzed by 2D gel electrophoresis followed by MALDI–TOF MS.

3.2. Materials and Methods

3.2.1. Strain and culture conditions

Glucan producing strain *Agrobacterium sp.* ATCC 31750 was cultured in same culture medium as chapter 2. The control culture was done without uracil addition. The other culture was started at same moment and when the culture time was 90 hrs, added 5 g/ℓ uracil to the fermentor to improve the curdlan productivity. Cell growth was monitored by measuring the absorbance of the sampled culture at 600 nm.

3.2.2. Analytical methods

The cells and curdlan concentrations were determined by measuring the dry weight. A 1 mℓ sample from the fermentor was centrifuged at 12000 rpm for 5 min. After harvesting the sample, curdlan was dissolved in a 3 N NaOH solution to measure the cell mass. The sample was washed 3 times with distilled water. The pellet was then dried and the cell mass was measured. After dissolving curdlan in the NaOH solution, 3 N HCl was added to the solution to acidify the solution, and the resulting solution was centrifuged at 8000 rpm for 15 min. The supernatant was removed from the tube. The remaining pellet was curdlan. The curdlan was washed 3 times with distilled water and dried to measure the curdlan concentration. The sucrose concentration was determined using the

dinitrosalicylic acid method after hydrolyzing the samples with 20 μl 2N HCl at 100 °C for 15 min. The ammonium concentration was determined using the indophenol method [65].

3.2.3. Sample preparation

Three samples were selected by analysis. The control sample was the cell growth phase; sample was taken after the cell cultured for 22 hr. The second sample was taken after the cell cultured for 94 hrs in control fermentation without uracil addition. The third sample was taken at same time as second sample in the uracil added fermentation.

Three samples were treated for 2-D SDS-PAGE, the methods for sample treatment was same as recorded in chapter 2.

3.2.4. 2-D SDS-PAGE analysis

45 μg of three protein samples were prepared for 2-D SDS-PAGE analysis. The methods were same as recorded in chapter 2.

The 2-D gel of the three samples was detected spot intensities using image master software V4.01. The reference gel was shared with gel C2 (pH 7.0, 22 hr) from chapter 2.

3.2.5. Detection of key metabolites

The key metabolites of UTP and UDP-glucose were detected by HPLC. The HPLC methods were recorded in chapter 2.

The activity of β -1,3-glucan synthase was detected by fluorescence assay and method also was same as recorded in chapter 2.

3.3. Results and discussion

3.3.1. Effect of uracil addition at 90h

As shown in Figure 3.1, the production of curdlan was initiated after the ammonium had been depleted at 24 hrs. After 90 hrs fermentation, the curdlan concentration was approximately 51 g/ℓ. The rate of curdlan production decreased thereafter. 1.5 g uracil was added to the 3 ℓ fermentor at 90 hrs to activate curdlan production. As a result, the rate of curdlan production was increased and its concentration was increased to 72 g/ℓ. The control fermentation was done at same condition without uracil addition. Three samples were taken. The control sample was taken at cell growth stage (22 hr) and sample at curdlan producing stage (94 hr) were taken at control fermentation and uracil added fermentation respectively. The Three samples were prepared to check changes in the metabolite and enzyme levels in the cell.

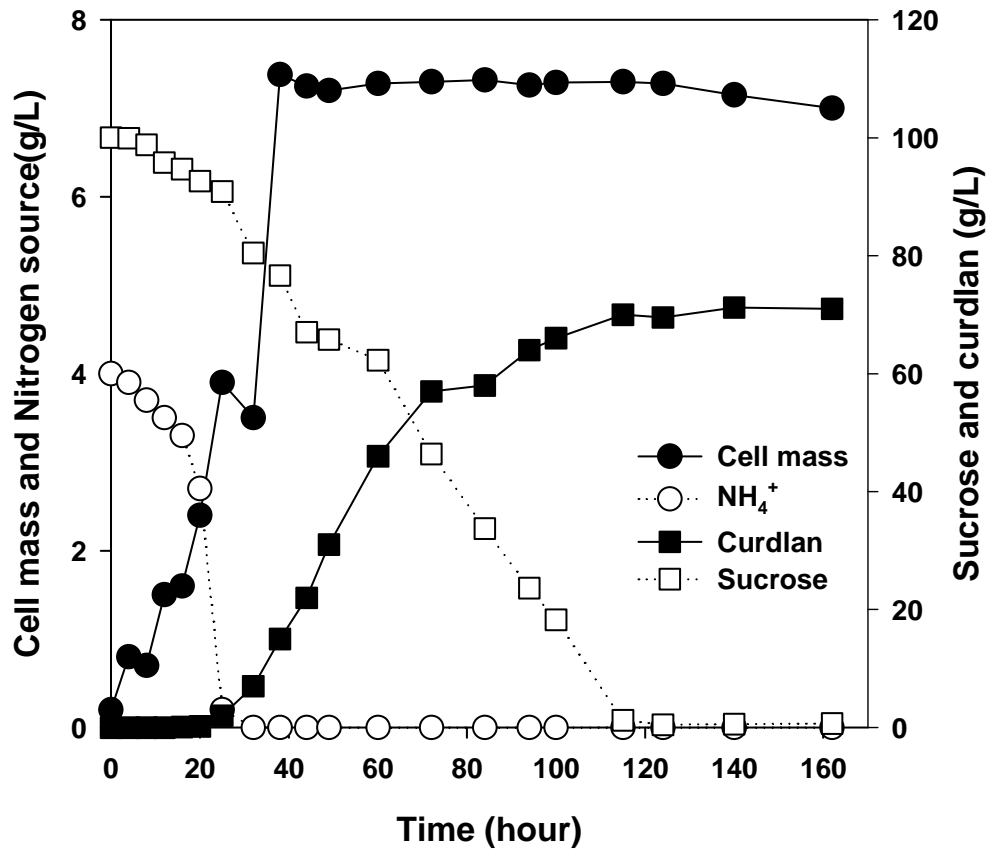


Figure 3.1. Effect of uracil addition (at 90 hrs) on curdian production with *Agrobacterium* sp. ATCC 31750.

pH was controlled from 7.0 to 5.5 after 25 hrs fermentation

3.3.2. Analysis enzymes expression levels with 2-dimensional electrophoresis

The cell broth was harvested at 22hrs and pH 7.0, and used to determine the reference protein profiles. More than 600 protein spots were identified (in preparation). This study focused on the changes in the key metabolic enzymes after the addition of uracil. Figure 3.2, 3.3 and 3.4 shows the proteomic profiles of the three samples from fermentation of *Agrobacterium* sp. ATCC31750. Figure 3.2 was cell growth stage, at that time, the cell was grown 22hrs. Figure 3.3 was the sample taken in the control fermentation, at that time, cell was grown 94 hrs. Figure 3.4 was also taken at same time with control fermentation, but the cell was grown 90 hrs, there were added 0.5 g/ℓ uracil.

Silver-stained 2-D SDS-PAGE gel at control, none, and uracil phases showing 11 protein spots listed in Table 3.1. The protein spots inside the circles indicate the induced proteins after uracil added. The protein spots inside the rectangles indicate the repressed protein after uracil added.

Figure 3.5 shows the spot intensity of 11 protein spots in the control culture (at pH 7.0, 22 hr); None, without uracil added, uracil, with uracil added. Uracil was added at fermentation time 90 hr and sample was taken at 94 hrs both in uracil added and control fermentation. The changes in the level of protein expression were detected using Image Master Software V4.01 (Amersham Biosciences, Uppsala, Sweden). This is because the key enzymes were identified using the

mass spectroscopy data of *Agrobacterium tumefaciens*, which has 98 % rRNA similarity to *Agrobacterium* sp. ATCC 31750. The PI values and molecular weights of the enzymes in the 2D gel might have different values from those in the DB sources (ExPASy at <http://www.expasy.ch/>).

Table 3.1 provides information on the 11 protein spot in the 2D-gel. In this Table, UTP-glucose-1-phosphate uridylyltransferase, phosphoglucomutase, and β -1,3-glucan synthase catalytic subunit which are key metabolic enzymes in the curdlan biosynthesis pathway, were more than 3.5 %, 30 %, 35 % higher in the uracil added culture. In addition, uracil phosphoribosyltransferase which converts uracil to the UMP were also up-regulated 79 % than control fermentation. However, the level of Orotidine 5-phosphate decarboxylase, Glucose-1-phosphate adenylyltransferase and Glucose-6-phosphate isomerase expression decreased after uracil addition (Table 3.1). Therefore, the addition of uracil during fermentation activates production of the enzymes related to the glucan synthesis metabolism and increase the rate of β -1,3-glucan production.

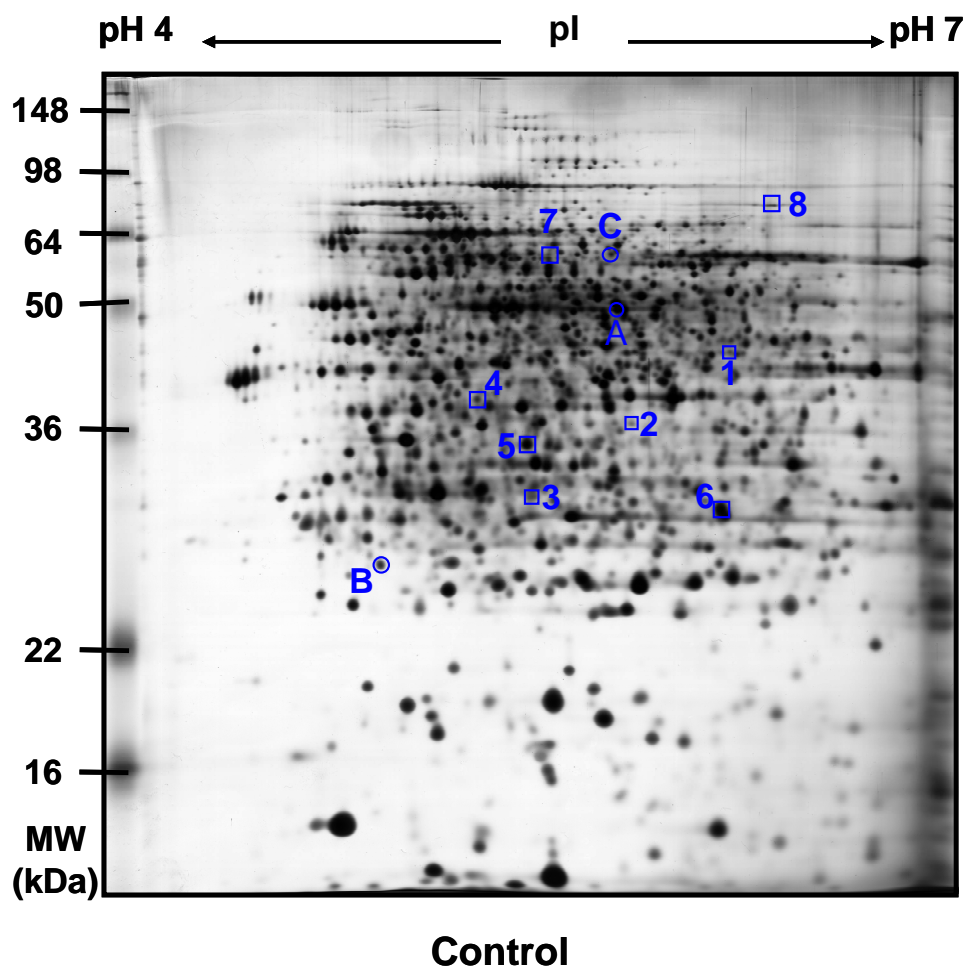


Figure 3.2. Silver-stained 2-D SDS-PAGE gel at the cell growth phase

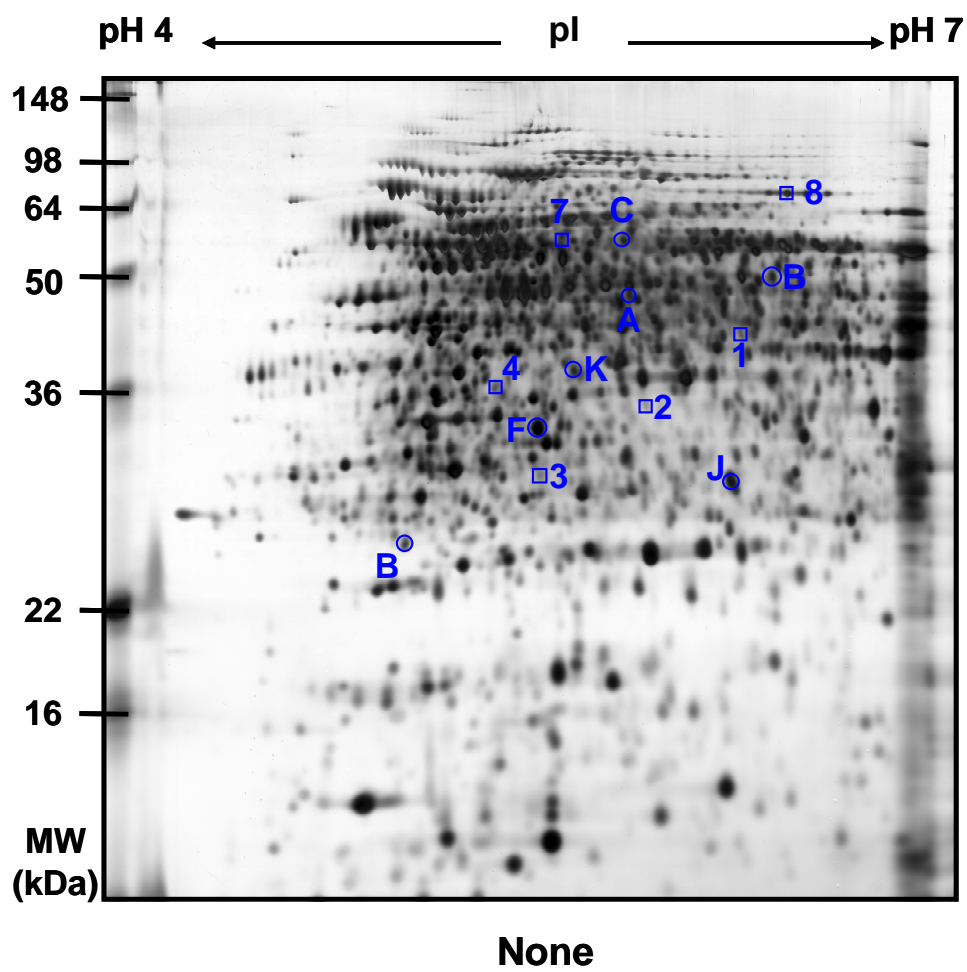


Figure 3.3. Silver-stained 2-D SDS-PAGE gel at the curlan producing phase without uracil addition

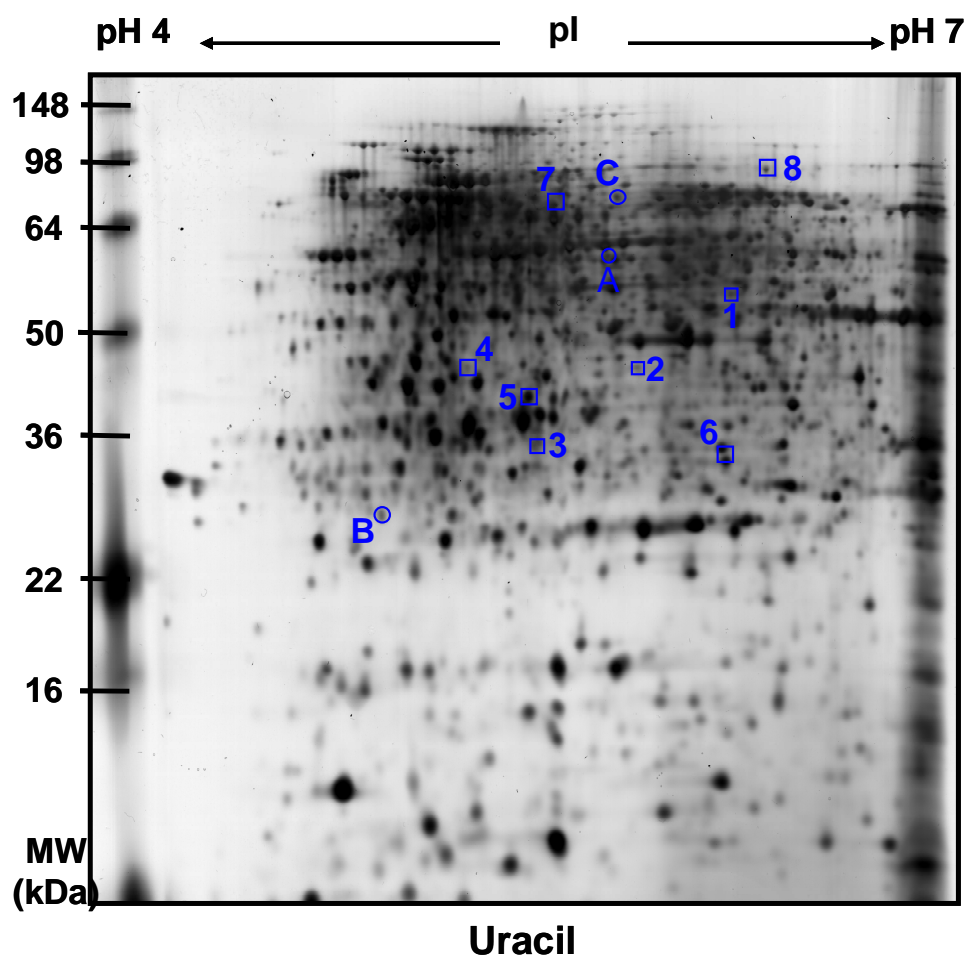


Figure 3.4. Silver-stained 2-D SDS-PAGE gel at the curlan producing phase with uracil addition

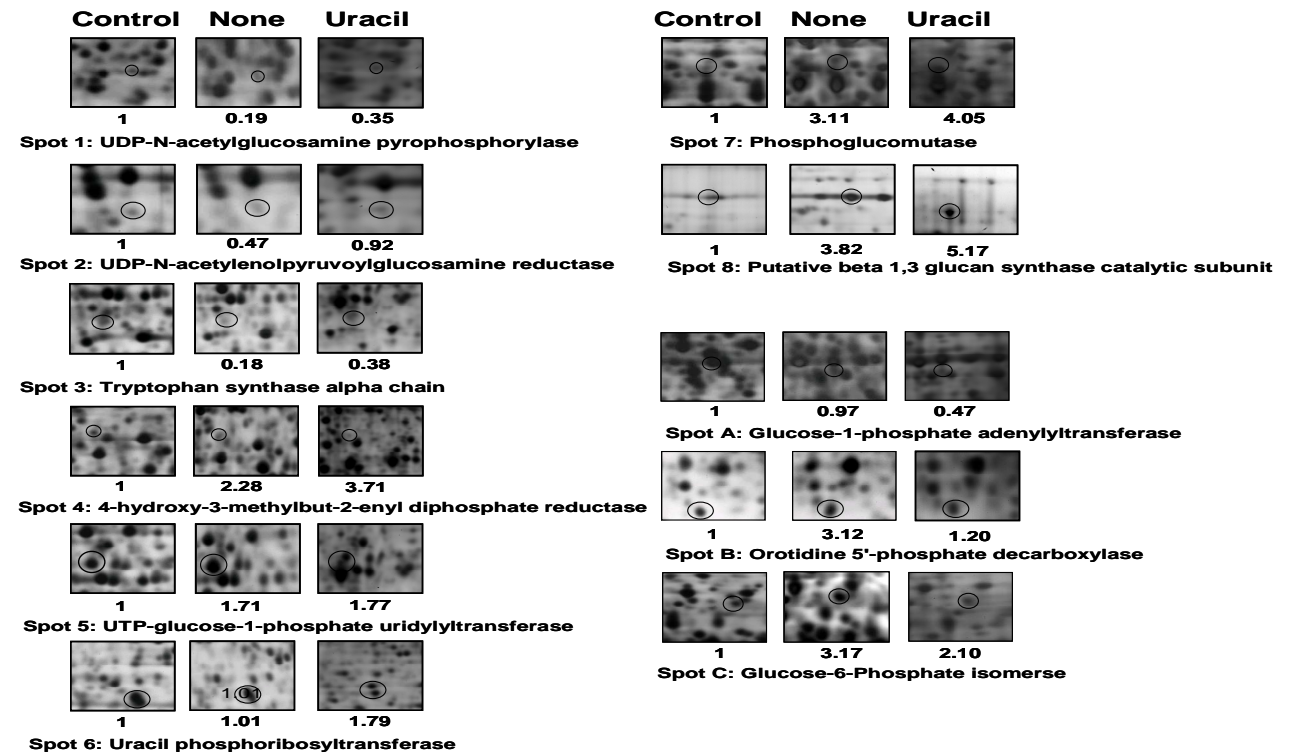


Figure 3.5. with and without uracil added samples in spot intensity

11protein spots in the control culcure(at pH7.0, 22hr); None , without uracil added , uracil, with uracil added. Uracil was added at fermentation time 90hr and sample was taken at 94hrs both in uracil added and control fermentation

Table 3. 1. Key metabolic enzymes showing a significant difference in intracellular protein expression level (i.e. spot intensity) during the whole period of cell growth and curdlan production with uracil addition

Spot No	Gene name	Protein name	pI	MW (kDa)	Accession Number ^a	% Sequence Coverage ^b	Control	None uracil added	uracil added
1	glmU	UDP-N-acetylglucosamine pyrophosphorylase	6.28	47.2	Q2K8G2	57	1.00	0.19	0.35
2	murB	UDP-N-acetylenolpyruvoylglucosamine reductase	5.83	34.83	Q8UDN0	51	1.00	0.47	0.92
3	trpA	Tryptophan synthase alpha chain	5.31	29.27	Q8UJA9	44	1.00	0.18	0.38
4	ispH	4-hydroxy-3-methylbut-2-enyl diphosphate reductase	5.48	37.54	P58673	63	1.00	2.28	3.71
5	exoN	UTP-glucose-1-phosphate uridylyltransferase	5.84	33.74	Q8U8P0	68	1.00	1.71	1.77
6	upp	Uracil phosphoribosyltransferase	6.32	23.2	Q8UJ06	72	1.00	1.01	1.79
7	pgm	Phosphoglucomutase	5.3	57.8	P39671	58	1.00	3.11	4.05
8	crd	Putative beta 1,3 glucan synthase catalytic subunit	6.81	73.12	Q9X2V0	65	1.00	3.82	5.17
A	glgC	Glucose-1-phosphate adenylyltransferase	5.24	47.03	P39669	68	1.00	0.97	0.47
B	pyrF	Orotidine 5-phosphate decarboxylase	5.18	25.05	P58638	46	1.00	3.12	1.20
C	pgi	Glucose-6-Phosphate isomerase	5.79	58.71	Q8UI94	67	1.00	3.17	2.10

^a Accession code refers to the SWISS-2DPAGE database

^b Mass tolerance in protein identification through PMF experiment was 10 ppm

3.3.3. Effect of uracil addition on metabolite concentration

The concentrations of the key metabolites were measured by HPLC (Figure 3.7, 3.8). In the cell growth phase, 1.4 mg/ℓ and 0.3 mg/ℓ of UDP-glucose and UTP were detected and prior to uracil addition, 3.3 mg/ℓ and 3.2 mg/ℓ of UDP-glucose and UTP were detected. However, after uracil addition, 4.2 mg/ℓ and 4.5 mg/ℓ of UDP-glucose and UTP was detected. UTP and UDP-glucose might not be necessary for cell growth but is essential for curdlan production: as both a precursor for curdlan and to transfer glucose to the curdlan polymer. Show in 2D gel, we also suggest that uracil addition activates uracil phosphoribosyl transferase, which catalyzes the reaction from Uracil to UMP which was the precursor of UTP. Since the raw material concentration increased, the enzymes related to the metabolic reaction were expressed more than without uracil addition. The level of intermediate metabolites from Uracil to UMP, Glucose-6P to Glucose-1P, UDP-glucose to β -1,3-glucan synthase were increased after the addition of uracil. Moreover, the levels of UTP-glucose-1-phosphate uridylyltransferase was almost not changed with uracil addition

3.3.4. Change of β -1,3-glucan synthase activity

The activity of β -1,3-glucan synthase was detected using a fluorescence assay. The β -1,3-glucan synthase activity changes the rate of β -1,3-glucan synthesis because it is the final reaction enzyme in the synthesis of β -1,3-

glucan [66]. Figure 3.6 shows the changes in the β -1,3-glucan synthase activity, which increased rapidly after the addition of uracil with a concomitant increase in the rate of β -1,3-glucan synthesis. When the cell conditions were changed from cell growth to β -1,3-glucan production at 22 hrs, the β -1,3-glucan synthase activity was increased to prepare β -1,3-glucan synthesis. The β -1,3-glucan synthase activity increased continuously with fermentation without uracil addition, and the level of β -1,3-glucan synthesis was also increased, as shown in Figure 3.1. After the addition of uracil, the β -1,3-glucan synthesis metabolism was activated resulting in an increase in β -1,3-glucan synthase activity.

3.3.5. Change of enzymes expression level

Figure 3.9 shows the pathway changes in β -1,3-glucan synthesis. Two independently prepared fractions were used for multidimensional proteome analysis: from the cells in the growth stage before uracil addition at 22 hrs and from the cells in the curdian production stage after uracil addition at 94 hrs. The replicate gels were scanned, averaged using imaging software, and compared by spot matching and spot densitometry.

The level of the key metabolites of UDP-glucose and β -1,3-glucan were increased. The key metabolic enzymes, such as, uracil phospharibosyltransferase, phosphoglucomutase, and β -1,3-glucan synthase catalytic subunit, were

significantly increased in 2D gel. Although the important key metabolite UTP-glucose-1-phosphate uridylyltransferase only increased 3.5 % after uracil addition. This suggests that UTP-glucose-1-phosphate uridylyltransferase is a target protein in the curdlan producing process. It is expected that the productivity of curdlan will be improved if the level of UTP-glucose-1-phosphate uridylyltransferase can be increased.

And Orotidine 5-phosphate decarboxylase, Glucose-1-phosphate adenylyltransferase and Glucose-6-phosphate isomerase showed a decrease in the 2D gel. In here, Glucose-1-phosphate adenylyltransferase and Glucose-6-phosphate isomerase were catalyzed side reaction of the curdlan synthesis, so their repression can improve the curdlan production.

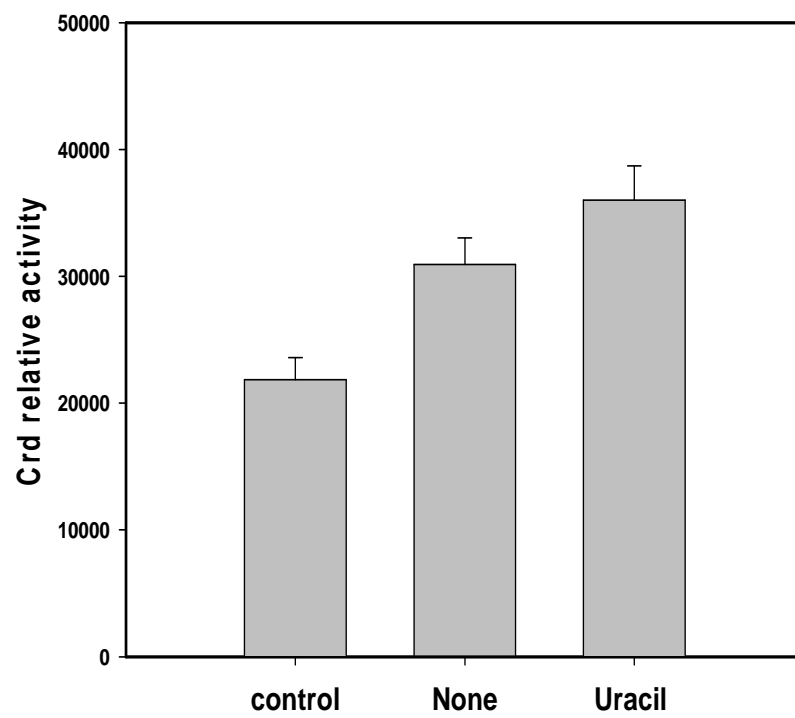


Figure 3.6. Detection of β -1,3-glucan synthase activity with fluorescence assay

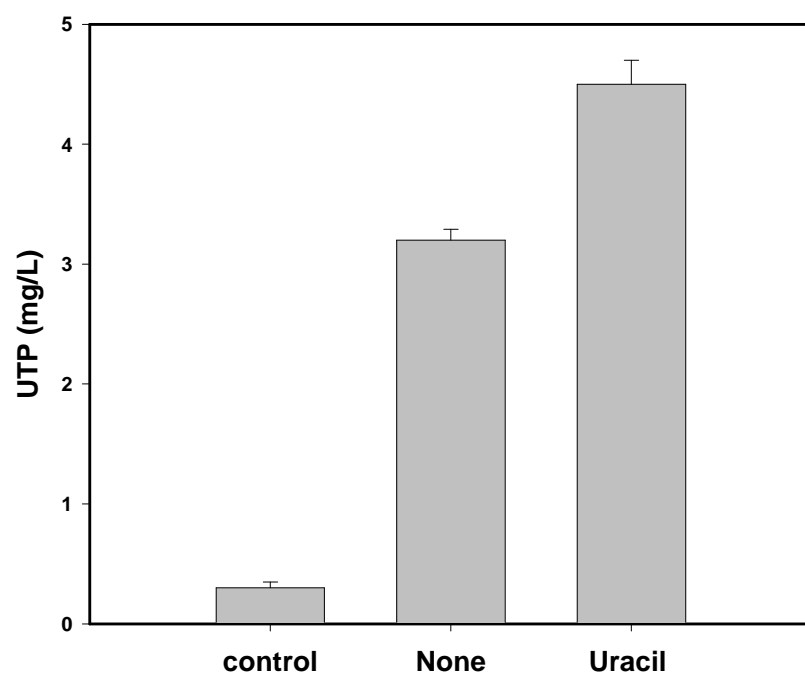


Figure 3.7. Detection of UTP levels from three difference samples

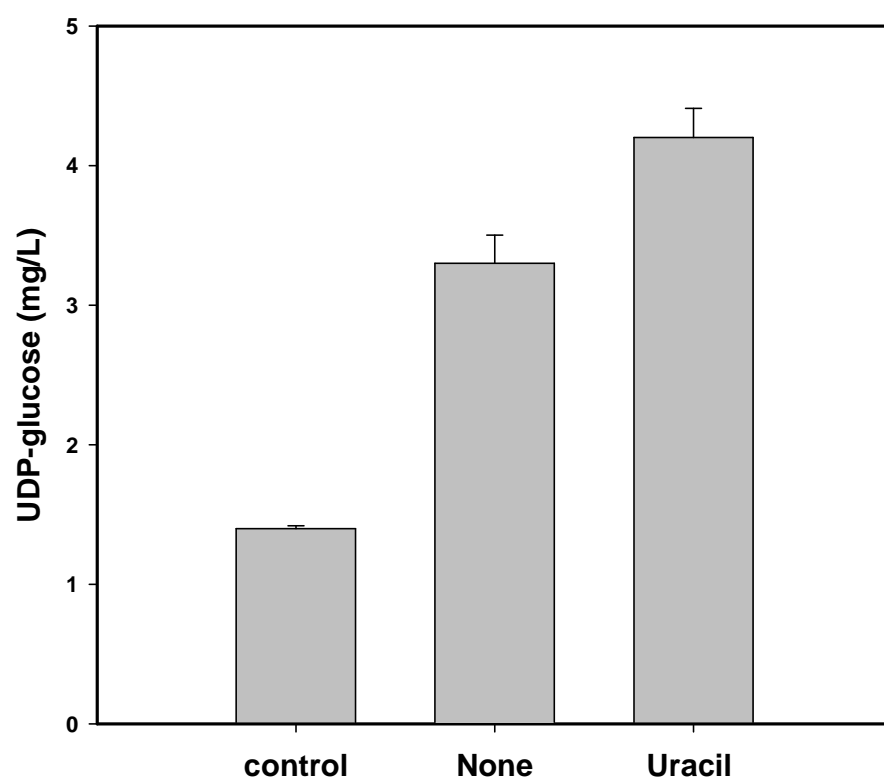


Figure 3.8. Detection of UDP-glucose levels from three difference samples.

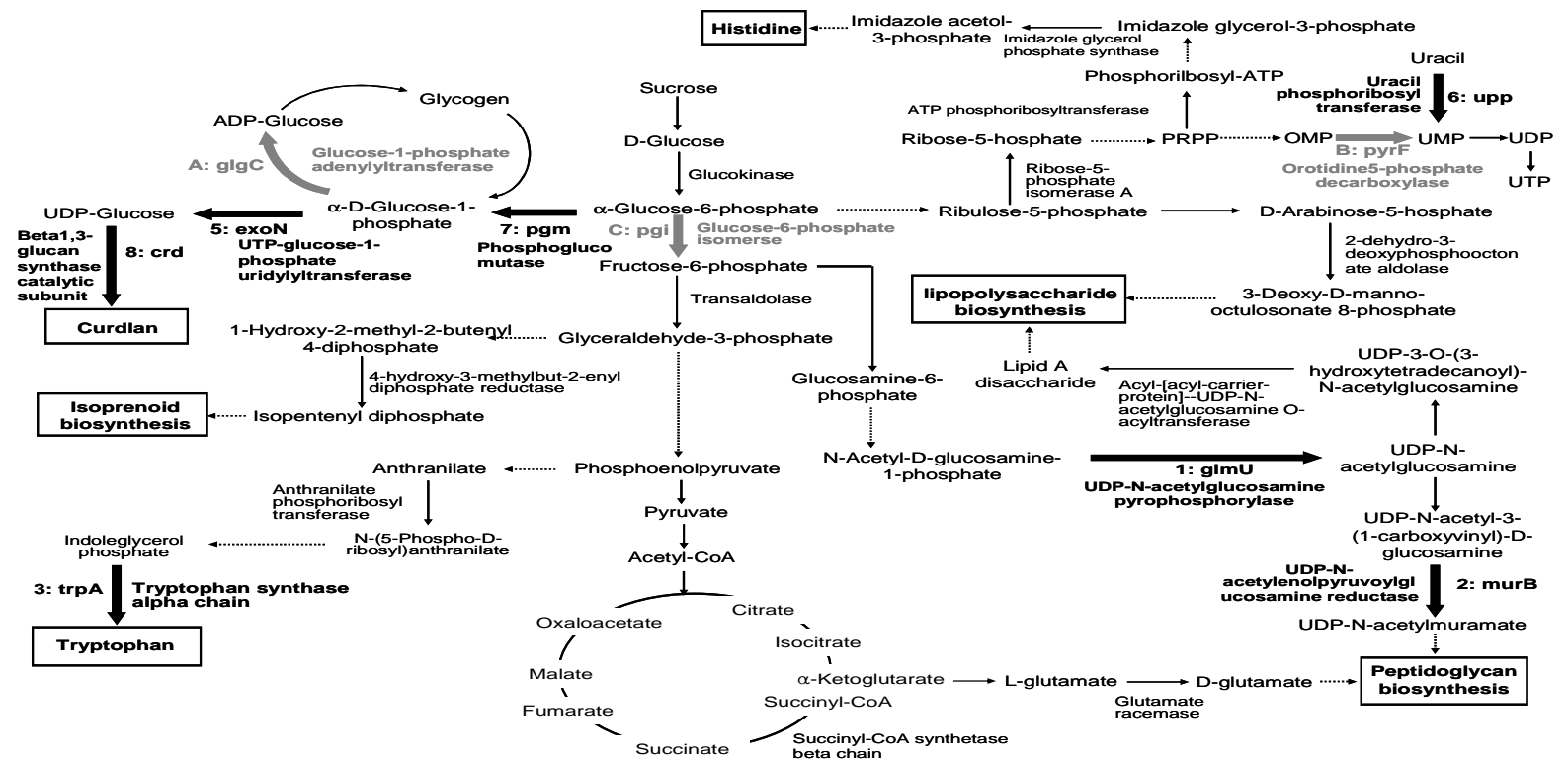


Figure 3.9. Metabolic pathway and changes in the level of enzyme expression during β -1,3-glucan (curdlan) synthesis.

The bold arrows show that the metabolic enzymes were over expressed and the dotted arrow indicate the enzymes under expressed.

The thick black arrow shows that the metabolic conversion was significantly activated after uracil added. In addition, the thick gray

arrow indicates that the metabolic conversion was repressed.

3.4. Conclusion

Systematic approaches for optimizing the production of β -1,3-glucan using metabolic and proteomic measurements were proposed. The intracellular level of enzymes and metabolites were measured at cell growth phase, without adding uracil and with adding uracil as a UDP-glucose precursor, and were used to explain the increase in the β -1,3-glucan synthase rate. After uracil addition, all key metabolic enzymes used for the synthesis of β -1,3-glucan were significantly activated with the exception of UTP-glucose-1-phosphate uridylyltransferase, and the enzymes, such as, Glucose-1-phosphate adenylyltransferase and Glucose-6-phosphate isomerase were catalyzed side reaction of the β -1,3-glucan synthase was repressed.

Chapter 4

The Change in the Proteomic Profiles of Genetically Modified 1,3-Propanediol Producing Recombinant *E. coli*

4.1. Introduction

With the development of sustainable technology, renewable materials produced by agriculture as feedstock for industry and energy, and industrial bio-based processes, will form a vital part in the future biotechnology. Biological resources and biodiversity from nature will have a significant impact by providing bio-based industrial feedstock and products from non-food crops [67–69]. 1,3-Propanediol (PDO) is one of the key bio-based industrial feed stocks. It has a wide variety of applications in polymers, cosmetics, foods, lubricants, and medicines. 1,3-PDO is an important intermediate chemical in the synthesis of polyester. Thousands of tons of polyester are produced every hour worldwide with polyethylene terephthalate (PET) comprising a major fraction of this amount. 1,3-Propanediol (PDO) is a key intermediate in the synthesis of PET.

Copolymerization with terephthalic acid leads to materials ideal for textiles owing to its appropriate mechanical and electrostatic characteristics [70–72].

Metabolic engineering, i.e. the design, modification, and construction of biochemical pathways, is an important technology in the chemical, biochemical, and environmental industries. Recent progress in metabolic engineering has combined with classical fermentation, recombinant DNA technology, and protein engineering [73, 74]. In this study, the conversion of glucose to 1,3-PDO was used as a biocatalytic conversion model system [70, 75–79].

Microbial fermentation for 1,3-PDO production has been studied extensively in species belonging to the family Enterobacteriaceae (*Enterobacter* sp., *Klebsiella* sp. and *Citrobacter* sp.) or the genus *Clostridium* sp. [80–85]. 1,3-PDO production by recombinant *E. coli* has attracted considerable interest with particular focus on the metabolic pathway to make a new metabolic pathway or increase the metabolic flux [76–78, 86]. The fermentation processes used in the production of glycerol and 1,3-PDO have been well studied [70, 87–90]. However, there are no reports of proteomic analysis of the expression level of the relevant enzymes under different fermentation conditions.

In this study, a recombinant *E. coli* was chosen as a model organism for the

production of 1,3-PDO, and the utilization of glucose for the production of 1,3-PDO by *E. coli* was investigated. A change in the protein expression levels related to the two natural metabolic pathways (glucose to glycerol and glycerol to 1,3-PDO) were detected.

4.2. Materials and methods

4.2.1. Recombinant strain

The recombinant strain, *E.coli* $\Delta 6$ mutant (galR, glpK, gldA, IdhA, lacI, tpiA), was used. This strain harbors the plasmids containing the genes for glycerol formation and 1,3-PDO transformation. Recombinant *E. coli* was cultured in a defined minimal media (12.8 g/l Na₂HPO₄·7H₂O, 3 g/l KH₂PO₄, 0.5 g/l NaCl, 1 g/l NH₄Cl, 3 mg/l CaCl₂, and 1 mM MgSO₄) containing a final concentration of 0.3–0.5 % (w/v) glucose, 50 µg/ml ampicillin, 100 µg/ml kanamycin, and 0.1mM CoCl₂ . Seed cultures for batch fermentation were prepared using two 100 ml culture volumes in 500 ml Erlenmeyer flasks at 250 rpm and 37°C. When the cells were in the exponential growth phase, they were transferred to a batch fermentor with 3 l of culture media. When the cell density reached 2.0 (OD₆₀₀), 0.5 mM of IPTG was added to induce the expression of the recombinant protein. After induction, 10 ml of the culture broth was harvested to measure the cell density, glucose, glycerol, acetate and 1,3-PDO.

4.2.2. Protein Preparation

For the analytical gels, 1 ml of the pulse labeled cells was washed twice in 20

mM of a phosphate buffer at pH 7, and then lysed in 200 μ l of a lysis buffer containing 8 M urea, 4 % cholamidopropyl– dimethyl–ammonio–propane sulfonate, 0.8 % ampholytes, pH 3~10 (Pharmalyte, Amersham Pharmacia), 65 mM DTT, and a few grains of bromophenole blue. The incorporated radioactivity of the trichloroacetic acid precipitated proteins was determined using a scintillation counter. For the preparative gels, 250 μ l of a suspension containing the cells was washed in 20 mM phosphate buffer at pH 7, and resuspended in 8 μ l of the breaking buffer (20 mM phosphate buffer, pH 7, 5 % sucrose) containing a protease inhibitor mixture (Complete, Roche Diagnostics, Rotkreuz, Switzerland), 4 mg/ μ l of RNase, and 16 mg/ μ l DNase. The suspension was passed twice through a precooled French pressure cell at 1000 psi and centrifuged at $120000\times g$. The soluble proteins were concentrated and washed twice with H_2O in an Amicon filtration cell using a membrane with a molecular weight cutoff of 10000. Solid urea and concentrated lysis buffer were added to the protein solution to give the same final concentration as that described above.

4.2.3. 2D Gel Electrophoresis

The proteins were separated using 18 cm Immobiline DryStrips, pH 4~7

(Amersham Pharmacia) in the first dimension and on continuous 12 % SDS gels in the second dimension. The analytical and preparative gels were loaded with 10^6 cpm and 2 mg of protein, respectively. The radioactivity was detected by storage phosphor imaging, and the preparative gels were stained with stained with ammoniacal silver. The protein size (10~100 kDa) and isoelectric point range (pH 4~7) of the 2-D gels were determined using 2D gel marker proteins (Bio-Rad).

4.2.4. Data Processing and Analysis

Samples from three independent labeling experiments were resolved on three independent 2-D gels at each time point investigated. The 2-D gel autoradiographs were matched and quantified by image analysis using Image Master software V4.01 (Amersham Bioscience, Uppsala, Sweden). The data was then analyzed with S-PLUS (MathSoft, Cambridge, MA) and Excel (Microsoft) as follows: (i) The spot intensities were converted to parts per million of the total gel intensity and normalized. (ii) The spots were removed from the data set of a given time point if they had been detected in less than one of the three repeats. (iii) All the spots were present on the gels of the non-synchronous

cultures were removed but they could not be detected on any of the gels of the cell cycle time points and *vice versa*. (iv) Spots with the highest intensity < 200 ppm showed high experimental variation and were removed. Finally, the highly reproducible protein spots determined by comparing the ExPASy protein server data were used as the data set for statistical analyses. The dried gel pieces were incubated in a trypsin digestion solution containing 12.5 $\mu\text{g}/\text{ml}$ trypsin 50 mM ABC containing 2 mM CaCl_2 on ice for 45 min. After 1 hour, the unabsorbed solution was removed and the same solution (without trypsin) was added to cover the pieces and the solution was stored overnight at 37 °C. The resulting peptides were extracted by sonication in 50 % acetonitrile/0.1 % TFA, and desalted using C18 Ziptips (Millipore). The peptide solution was prepared using an equal volume of saturated α -cynao-4hydroxy-cinnamic acid solution in 50 % CAN/0.1 % trifluoroacetic acid on a MALDI-TOF-MS sample plate. The peptide mass fingerprints (PMFs) obtained from MALDI-TOF (Voyager DE-STR, PE Biosystem, Framingham, MA, USA) with 150–200 Hz pulsed nitrogen laser at 355 nm. The spectra were calibrated using a matrix and the tryptic auto digestion ion peaks as the internal standards. The peptide mass fingerprints were analyzed using web-based software programs, Mascot (Matrix Science Ltd., UK,

<http://www.matrix-science.com>), PeptIdent (Swiss Institute of Bioinformatics, <http://www.expasy.ch/tools/peptident.html>) and Knexus™ (Proteometrics Inc., <http://www.proteometrics.com>) were used to analyze the MALDI data using the public databases, NCBI nr and SWISS-PROT/TrEMBL.

4.2.5. Analytical Procedure

The glucose concentration was measured using the DNS method. Samples of the fermentation broth were centrifuged ($13000\times g$, 5 min) and 100 $\mu\ell$ of the supernatant was mixed with 900 $\mu\ell$ of a DNS solution. The mixture was heated to 100 °C for 15 min. After cooling, 1 ml of water was added and the absorption at 575 nm was measured using a UV spectrophotometer (Shimadzu, Japan). Glucose was used as the standard.

4.2.6. High Performance Liquid Chromatography Analysis

1,3-PDO, glycerol, and other fermentation byproducts such as lactic acid and acetic acid were analyzed using a Shimadzu HPLC system (Japan) that was fitted with a refractive index detector and a Bio-Rad Aminex HPX-87H organic acids column (Richmond, CA). The column temperature was maintained at 30 °C. A 1.0 mL/min flow rate of 0.01 N sulfuric acid was used as the mobile phase. The

samples were filtered through 0.45 μm Supor membranes (Gelman Sciences, Ann Arbor, MI), and 20 μl was injected into the column.

4.3. Result and discussions

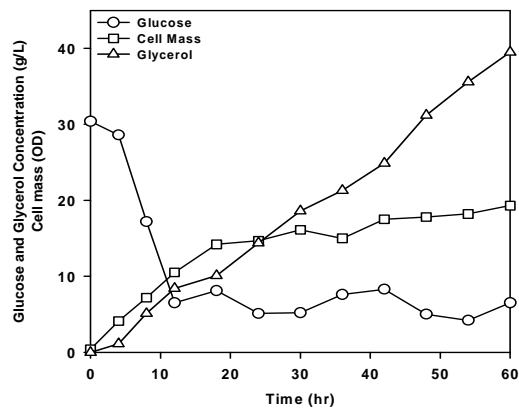
4.3.1. Effect of controlled glucose level on glycerol, 1,3-PDO, and acetic acid

Fed-batch reactors are used widely in industrial applications because they combine the advantages from both batch and continuous processes. The process is first started as a batch process but it is prevented from reaching a steady state using the starting substrate feed when the initial glucose is consumed[91]. A simple fed-batch fermentation process was used to maximize the level of 1,3-PDO production. The glucose level was maintained with the feedback control by measuring the glucose concentration and manipulating the glucose feed rate. A single fed-batch experiment was performed by controlling the glucose concentration between 5–10 g/ℓ and the other fed-batch experiment was carried out by controlling the glucose concentration at a minimum level < 1 g/ℓ i.e. limited glucose concentration.

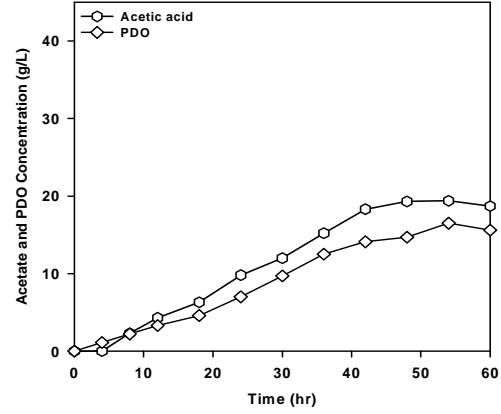
With a high glucose concentration, there was an increase in acetic acid production due to the high glucose metabolic rate. The level of acetic acid production decreased with decreasing glucose concentration. Glycerol also accumulated with high glucose concentrations and the level of 1,3-PDO

production decreased due to glycerol inhibition of the reaction for 1,3-PDO production. A high glucose level enhanced glycerol production and decreased the level of 1,3-PDO production. The glucose concentration affects glycerol production and also alters the level of 1,3-PDO production. The glycerol production rate increased with increasing glucose concentration. The glycerol produced inhibits the production of 1,3-PDO through reactant inhibition.

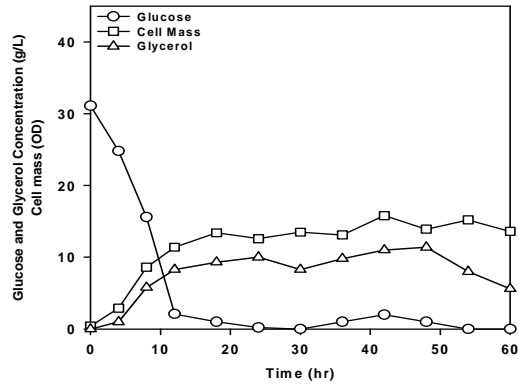
The 1,3-PDO yield from glucose was approximately 30 % when the glucose level was controlled to between 5–10 g/ℓ, and that for low glucose concentration level control was 38 %. The increase in yield due to the low glucose concentration was attributed to a decrease in the formation of byproducts as a result of the limited nutrient source inhibiting 1,3-PDO formation.



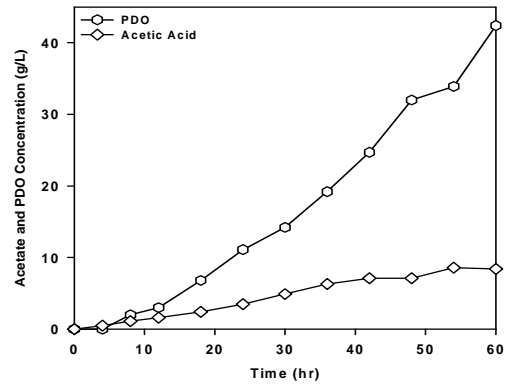
(a)



(b)



(c)



(d)

Figure 4.1. Cell growth and 1,3-PDO production with feedback glucose concentration control between 5–10 g/ℓ.

(a) cell mass, glycerol, and glucose concentrations (b) 1,3-PDO and acetic acid concentrations (c) cell mass, glycerol, and glucose concentrations and (b) 1,3-PDO and acetic acid concentrations when the glucose level was reduced

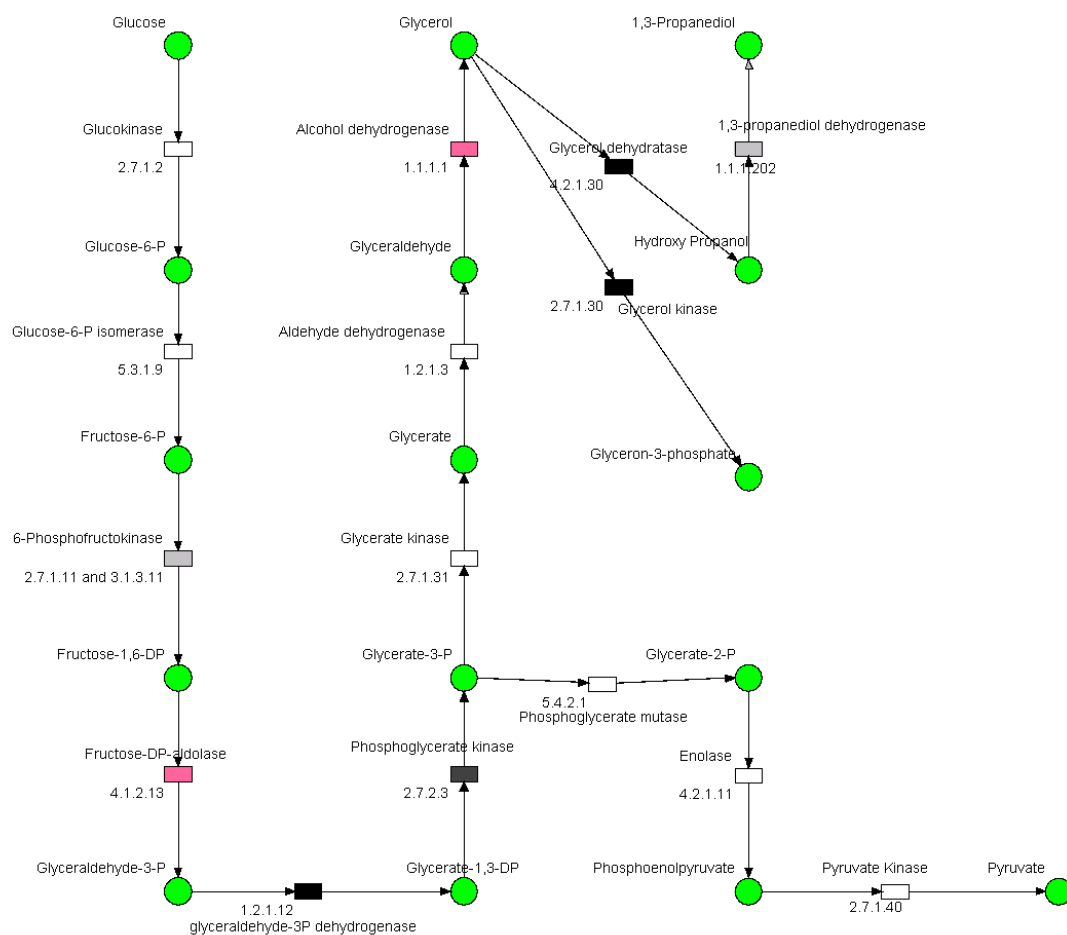


Figure 4.2. 1,3-PDO production metabolic pathway from glucose as a carbon source.

The open rectangle in enzyme notation showed that the enzymes could not be identified in this study. The shade density represents the enzyme expression levels (light shade, 1–2 folds; dark shade, 2–3; black, 3–4; pink, 0–1; blank, unknown).

4.3.2. Analysis of 1,3-PDO synthesis metabolic pathway

Information on gene expression at the protein level provides critical data on the metabolic activity of 1,3-PDO metabolism. Such data is essential for understanding this nonlinear relationship and is necessary for metabolic and cellular engineering efforts. For increased accuracy, sample preparation and the 2D gel electrophoresis was repeated three times, each time starting with an independent colony[92]. The Expert Protein Analysis System (ExPASy at <http://www.expasy.ch/>) was found to be an excellent resource for internet-accessible proteome databases for protein identification. The functions of the proteins identified were assigned by comparing their sequences with those in the public protein database. Table 1 lists the homologue proteins with the highest sequence similarity under the corresponding annotation for each protein identified. Wang et al.[93] reported that two subunits of glycerol dehydratase (EC 4.2.1.30) converted glycerol to hydroxyl glycerol, the beta subunit (MW 24.3 KDa, PI 6.53) and a small subunit (MW 16.8 KDa, PI 6.66). They also showed that the molecular weight and PI of 1,3-propanediol dehydrogenase (EC 1.1.1.202) were 41.5 KDa and 5.91, respectively. From these results, the beta subunit of glycerol dehydratase and 1,3-propanediol dehydrogenase was

identified from the 2-D gel.

Seven of the 11 enzymes associated with the metabolism of 1,3-PDO synthesis from glucose were identified. Glycerol kinase phosphorylate glycerol was also identified in this study. Figure 2 shows the enzyme expression level with the change in cell state from growth to 1,3-PDO production. Five out of 7 enzymes identified in the metabolism of 1,3-PDO synthesis were upregulated, and the level of 1,3-PDO production was increased. The energy metabolism related enzymes from glycerate to pyruvate were not identified. Therefore, it is essential to identify the changes in flux as the process moves from the energy metabolism to the production metabolism. The level of alcohol dehydrogenase expression during 1,3-PDO production decreased to 20 % of that in the cell growth state. This can be interpreted as the alcohol dehydrogenase being strongly inhibited by glycerol formation during fermentation. The open rectangle in the enzyme notation showed that the enzymes could not be identified from this study. The shade density represents the enzyme expression levels (light shade, 1-2 folds; dark shade, 2-3; black, 3-4). The two enzymes, glycerol dehydratase (from *dha B*) and 1,3-propanediol dehydrogenase (from *dha T*), showed a high level expression during 1,3-PDO production.

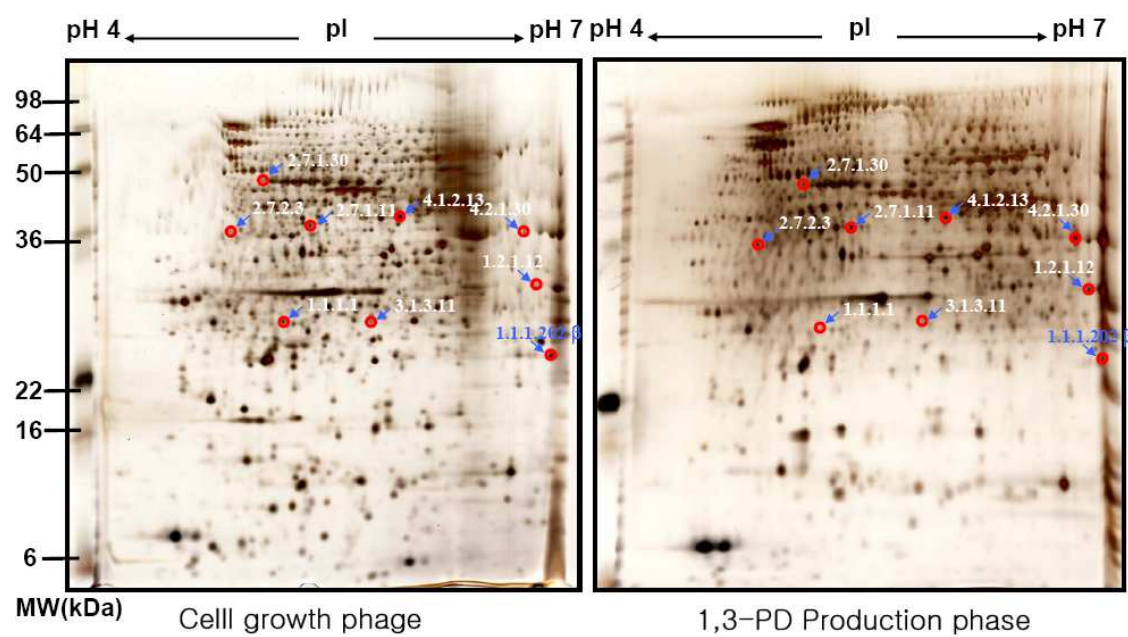


Figure 4.3. Protein images of the mutant *E. coli* $\Delta 6$ producing 1,3-PDO separated by 2D-PAGE and stained with ammoniacal silver.

The pH gradient(horizontal direction) runs from pH 4~7, and the SDS-PAGE separation (vertical direction) was performed in a 12 % gel. The key metabolic enzymes were identified and their expression levels were measured.

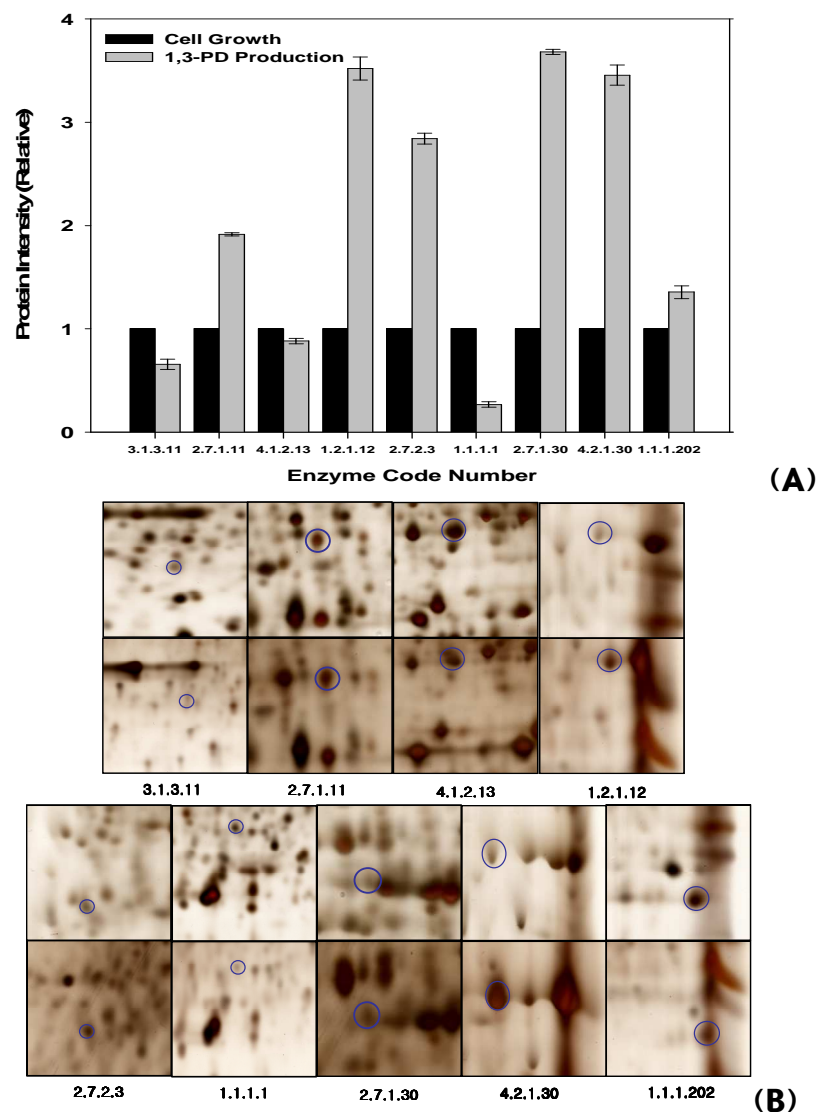


Figure 4.4. The change in enzyme expression level in the cell growth phase and 1,3-PDO production phase.

(A) The shade bar represents the enzyme expression level for the cell growth phase and the hatched bar represents the enzyme expression level for the 1,3-PDO production phase. (B) Enlarged protein spots. The enzymes code numbers and their names are listed in Table 4.1.

Table 4. 1. The identification of the proteins from the *E.coli* $\Delta 6$ mutant

Cross-species identification using public protein databases with identification using the specific protein database for the identification of the proteins from the *E.coli* $\Delta 6$ mutant.

Code	Proteins	PI	MW(Da)	Sequence coverage (%)	Mascot Score
3.1.3.11	fructose-bisphosphatase	5.68	32,568	32	113
2.7.1.11	6-Phosphofructokinase	5.45	38,156	38	198
4.1.2.13	Fructose-P2-aldolase	5.55	40,651	40	98
1.2.1.12	glyceraldehyde-3P dehydrogenase	6.28	36,748	24	142
2.7.2.3	phosphoglycerate kinase	5.07	41,960	31	103
1.1.1.1	alcohol dehydrogenase	5.17	25,083	48	86
2.7.1.30	glycerol kinase	5.3	25,083	43	174
4.2.1.30	glycerol dehydratase β	6.53	50,642	28	101
	glycerol dehydratase small unit	6.66	24,300	36	71
1.1.1.202	1,3-propanediol dehydrogenase	5.91	16,800	58	63

4.4. Conclusion

Proteomic studies integrating the protein expression level and metabolism have the greatest potential to accelerate metabolite production research. The cellular biological technique and approach together can become extremely powerful tools providing greater information for the production of various metabolites.

This is the first report showing the changes in the proteomic profiles in 1,3-PDO producing recombinant *E. coli* using 2-D gel electrophoresis. Seven out of 11 enzymes in the 1,3-PDO production metabolism were identified and their changes in expression from cell growth to 1,3-PDO production were studied and presented. The major enzymes except for alcohol dehydrogenase were over expressed to enhance 1,3-PDO production.

Glycerol, an intermediate compound for 1,3-PDO production, was produced rapidly when the glucose concentration was $> 5 \text{ g/}\ell$ and inhibited the production of 1,3-PDO. As a result, 1,3-PDO accumulation was went up to $35 \text{ g/}\ell$. The level of 1,3-PDO production increased when the glucose concentration was $< 1 \text{ g/}\ell$, which prevented the overproduction of glycerol. $43 \text{ g/}\ell$ of 1,3-PDO was produced after 60 hrs fed-batch fermentation.

Chapter 5

Conclusion

2-DE is very useful for understanding the quantitative proteomic responses of curdlan-producing *Agrobacterium* sp. ATCC 31750 to a pH downshift during well-controlled batch fermentation by analyzing the time-course variations in the protein level in detail. Comparative proteome analyses of the control culture (pH 7.0) and low pH culture (pH 5.5) showed that curdlan overproduction was accompanied by significant changes in the synthesis of the key metabolic enzymes involved in curdlan biosynthesis and the nucleotide biosynthesis pathway. These results strongly suggest that altered metabolic conversion leading to the accumulation of UTP and UDP-glucose, as well as inhibition of the lipopolysaccharide and peptidoglycan biosynthesis pathways and key precursors play important roles in the production of large amounts of curdlan. For further metabolic engineering of the strain for industrial applications, more complete information on the overall regulation characteristics of curdlan overproduction will be needed through a detailed analysis of the transcriptomic responses at the gene expression level.

Systematic approaches for optimizing the production of β -1,3-glucan using metabolic and proteomic measurements were proposed. The intracellular level of enzymes and metabolites were measured at the cell growth phase with and

without adding uracil as a UDP-glucose precursor, and were used to explain the increased rate of β -1,3-glucan synthase production. After uracil addition, all key metabolic enzymes used for the synthesis of β -1,3-glucan were significantly activated with the exception of UTP-glucose-1-phosphate uridylyltransferase. Enzymes, such as glucose-1-phosphate adenylyltransferase and glucose-6-phosphate isomerase, which were catalyzed as side reactions of the β -1,3-glucan synthase, was repressed.

Proteomic studies integrating the protein expression level and metabolism have the greatest potential to accelerate research in metabolite production. The cellular biological technique and approach can become an extremely powerful tool for providing greater information on the production of many metabolites.

This is the first report showing the changes in the proteomic profiles in 1,3-PDO producing recombinant *E. coli* using 2-D gel electrophoresis. Seven out of 11 enzymes in the 1,3-PDO production metabolism were identified and their changes in expression from cell growth to 1,3-PDO production were examined. The major enzymes except for alcohol dehydrogenase were over expressed to enhance 1,3-PDO production.

Glycerol, an intermediate compound for 1,3-PDO production, was produced rapidly when the glucose concentration was $> 5 \text{ g/l}$ and inhibited 1,3-PDO production. As a result, the level of 1,3-PDO accumulation increased to 35 g/l . In addition, the level of 1,3-PDO production increased when the glucose

concentration was $< 1 \text{ g/}\ell$, which prevented the overproduction of glycerol. $43 \text{ g/}\ell$ of 1,3-PDO was produced after 60 hrs of fed-batch fermentation.

Chapter 6

The other studies during the course work:

Enzyme immobilization and it' s used in chemical transformation

6.1 Introduction

Immobilization of proteins and enzymes on a solid support is certainly among the most important problems in modern biotechnology [94–97]. Such a support must immobilize the enzymes in an efficient way, thereby preventing the leaching out of the precious biomolecules during reaction and workup [98, 99]. On the other hand, the immobilization must not impede the biological activity and the binding must be done by an approach that does not disturb the secondary or tertiary structure of the proteins [99–103]. A further point to be considered is the possible resistance of the carrier to the transport of educts and products to the immobilized enzyme [104, 105]. In the worst case, the enzyme may be buried in the carrier so that it cannot be accessed by the reagents. This will render the quantitative analysis of the activity of the bound enzyme a difficult task. Hence, the number of studies in which the reaction rate has been analyzed

quantitatively in terms of classical Michaelis–Menten kinetics is relatively small when compared with the entire number of articles devoted to the immobilization of enzymes.

The solid support for enzyme immobilization was most important in immobilized enzyme properties. Enzymes have been immobilized on a variety of support materials, such as Sephadex, alginate, k-carrageenan, chitosan, porous glass, agarose, polyvinyl alcohol polymer, DEAE–cellulose, Eupergit C (epoxy activated acrylic beads), nylon, polyurethane foams, or zeolite[106]. The immobilized enzymes have been used in both batch and continuous reactors [107–112]. Enzymes have a high sensitivity to a number of denaturing agents, are unstable in room temperature and too expensive for large-scale process. However, these limitations can be overcome using immobilized enzymes. The immobilized enzyme is more stable than the free enzyme at room temperature, can recycle, and has activity in several denaturing agents.

This study, we developed many different solid materials for enzyme immobilization. For instance, polyaniline nanofiber(PANI), magnetically separable polyaniline nanofiber(PAMP), magnetically separable CM cellulose(CMC), magnetically separable DEAE cellulose(DEAE), etc. These materials used in various kinds of enzyme immobilization, some immobilized enzymes can be used for chemical transformation, some can be used for biosensors. I showed the characters of each enzyme immobilized on the above materials. Finally, there

showed the immobilization methods with difference cross linkers. For example, glutaraldehyde (GA), 1-Ethyl-3-[3-dimethylaminopropyl] carbodiimide hydrochloride (EDC), etc.

6.2 Materials and Methods

6.2.1 Materials

Lactase (E.C.3.2.1.23) from *Agaricus visporus* biochemika powder and Laccase (E.C.1.10.3.2) from *Agaricus bisporus* were purchased from Fluka AG (Switzerland). Alcohol dehydrogenase from *Saccharomyces cerevisiae* and urease from Jack bean were purchased from Sigma (St. Louis, MO). Catalase (Sigma C1345), iron oxide nanopowder, hydrogen peroxide, glutaraldehyde (GA) and aniline were purchased from Sigma (St. Louis, MO). O-nitrophenyl β -D-galactopyranoside (ONGP), bovine serum albumin standard (BSA), polyaniline, magnetic DEAE-Cellulose, and lactose were obtained from Sigma-Aldrich (St. Louis, USA) and used without further purification. All chemicals used were of analytical grade, and all solvents were of the highest quality commercially available.

6.2.2 Methods

6.2.2.1. Preparation and characterization of the supporting magnetized nanomaterials

1. PANI and PAMP

Polyaniline nanomaterials (PANI) were produced by rapidly mixing 0.1 %

(weight fraction) of the initiator (ammonium peroxydisulfate) with 5 ml of the aniline monomer solutions (with different weight fractions) in 1 M HCl. Magnetically separable nanomaterials (PAMP) were produced using the above protocols in the presence of 0.05 g of an iron oxide nanopowder (Sigma). Once the initiator molecules had been depleted during nanomaterial formation, there was no further polymerization that could lead to overgrowth. The samples were washed 4 times with distilled water to remove the HCl remaining and were stored in a refrigerator prior to use.

The nitrogen adsorption-desorption measurements were carried out at 77K using a Belsorp II (BEL Japan Inc.) to determine the Brunauer–Emmett–Teller (BET) surface area and Barrett–Joyner–Halenda (BJH) pore size distribution. All samples were freeze dried and pretreated at 300 °C for 12h before the measurements.

2. CMC and DEAE

For a typical preparation, nanoferrite (100 mg) was introduced with 10 ml of swelled CMC and DEAE. This mixture was agitated vigorously for 2 h at 500 rpm. The mixture was washed with distilled water to remove ferrite nanoparticles that were located outside of the bead. The supernatant was decanted and the sediment was washed with distilled water several times until further free ferrite was observed. Finally, sediments were washed twice with 100 mM phosphate

buffer and dried for future use

6.2.2.2. Enzyme immobilization process

1. Glutaraldehyde (GA) as a crosslinker

The solid materials (2 mg) were incubated in 1 mL of a 20 mM phosphate buffer containing 10 mg of each enzymes. The vials were shaken at 200 rpm at room temperature for 30 min, a GA solution was added to a final GA concentration of 0.5 % w/v, and the mixture was placed on a rocker (30 rpm) at 25 °C for 2 h. The enzyme aggregate-coated nanomaterials were transferred to a new glass vial and washed with 20 mM phosphate buffer and 100 mM Tris-HCl (pH 7.9). The unreacted aldehyde groups were capped by incubating the nanomaterials in a Tris-HCl buffer for 30 min. After capping, the nanomaterials were washed excessively with the 20 mM phosphate buffer until no enzyme was released into the washing solution. The enzyme aggregate-coated nanomaterials were then stored in 20 mM phosphate buffer at 4 °C for further use. A control sample was also prepared as a comparison with the enzyme aggregate-coated nanomaterials.

2. 1-Ethyl-3-[3-dimethylaminopropyl] carbodiimide hydrochloride (EDC) as a crosslinker

The solid materials (2 mg) were incubated in 1 mL of a 100 mM MES buffer

containing 10 mg of each enzymes. The vials were shaken at 200 rpm at room temperature for 30 min, a 2 mg/mL EDC solution was added to a final EDC concentration of 0.5 mg/mL, and the mixture was placed on a rocker (30 rpm) at 25 °C for 2 h. The enzyme aggregate-coated nanomaterials were transferred to a new glass vial and washed with 20 mM phosphate buffer (pH 7.0). The nanomaterials were washed excessively with the 20 mM phosphate buffer until no enzyme was released into the washing solution. The enzyme aggregate-coated nanomaterials were then stored in 20 mM phosphate buffer at 4 °C for further use.

6.2.2.3. Scanning electron microscopy (SEM)

SEM images were obtained using a Hitachi S-4800 scanning electron microscope (Hitachi, Tokyo, Japan). Images of the PANI and PAMP were obtained and digitized under the following conditions: files, 1280 × 960 pixel; voltage, 15 kV; probe size, 20 nm; and magnification, 10000×

6.2.2.4. Activity measurement

1. Lactase

The activity of the free and immobilized-lactase were determined at 37 °C

using chromogen ONPG as the substrate. The reaction mixture contained 20 mM phosphate buffer (pH 6.5), and 1.6 mM ONPG. After adding the free and immobilized-lactase, a 50 μl sample was taken every minute and diluted 20 fold. The absorbance was detected at 410 nm with a spectrophotometer. One unit of enzyme activity (EU) was defined as the amount of enzyme hydrolyzing one μmole of the substrate per minute under the above defined conditions.

2. Laccase

The activities of the free and immobilized-laccase were determined at room temperature using 2 mM syringaldazine as substrate. Reaction mixture contained 50 mM citrate-phosphate buffer (pH 5.0), 2 mM syringaldazine. After addition 10 μl of free and immobilized-laccase, the reaction was started. At every minute, the absorbance was detected at 525 nm with UV spectrophotometer.

3. Lysing enzyme

The activity of PAMP-lysing enzyme was determined the hydrolyzed sugars from cellulose or curdlan etc. The reduced sugars detected by HPLC shodex SH1011 sugar series columns (Showa DenKo, Japan).

4. Alcohol dehydrogenase (ADH)

The activity of ADH and immobilized ADH were determined the NADH concentration at 340 nm with UV spectrophotometer. The reaction mixture contained 100 μl of 20 mM NAD, 100 μl of 100 mM alcohol solution and 790 μl of 20 mM sodium phosphate buffer (pH 8.5). The reaction was started after adding

10 $\mu\ell$ of 1 mg/ml ADH.

6.2.2.5. Application of the immobilized enzymes

1. Laccase was used in pectin gelation

Ferulic acid convert to its radical form was catalyzed by PAMP-laccase
PAMA-laccase can convert ferulic acid to radical form at room temperature.
The 1 ml volume of the reaction mixture only contains 100mM ferulic acid and 1 mg PAMP-laccase. The reaction time was 1, 5, and 10 min respectively.
Ferulic acid radical form was obtained to remove PAMP-laccase by magnetic.
The radical formed ferulic acid was added to 10 g/l pectin solution. At that instant, pectin solution converts to the gel.

2. Lactase was used in lactose analysis and recycle

Free and immobilized lactase can convert lactose to glucose and galactose.
There the reaction mixture contains 2 mg/ml immobilized-lactase and 5 mM lactose solved in 50 mM sodium phosphate buffer (pH 6.5).
The immobilized lactase can recover simply magnet and can reuse several times.

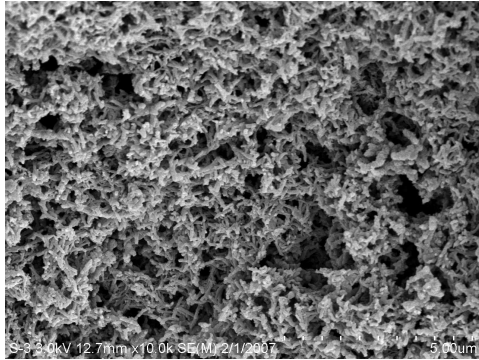
3. Immobilized lysing enzyme can hydrolyze the various carbohydrates

10mg of immobilized lysing enzyme can hydrolyze the various carbohydrates such as curdlan, agarose, cellulose, cellulose fiber, seaweed. In this time, the immobilized lysing enzyme can reuse several times.

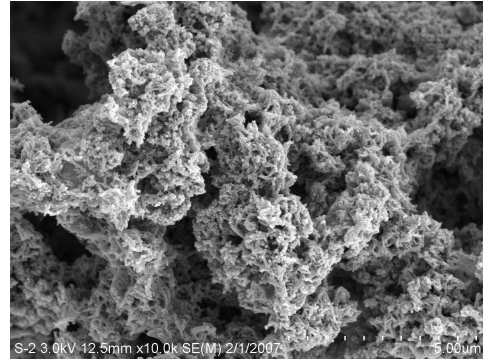
6.3 Results and Discussion

6.3.1 SEM images of PANI and PAMP

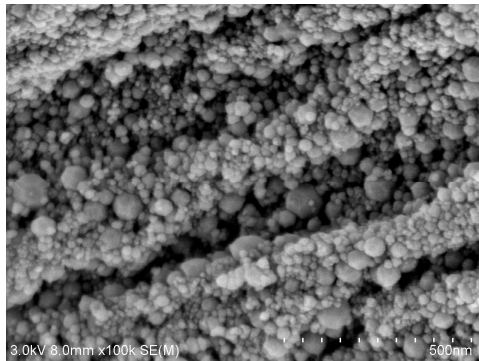
Pure polyaniline nanofibres were developed by the rapid mixing of an aniline solution in 1 N HCl mixed with ammonium peroxydisulphate (Figure 6.1(a)). The nanofibers were interconnected and the porosity was found to depend on the aniline concentration. The formation of nanopores by nanofiber cross-linking is observed when the rapid polymerization of polyaniline occurs with vigorous mixing. Figure 6.1(b) shows the polyaniline nanomaterials mixed with iron oxide nanoparticles. SEM revealed significant differences in morphology. Enzyme coated diethylaminoethyl cellulose (DEAE) and carboxymethyl cellulose (CMC) fibers were observed in SEM analysis (Figure 6.1(c,d)).



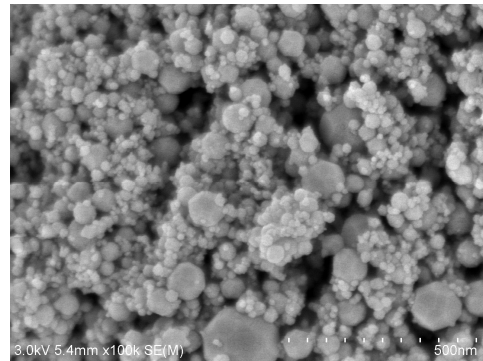
(a) PANI



(b) PAMP



(c) DEAE



(d) CMC

Figure 6.1. SEM images of the four nanomaterials.

Manufactured (b) with and (a) without the iron oxide nanoparticles and (c) DEAE-immobilized enzymes, (d) CMC-immobilized enzymes. The images are taken at a $10000\times$ magnification and the scale bar represents $5\text{ }\mu\text{m}$.

6.3.2 Properties of nanomaterials

6.3.2.1. BET and BJH of the PANI and PAMP

BET is used to determine the surface area, pore size and pore size distribution, and void structure of solid materials. The surface area of the developed nanomaterials is an important factor in determining the immobilization efficiency as a carrier. The porous structure and pore size distribution is an important factor in enzyme immobilization. These parameters control the catalytic activity of immobilized enzymes by controlling the mass transfer phenomena.

Table 6.1 summarizes the fundamental BET of the nanomaterials with the addition of iron oxide. The BET surface area for PANI and PAMP was 58.37 m²/g and 46.36 m²/g, respectively, and the average pore diameter was 12.26 nm and 20.33 nm, respectively. The pore size increased after the addition of iron oxide nanoparticles while the BET surface area decreased.

The BJH graph (Figure 6.2(b)) provided important information on the surface and pore volume of nanomaterials. The pore size calculated from desorption profiles using the BJH (Barrett–Joyner–Halenda) method was 20 nm (Figure 6.2).

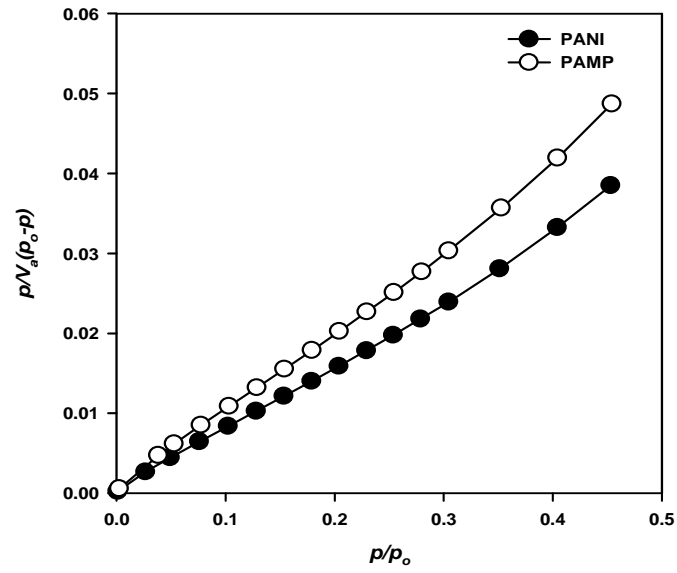
Figure 6.3 shows the nitrogen adsorption–desorption isotherms of PANI and PAMP. No substantial hysteresis was observed in the two samples. This suggests that nitrogen can be recovered fully during desorption. At a relative pressure (P/P_0) between 0.9 and 0.99, the sample adsorbed and desorbed a

significant amount of gas. This was attributed to the nitrogen molecules that were either adsorbing or desorbing from the surface layers, resulting in a small difference in surface tension between adsorption and desorption

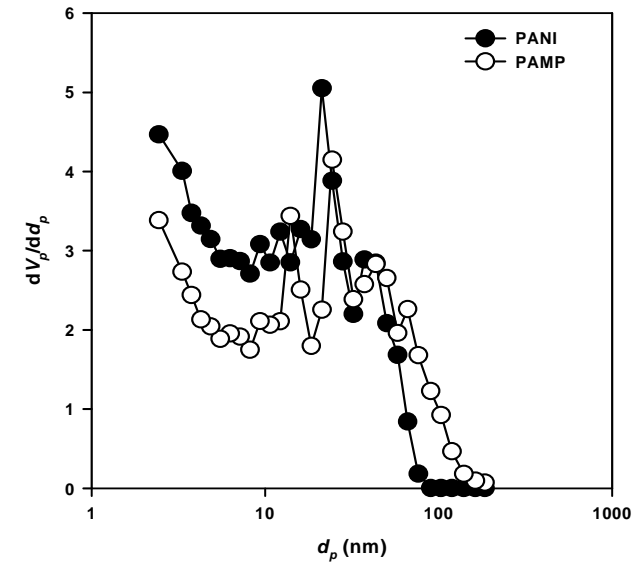
Table 6. 1. Properties of PANI and PAMP

BET surface area, BJH pore volume, and average pore diameter of the PANI and PAMP nanomaterials.

	PANI	PAMP	Unit
$a_{s,BET}$	58.374	46.364	$[m^2\ g^{-1}]$
Total pore volume ($p/p_0=0.990$)	0.1789	0.2357	$[cm^3\ g^{-1}]$
Average pore diameter	12.257	20.331	[nm]



(a) BET changes with the change of nanomaterials



(b) BJH changes with the change of nanomaterials

Figure 6.2. Changes in the BET and BJH of the two nanomaterials.
Porous repartitions obtained from the adsorption and desorption curves.

6.3.2.2. Long term stability and characterization

In this page, I show the long term stability and enzyme characterization about the lactase immobilized on the solids materials. In this reaction, ONPG was used as a substrate to measure the initial enzyme reaction rate. The maximum reaction rate (V_{max}) and Michaelis–Menten constant (K_m) for the free and immobilized lactase was estimated from statistical analysis of the experimental data. The catalytic activity (k_{cat}) represents the maximum enzyme reaction rate for the same amount of free and immobilized enzyme. Table 6.2 shows the estimated kinetic parameters of the free and immobilized lactases. The K_m value of PAMP–lactase was 2.34 times lower than that of the free enzyme (see Table 6.2) but that of PANI–lactase was 4.39 higher. The decrease in K_m in PAMP–lactase might be due to structure changes in the enzyme after immobilization. The substrate can easily access the active sites after immobilization. The k_{cat} values for free, PANI, PAMP, magnetic CMC and DEAE–Cellulose were 4.02, 2.05, 0.59, 0.038, 0.042 mM/min mg protein, respectively.

The free and the immobilized lactase were incubated at room temperature under rigorous stirring conditions at 200 rpm. Many studies have reported that immobilized lactase has excellent stability at 4 °C [113]. Table 6.3 gives a summary of the experimental results. The immobilized lactases onto PANI and PAMP showed almost 100 % residual activity under room temperature and vigorous shaking conditions.

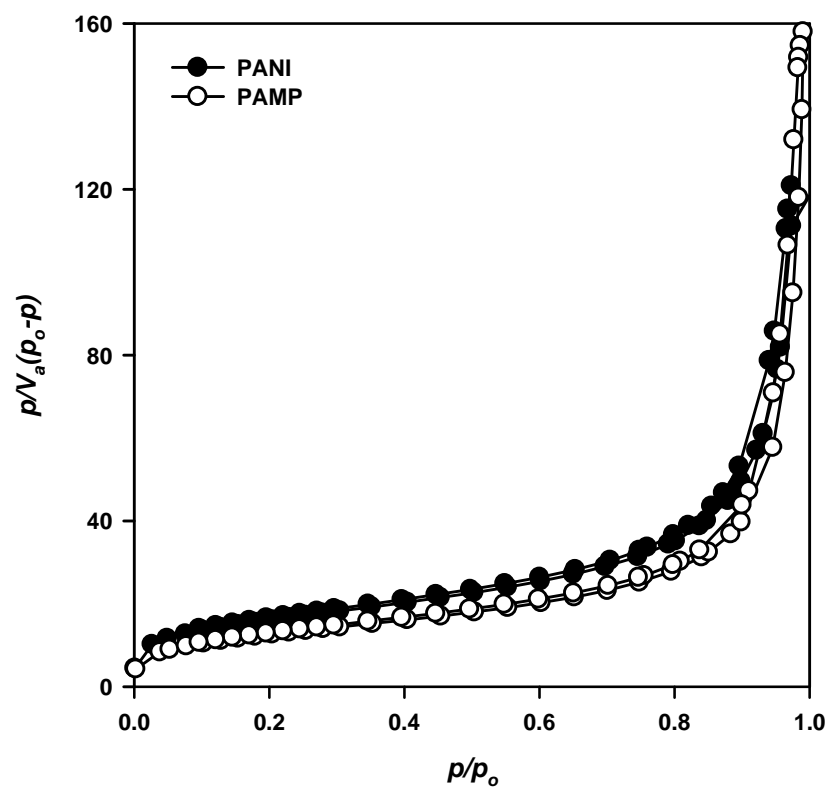


Figure 6.3. Adsorption and desorption isotherms of PANI and PAMP

Table 6. 2. Catalytic activity of free lactase and immobilized lactases with various supporting nanofibers

Polymer nanofiber	Amount of lactase used (mg/ml)	K_m (mM)	V_{max} (mmol/min)	k_{cat} (mmol/min mg protein)
Free	0.5	2.7	2.01	4.02
PANI	1	4.39	2.05	2.05
PAMP	1	2.34	0.59	0.59
CMC	10	7.21	0.38	0.038
DEAE	10	6.53	0.42	0.042

Table 6. 3. Stability of immobilized lactase using various supporting materials.

Support materials	Retention activities (%)	Storage condition	Storage period (month)	Reference
crosslinked concanavalin A–beta–galactosidase complex	93	4°C	2	[113]
Magnetic poly (GMA–MMA) Beads	94	4°C, dry sample	2	[107]
	59	4°C , wet sample	2	
CPC–silica and agarose	100	4°C	2	[114]
Langmuir–Blodgett films of poly (3–hexyl thiophene) stearic acid)	80~82	4°C	3	[115]
Graphite surface	86	4°C	1	[116]
Cellulose–gelatine carrier system	80	4°C	1	[117]
Fiber composed of alginate and gelatin	56	4°C	1	[118]
Magnetic CMC	17.6	25°C	2	In this study
Magnetic DEAE	19.8	25°C	2	In this study
PANI	100	25°C	3	In this study
PAMP	100	25°C	3	In this study

6.3.3 Application of the immobilized enzymes.

6.3.3.1 Pectin gellation with immobilized laccase

Laccase can convert ferulic acid to radical forms (Figure 6.4), PAMP-laccase can do this conversion really well, Figure 6.5 shows the pectin gellation with radical form's ferulic acid which converted by PAMP-laccase. When the conversion time was 1min, a few of the pectin was polymerized and conversion time was 10min, the pectin was completely changed to gel type. Laccase was not permitted to the food industry, but in this case the immobilized laccase can be removed clearly by the magnets.

6.3.3.2. Immobilized lactase hydrolyze the lactose and can recycle.

The reaction volume was 1ml in 5 ml vial at 37 °C. The PANI, PAMP and DEAE-lactase show high percentages of lactose conversion (46 %, 45 % and 24 %) after 1hr in batch reactor (Figure 6.6).

Immobilized lactase was recycled 10 folds for the lactose hydrosis. After 30 min hydrosis, the produced glucose was detected by glucose oxidase-peroxidase method (Figure 6.7). After recycled 10 folds, the produced glucose decreased only 3~14 % and PANI, PAMP and DEAE lactase shows 86 %, 96 % and 97 % production abilities.

6.3.3.3. Immobilized lysing enzyme produce the glucose from carbohydrates.

Lysing enzyme was the enzyme mixture, it contains β -glucanase, cellulase, protease, and chitinase. In this study, we immobilized the lysing enzyme on the PAMP. Show in Figure 6.7, this is the degradation of polysaccharide such as Agarose(a), cellulose fiber(b), sea weed(c), and curdlan(d), with magnetically separable immobilized lysing enzyme. The degradation rate was showed in Figure 6.8. Immobilized lysing enzyme shows different reaction rate in different substrates. When it was reaction in the curdlan solution, the reaction rate was 2 or 3 times quickly than it's in other substrates. That time, the reaction rate was approximately 1 g/ ℓ /h.

Show in Figure 6.9, Immobilized lysing enzyme also can recover simply with magnets. The picture shows when the immobilized lysing enzyme suspended in the buffer solution (Figure 6.9(b)) and when the magnets come, all of the particles could recover and the solution immediately changed clearly (Figure 6.9(c)). Because of this process, all of the immobilized enzymes can re use and the remained activity was more than 70 % when it's reused 10 times.

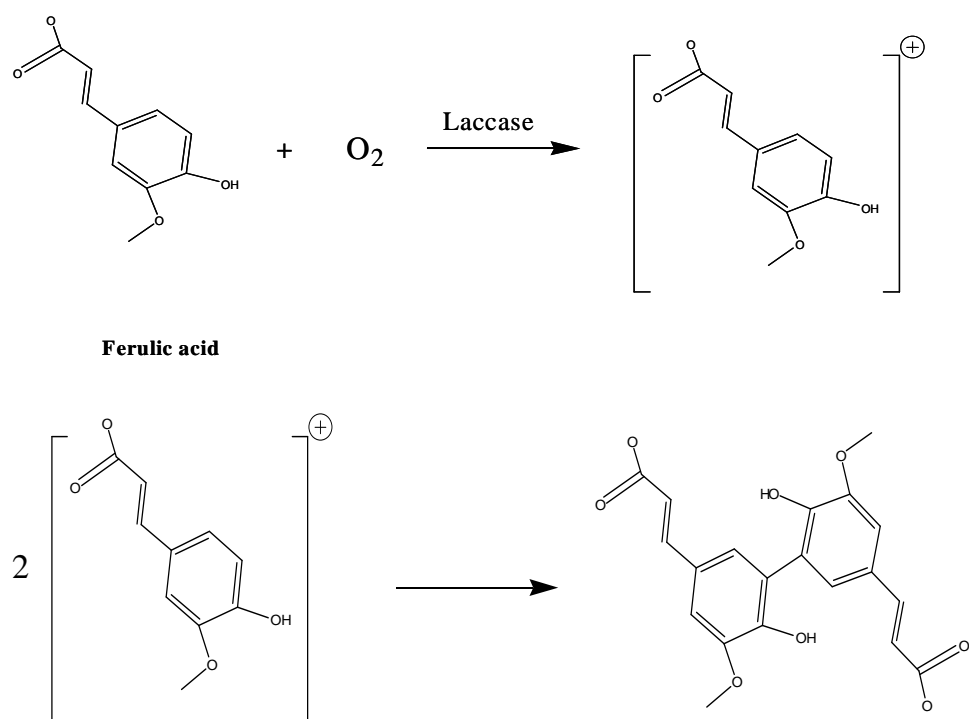


Figure 6.4. Ferulic acid was converted to radical form by laccase.

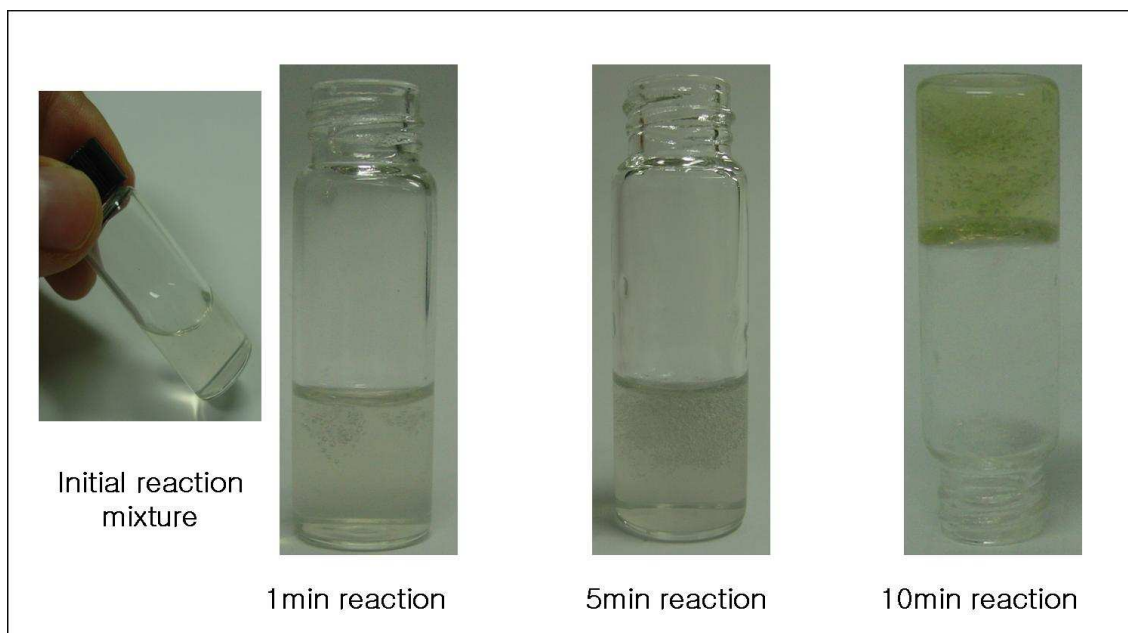


Figure 6.5. Pectin was gelled by radical formed ferulic acid.

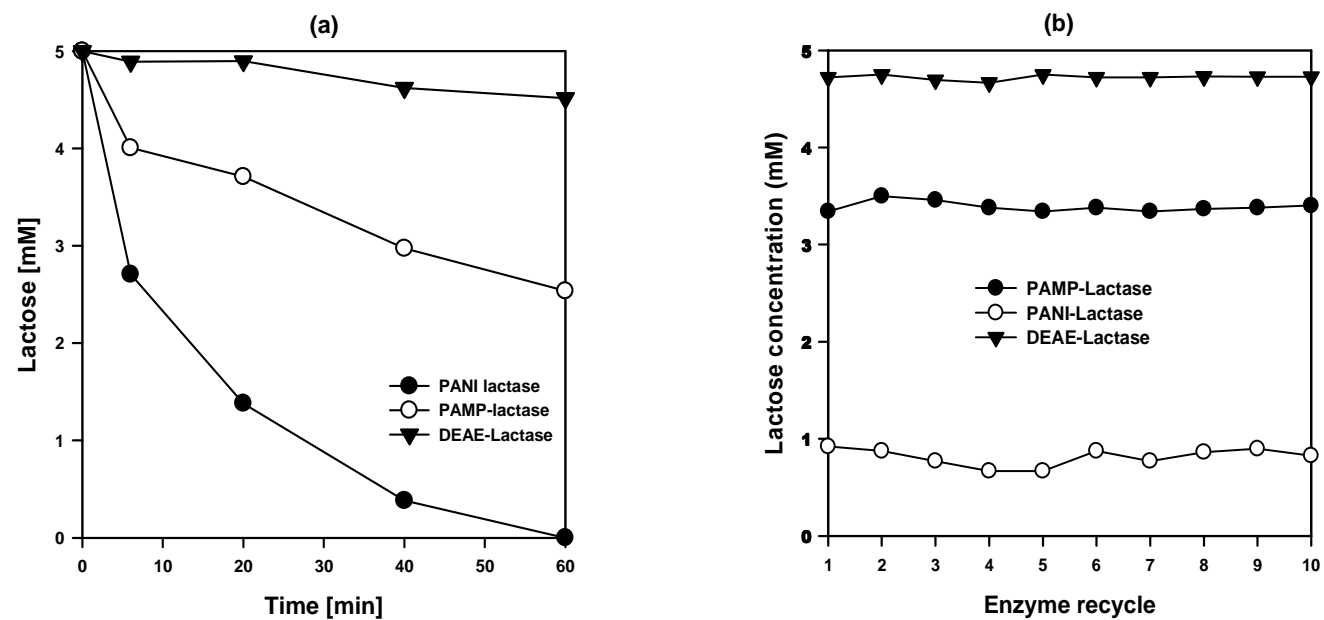
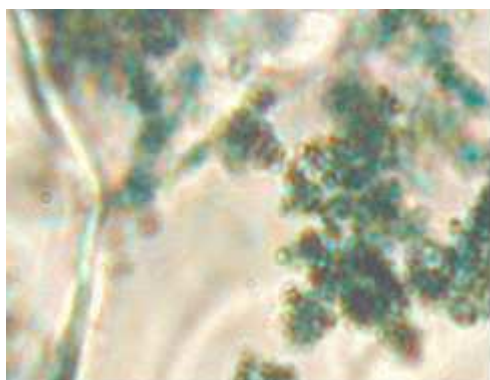
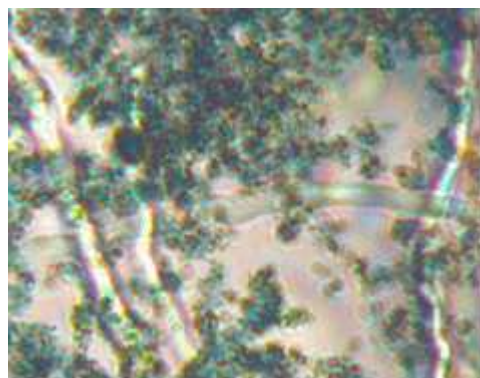


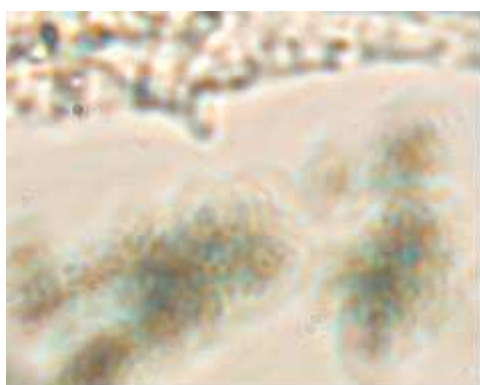
Figure 6.6. Batch lactose hydrolysis using recycled immobilized lactase.
 (a) Lactose degradation with the immobilized lactase and lactose concentration (b) after immobilized lactase recycle. The lactose concentration was measured after 30 min reaction. After 10 recycling steps, lactase residual activity was 98%, 96% and 97%.



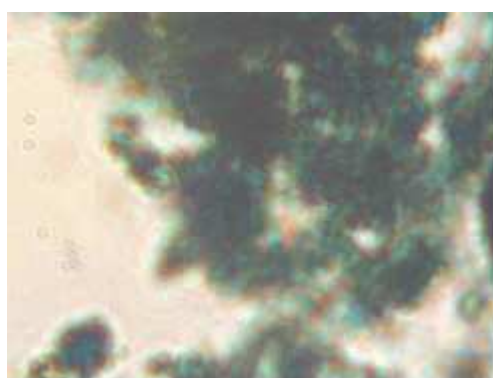
(a)



(b)



(c)



(d)

Figure 6.7. Degradation of polysaccharide with magnetically separable immobilized lysing enzyme.

(a) Agarose, (b) cellulose fiber, (c) sea weed, and (d) curdlan degradation.

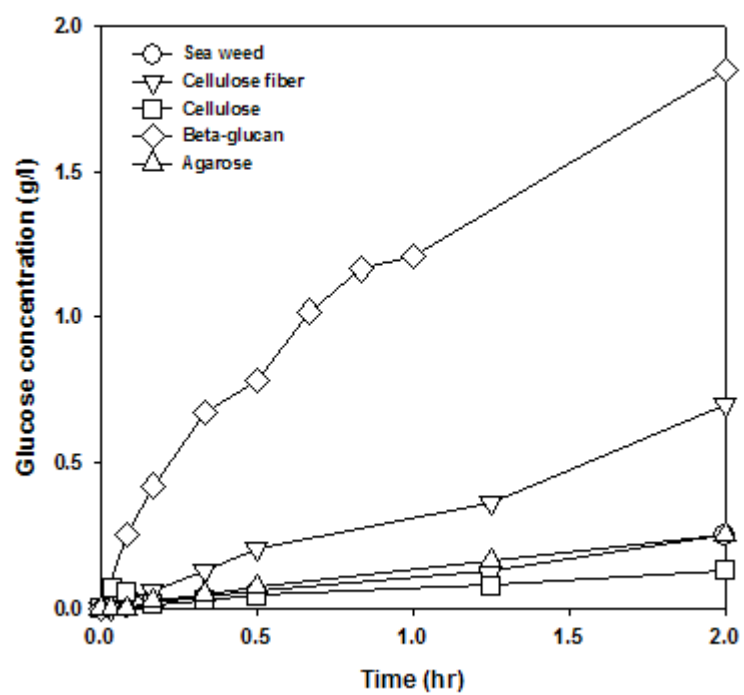
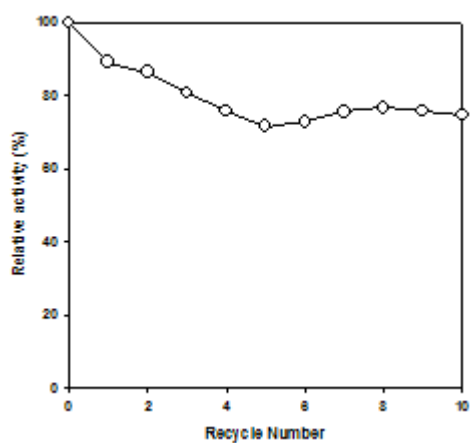


Figure 6.8. Production of glucose using various carbohydrate using PAMP immobilized lysing enzyme.



(a)



(b)



(c)

Figure 6.9. Effect of immobilized enzyme recycle.

(a) enzyme activity. The immobilized enzymes are homogenized (b) and recovery with magnets (c)

References

1. McIntosh M, Stone, B.A., Stanisich, V.A.: Curdlan and other bacterial (1→3)- β -D-glucans. *Appl Microbiol Biotechnol* 2005, 68:163–173.
2. Chan TW, Chan, P.K. and Tang, K.Y.: Determination of molecular weight profile for a bioactive beta-1,3 polysaccharides(curdlan). *Analytical chimical Acta* 2006, 556:226–236.
3. Lee IY: Curdlan, Biopolymers. In A. Steinbuchel, E.J. Vandamme, &S. de Baets(Eds.) vol. 5. Weinhein: Wiley–VCH; 2000.
4. Jagodzinski PP, Wiaderkiewicz, R., Kurzawski, G. : Mechanism of the inhibitory effect of curdlan sulfate on HIV–1 infection in viro. *Virology* 1994, 202:735–745.
5. Mikio K, Yoshiro, O, Hirotoomo, O: Water soluble beta-1,3-glucan derivative and antiviral agent containing the derivative. In. Japan; 1995.
6. Shimizu J, N. Tsuchisashi, K. Kudoh, M. Wada, T. Tarika and S. Innami: Dietary curdlan increases proliferation of bifidobacteria in the cecum of rats. *Bioscience Biotechnology and Biochemistry* 2001, 65(2):466–469.
7. Grandpierre C, Janssen HG, Laroche C, Michaud P, Warrand J: Enzymatic and chemical degradation of curdlan targeting the production of [beta]-(1?→?) oligoglucans. *Carbohydrate Polymers* 2008, 71(2):277–286.
8. Tara Karnezis HCF, Gregory M. Neumann, Bruce A. Stone, and Vilma A. Stanisich: Cloning and Characterization of the phosphatidylserine synthase gene of *Agrobacterium* sp. Strain ATCC 31749 and Effect of Its inactivation on Production of High–Molecular–Mass (1→3)-beta-D-Glucan(Curdlan). *Journal of Bacteriology* 2002, 184(15):4114–4123.
9. Erh–Min Lai H–WS, Sy–Ray Wen, Min–Wen Cheng, Hau–Hsuan Hwang, Shih–Hua Chiu,: Proteomic analysis of <I>Agrobacterium tumefaciens</I> response to the gene inducer acetosyringone.

- Proteomics* 2006, 6(14):4130–4136.
10. Ran Rosen AS, Nelia Shechter, D?te Becher, Knut B?tner, Dvora Biran, Michael Hecker, Eliora Z. Ron,: Two–dimensional reference map of <I>Agrobacterium tumefaciens</I> proteins. *Proteomics* 2004, 4(4):1061–1073.
 11. Anderson LaS: A comparison of selected mRNA and protein abundances in human liver. *Electrophoresis* 1997, 18:533–537.
 12. Mchael JDaKHL: Proteomic analysis. *Current opinion in biotechnology* 2000, 11:1176–1179.
 13. Andreson LNaANG: Proteome and proteomics: New technologies, new concepts, and new words. *Electrophoresis* 1998, 19:1853–1861.
 14. Wilkins MR, Williams, K. L., Appel, R. D. and Hochstrasser, D. F. : Proteome Research: New frontiers in functional genomics. . New York: Springer; 1997.
 15. Issaq HJ: The role of separation science in proteomics research. *Electrophoresis* 2001, 22:3629–3638.
 16. Lauber WM, Carroll, J. A., Dufield, D.R., Kiesel, J.R., Radabaugh, M.R. and Malone, J.P.: Mass spectrometry compatibility of two–dimensional gel protein stains. *Electrophoresis* 2001, 22:906–918.
 17. le Coutre J, Whitelegge, J. P., Gross, A., Turk, E., Wright, E. M., Kaback, H.R. and Faull, K. F. : Proteomics on full–length membrane proteins using mass spectrometry. *Biochemistry* 2000, 39:4237–4242.
 18. Nuttall ME: Drug discovery and target validation. *Cells Tissues Organs* 2001, 169:265–271.
 19. Kim MK, Lee, I.Y., Ko, J.H., Rhee, Y.H., Park, Y.H.: Higher intracellular levels of uridinemonophosphate under nitrogen–limited conditions enhance metabolic flux of curdlan synthesis in *Agrobacterium* species. *Biotechnol Bioeng* 1999, 62:317–323.

20. Lee JH, Lee, I.Y., Kim, M.K., Park, Y.H.: Optimal pH control of batch processes for production of curdlan by *Agrobacterium* species. . *J Ind Microbiol Biotechnol* 1999, 23:143–148.
21. Harada T: Production, properties, and application of curdlan. In: Sanford, P.A., Laskin, A. (Eds.), Extracellular microbial polysaccharides. *American Chemical Society* 1997:265–283.
22. Renn DW: Purified curdlan and its hydroxyalkyl derivatives: preparation, properties and applications. . *Carbohydr Polym* 1997, 33:219–225.
23. report Tt: Pureglucan: Basic properties and food applications. Japan: Takeda Chemical Industries; 1997.
24. Kanke ME, Tanabe, H., Katayama, Y.K., Yoshitomi, Y.: Application of curdlan to controlled drug delivery. III. Drug release from sustained release suppositories in vitro. *Biol Pharm Bull* 1995, 18:1154–1158.
25. Takeda HN, Neoh, L.P., Akimoto, H., Kaneko, H., Hishikawa, T., Sekigawa, I., Hashimoto, H., Hirose, S., Murakami, T., Yamamoto, N., Mimura, T., Kaneko, Y.: Role of curdlan sulfate in the binding of HIV–1 gp120 to CD4 molecules and the production of gp120–mediated TNF–alpha. *Microbiol Immunol* 1997, 41:741–745.
26. Davis WB: Unique bacterial polysaccharide polymer gel in cosmetics, pharmaceuticals and foods. In., vol. US patent 5,158,772; 1992.
27. Lee IY: Curdlan. In: Vandamme, E.J., De Baets, S., Steinbüchel, A. (Eds.), Polysaccharides I: Polysaccharides from prokaryotes. *Biopolymers* 2002, 5:135–158.
28. Kim MK, Lee, I.Y., Lee, J.H., Kim, K.T., Rhee, Y.H., Park, Y.H.: Residual phosphate concentration under nitrogen–limiting conditions regulates curdlan production in *Agrobacterium* species. *J Ind Microbiol Biotechnol* 2000, 25:180–183.
29. Lee JH, Lee, I.Y.: Optimization of uracil addition for curdlan (beta–glucan)

- production by *Agrobacterium* species. . *Biotechnol Lett* 2001, 23:1131–1134.
30. Kim MK, Ryu, K.E., Choi, W.A., Rhee, Y.H., Lee, I.Y.: Enhanced production of $(1\rightarrow3)\text{-}\beta\text{-D-glucan}$ by a mutant strain of *Agrobacterium* species. *Biochem Eng* 2003, 16:163–168.
 31. Lee IY, Seo, W.T., Kim, G.J., Kim, M.K., Park, C.S., Park, Y.H.: Production of curdlan using sucrose or sugar cane molasses by two-step fed-batch cultivation of *Agrobacterium* species. *J Ind Microbiol Biotechnol* 1997, 18:255–259.
 32. Lee IY, Kim, M.K., Lee, J.H., Seo, W.T., Park, C.S., Park, Y.H.: Influence of agitation speed on production of curdlan by *Agrobacterium* species. *Bioprocess Eng* 1999, 20:283–287.
 33. Lee JH, Park, Y.H.: Optimal production of curdlan by *Agrobacterium* sp. with feedback inferential control of optimal pH profile. . *Biotechnol Lett* 2001, 23:525–530.
 34. Nakanishi I, Kimura, K., Kanamaru, T.: Studies on curdlan-type polysaccharide. I. Industrial production of curdlan-type polysaccharide. . *J Takeda Res Lab* 1992, 51:99–108.
 35. Harada T, Harada, A.: Curdlan and succinoglycan. In: Dumitriu, S. (Eds). *Polysaccharides in medical applications* 1996:21–57.
 36. Stasinopoulos SJ, Fisher P-R, Stone B-A, Stanisich V-A: Detection of two loci involved in $(1\rightarrow3)\text{-}\beta\text{-glucan}$ (curdlan) biosynthesis by *Agrobacterium* sp. ATCC 31749, and comparative sequence analysis of the putative curdlan synthase gene. *Glycobiology* 1999, 9(1):31–41.
 37. Karnezis T, Epa, V.C., Stone, B.A., Stanisich, V.A.: Topological characterization of an inner membrane $(1\rightarrow3)\text{-}\beta\text{-D-glucan}$ (curdlan) synthase from *Agrobacterium* sp. strain ATCC31749. *Glycobiology* 2003, 13:693–706.

38. Goodner B, Hinkle, G., Gattung, S., Miller, N., Blanchard, M., Quorllo, B., Goldman, B.S., Cao, Y., Askenazi, M., Halling, C., Mullin, L., Houmiel, K., Gordon, J., Vaudin, M., Iartchouk, O., Epp, A., Liu, F., Wollam, C., Allinger, M., Doughty, D., Scott, C., Lappas, C., Markelz, B., Flanagan, C., Crowell, C., Gurson, J., Lomo, C., Sear, C., Strub, G., Cielo, C., Slater, S.: Genome sequence of the plant pathogen and biotechnology agent *Agrobacterium tumefaciens* C58. *Science* 2001, 294:2323–2328.
39. Wood DW, Setubal, J.C., Kaul, R., Monks, D., Chen, L., Wood, G.E., Chen, Y., Woo, L., Kitajima, J.P., Okura, V.K.: The genome of the natural genetic engineer *Agrobacterium tumefaciens* C58. . *294* 2001, 2317 2323.
40. Lai EM, Shih, H.W., Wen, S.R., Cheng, M.W., Hwang, H.H., Chiu, S.H.: Proteomic analysis of *Agrobacterium tumefaciens* response to the vir gene inducer acetosyringone. . *Proteomics* 2006, 6:4130–4136.
41. Rosen R, Buettner, K., Schmid, R., Hecker, M., Ron, E.Z.: Stress-induced proteins of *Agrobacterium tumefaciens*. *FEMS Microbiol Ecol* 2001, 35:277–285.
42. Rosen R, Büttner, K., Becher, D., Nakahigashi, K., Yura, T., Hecker, M., Ron, E.Z.: Heat shock proteome of *Agrobacterium tumefaciens*: evidence for new control systems. *J Bacteriol* 2002, 184:1772–1778.
43. Rosen R, Sacher, A., Shechter, N., Becher, D., Büttner, K., Biran, D., Hecker, M., Ron, E.Z.: Two-dimensional reference map of *Agrobacterium tumefaciens* proteins. *proteomics* 2004, 4:1061–1073.
44. Srienc F, Arnold, B., Bailey, J.E.: Characterization of intracellular accumulation of poly- β -hydroxybutyrate (PHB) in individual cells of *Alcaligenes eutrophus* H16 by flow cytometry. *Biotechnol Bioeng* 1984, 26:982–987.
45. Shedletzky E, Unger, C., Delmer, D.P.: A microtiter-based fluorescence assay for (1,3)- β -glucan synthases. . *Anal Biochem* 1997, 249:88–93.

46. Ryll T, Wagner, R.: Improved ion-pair high-performance liquid chromatographic method for the quantification of a wide variety of nucleotides and sugar-nucleotides in animal cells. *J Chromatogr* 1991, 570:77–88.
47. Rabilloud T: Silver staining of 2-D electrophoresis gels. *Methods Mol Biol* 1999, 112:297–305.
48. Kim YH, Han, K.Y., Lee, K., Lee, J.: Proteome response of Escherichia coli fed-batch culture to temperature downshift. *Appl Microbiol Biotechnol* 2004, 68:786–793.
49. Harding NE, Raffo, S., Raimondi, A., Cleary, J.M., Ielpi, L.: Identification, genetic and biochemical analysis of genes involved in synthesis of sugar nucleotide precursors of xanthan gum by Xanthomonas campestris. *J Gen Microbiol* 1993, 139:447–457.
50. Atkinson DE: Cellular energy metabolism and its regulation. New York: Academic Press; 1977.
51. Ielpi L, Couso, R.O., Dankert, M.A.: Sequential assembly and polymerization of the polyprenol-linked pentasaccharide repeating unit of the xanthan polysaccharide in Xanthomonas campestris. *J Bacteriol* 1993, 175:2490–2500.
52. Sutherland IW: Microbial exopolysaccharide synthesis. In: Sanford, P.A., Laskin, A. (Eds.), Extracellular microbial polysaccharides. . *American Chemical Society* 1997:40–57.
53. West TP: Pyrimidine base supplementation effects curdlan production in Agrobacterium sp. ATCC 31749. *J Basic Microbiol* 2006, 46:153–157.
54. Nakahigashi K, Ron, E.Z., Yanagi, H., Yura, T.: Differential and independent roles of a σ^{32} homolog (RpoH) and an HrcA repressor in the heat shock response of Agrobacterium tumefaciens. . *J Bacteriol* 1999, 181:7509–7515.

55. Segal G, Ron. E.Z.: Heat shock transcription of the groESL operon of *Agrobacterium tumefaciens* may involve a hairpin-loop structure. . *J Bacteriol* 1993, 175:3083–3088.
56. Segal G, Ron, E.Z.: The dnaKJ operon of *Agrobacterium tumefaciens*: transcriptional analysis and evidence for a new heat shock promoter. . *J Bacteriol* 1995, 177:5952–5958.
57. Nakahigashi K, Yanagi, H., Yura, T.: Isolation and sequence analysis of rpoH genes encoding sigma 32 homologs from gram-negative bacteria: conserved mRNA and protein segments for heat shock regulation. *Nucleic Acids Res* 1995, 23:4383–4390.
58. Nakahigashi K, Yanagi, H., Yura. T.: DnaK chaperone-mediated control of activity of a σ 32 homolog (RpoH) plays a major role in the heat shock response of *Agrobacterium tumefaciens*. *J Bacteriol* 2001, 183:5302–5310.
59. Rosen R, Matthysse, A.G., Becher, D., Biran, D., Yura, T., Hecker, M., Ron, E.Z.: Proteome analysis of plant-induced proteins of *Agrobacterium tumefaciens*. . *FEMS Microbiol Ecol* 2003, 44:355–360.
60. Kandrór O, Goldberg, A.L.: Trigger factor is induced upon cold shock and enhances viability of *Escherichia coli* at low temperatures. . *Proc Natl Acad Sci U S A* 1997, 94:4978–4981.
61. Karanezis T, . , Fisher H-G, Neumann G-M, Stone B-A, Stanisich V-A: Cloning and characterization of the phosphatidylserine synthase Gene of *Agrobacterium* sp. strain ATCC 31749 and Effect of Its Inactivation on Production of High-Molecular-Mass (1- \rightarrow 3)-beta-D-glucan(curdlan). *Journal of Bacteriology* 2002, 184:4114–4123.
62. Griffin TJ, Gygi S-P, Ideker T, Rist B, Eng J, Hood L, Aebersold R: Complementary profiling of Gene Expression at the Transcriptome and proteome Levels in *Saccharomyces cerevisiae*. *Mol Cell proteome* 2002,

- 1:323–333.
63. Gygi SP, Rochon Y, Franza B–R, Aebersold R: Correlation between Protein and mRNA Abundance in Yeast. *Mol Cell Biol* 1999, 19:1720–1730.
 64. Ideker T, Thorsson V, Ranish J, Christmas AR, Buhler J, Eng JK, Bumgarner R, Goodlett D–R, Aebersold R, Hood L: Integrated Genomic and proteomic analyses of a systematically perturbed Metabolic Network. *Science* 2001, 292:929–934.
 65. Kothny EL, Cook WA, Cuddeback JE, Dimitriades B, Ferrand EF, McDaniel PW, Nifong GD, Saltzman BE, Weiss FT: Tentative method of analysis for ammonia in the atmosphere (indophenol method). *Health Lab Sci* 1973, 10(2):115–118.
 66. Inoue SB, Takewaki N, Takasuka T, Mio T, Adachi M, Fujii Y, Miyamoto C, Arisawa M, Furuichi Y, Watanabe T: Characterization and gene cloning of 1,3–beta–D–glucan synthase from *Saccharomyces cerevisiae*. *Eur J Biochem* 1995, 231(3):845–854.
 67. Lee SY, Hong SH, Lee SH, Park SJ: Fermentative production of chemicals that can be used for polymer synthesis. *Macromol Biosci* 2004, 4(3):157–164.
 68. Carole TM, Pellegrino J, Paster MD: Opportunities in the industrial biobased products industry. *Appl Biochem Biotechnol* 2004, 113–116:871–885.
 69. Wilke D: Chemicals from biotechnology: molecular plant genetics will challenge the chemical and the fermentation industry. *Appl Microbiol Biotechnol* 1999, 52(2):135–145.
 70. Nakamura CE, Whited GM: Metabolic engineering for the microbial production of 1,3–propanediol. *Curr Opin Biotechnol* 2003, 14(5):454–459.

71. Huang H, Gong CS, Tsao GT: Production of 1,3-propanediol by *Klebsiella pneumoniae*. *Appl Biochem Biotechnol* 2002, 98–100:687–698.
72. Cameron DC, Altaras NE, Hoffman ML, Shaw AJ: Metabolic engineering of propanediol pathways. *Biotechnol Prog* 1998, 14(1):116–125.
73. Kim I, Yun H, Jin I: Comparative proteomic analyses of the yeast *Saccharomyces cerevisiae* KNU5377 strain against menadione-induced oxidative stress. *J Microbiol Biotechnol* 2007, 17(2):207–217.
74. Lee SY, Jeoung D: The reverse proteomics for identification of tumor antigens. *J Microbiol Biotechnol* 2007, 17(6):879–890.
75. Gonzalez-Pajuelo M, Meynial-Salles I, Mendes F, Andrade JC, Vasconcelos I, Soucaille P: Metabolic engineering of *Clostridium acetobutylicum* for the industrial production of 1,3-propanediol from glycerol. *Metab Eng* 2005, 7(5–6):329–336.
76. Zhu MM, Lawman PD, Cameron DC: Improving 1,3-propanediol production from glycerol in a metabolically engineered *Escherichia coli* by reducing accumulation of sn-glycerol-3-phosphate. *Biotechnol Prog* 2002, 18(4):694–699.
77. Skraly FA, Lytle BL, Cameron DC: Construction and characterization of a 1,3-propanediol operon. *Appl Environ Microbiol* 1998, 64(1):98–105.
78. Tong IT, Liao HH, Cameron DC: 1,3-Propanediol production by *Escherichia coli* expressing genes from the *Klebsiella pneumoniae* dha regulon. *Appl Environ Microbiol* 1991, 57(12):3541–3546.
79. Chotani G, Dodge T, Hsu A, Kumar M, LaDuca R, Trimbur D, Weyler W, Sanford K: The commercial production of chemicals using pathway engineering. *Biochimica et Biophysica Acta (BBA) – Protein Structure and Molecular Enzymology* 2000, 1543(2):434.
80. Abbad-Andaloussi S, Manginot-Durr C, Amine J, Petitdemange E, Petitdemange H: Isolation and Characterization of *Clostridium butyricum*

- DSM 5431 Mutants with Increased Resistance to 1,3-Propanediol and Altered Production of Acids. *Appl Environ Microbiol* 1995, 61(12):4413–4417.
81. Barbirato F, Himmi EH, Conte T, Bories A: 1,3-propanediol production by fermentation: An interesting way to valorize glycerin from the ester and ethanol industries. *Industrial Crops and Products* 1998, 7(2–3):281.
 82. Boenigk R, Bowien S, Gottschalk G: Fermentation of glycerol to 1,3-propanediol in continuous cultures of *Citrobacter freundii*. *Applied Microbiology and Biotechnology* 1993, 38(4):453.
 83. Menzel K, Zeng AP, Deckwer WD: High concentration and productivity of 1,3-propanediol from continuous fermentation of glycerol by *Klebsiella pneumoniae*. *Enzyme and Microbial Technology* 1997, 20(2):82.
 84. Papanikolaou S, Ruiz-Sanchez P, Pariset B, Blanchard F, Fick M: High production of 1,3-propanediol from industrial glycerol by a newly isolated *Clostridium butyricum* strain. *Journal of Biotechnology* 2000, 77(2–3):191.
 85. Xiu Z-L, Song B-H, Wang Z-T, Sun L-H, Feng E-M, Zeng A-P: Optimization of dissimilation of glycerol to 1,3-propanediol by *Klebsiella pneumoniae* in one- and two-stage anaerobic cultures. *Biochemical Engineering Journal* 2004, 19(3):189.
 86. Altaras NE, Cameron DC: Metabolic engineering of a 1,2-propanediol pathway in *Escherichia coli*. *Appl Environ Microbiol* 1999, 65(3):1180–1185.
 87. Hartlep M, Hussmann W, Prayitno N, Meynial-Salles I, Zeng AP: Study of two-stage processes for the microbial production of 1,3-propanediol from glucose. *Appl Microbiol Biotechnol* 2002, 60(1–2):60–66.
 88. Knietsch A, Bowien S, Whited G, Gottschalk G, Daniel R: Identification and characterization of coenzyme B12-dependent glycerol dehydratase- and

- diol dehydratase-encoding genes from metagenomic DNA libraries derived from enrichment cultures. *Appl Environ Microbiol* 2003, 69(6):3048–3060.
89. Colin T, Bories A, Moulin G: Inhibition of *Clostridium butyricum* by 1,3-propanediol and diols during glycerol fermentation. *Appl Microbiol Biotechnol* 2000, 54(2):201–205.
 90. Biebl H, Menzel K, Zeng AP, Deckwer WD: Microbial production of 1,3-propanediol. *Appl Microbiol Biotechnol* 1999, 52(3):289–297.
 91. Lee YJ, Jung KH: Modulation of the tendency towards inclusion body formation of recombinant protein by the addition of glucose in the araBAD promoter system of *Escherichia coli*. *J Microbiol Biotechnol* 2007, 17(11):1898–1903.
 92. Seul KJ, Park SH, Ryu CM, Lee YH, Ghim SY: Proteome analysis of *Paenibacillus polymyxa* E681 affected by barley. *J Microbiol Biotechnol* 2007, 17(6):934–944.
 93. Wang W, Sun J, Nimtz M, Deckwer W-D, Zeng A-P: Protein identification from two-dimensional gel electrophoresis analysis of *Klebsiella pneumoniae* by combined use of mass spectrometry data and raw genome sequences. *Proteome Sci* 2003, 1(6):1–9.
 94. Norde ABaW: Physical Chemistry of Biological Interface. New York: Marcel Dekker; 1999.
 95. Kawaguchi H: Functional polymer microspheres. *Progress in polymer science* 2000, 25:1171–1210.
 96. Czeslik C: Factors Ruling Protein Adsorption. *Zeitschrift für Physikalische Chemie* 2004, 218:771–801.
 97. Wageesha Senaratne LA, and Christopher K. Ober: Self-Assembled Monolayers and Polymer Brushes in Biotechnology: Current Applications and Future Perspectives *Biomacromolecules* 2005, 6(5):2427–2448.

98. Hartmeier W: Immobilized Biocatalysts. Berlin: Springer; 1988.
99. Oliver Hollmann RSaCC: Structure and dynamics of α -lactalbumin adsorbed at a charged brush interface. *Physical Chemistry Chemical Physics* 2008, 10:1448–1456.
100. Oliver Hollmann TG, and Claus Czeslik: Structure and Protein Binding Capacity of a Planar PAA Brush *Langmuir* 2007, 23(3):1347–1353.
101. Wertz MMSaCF: Protein Spreading Kinetics at Liquid–Solid Interfaces via an Adsorption Probe Method *Langmuir* 2005, 21(22):10172–10178.
102. Santore CFWaMM: Adsorption and Reorientation Kinetics of Lysozyme on Hydrophobic Surfaces. *Langmuir* 2002, 18(4):1190–1199.
103. Santore CFWaMM: Fibrinogen Adsorption on Hydrophilic and Hydrophobic Surfaces: Geometrical and Energetic Aspects of Interfacial Relaxations *Langmuir* 2002, 18(3):706–715.
104. Schüler FCaC: Enzyme Multilayers on Colloid Particles: Assembly, Stability, and Enzymatic Activity *Langmuir* 2000, 16(24):9595–9603.
105. Frank Caruso DT, Helmuth Möhwald, and Reinhard Renneberg Enzyme Encapsulation in Layer-by-Layer Engineered Polymer Multilayer Capsules *Langmuir* 2000, 16(4):1485–1488.
106. Peppler H.J. RG: Enzymes in food and feed processing. *Biotechnology* 1987, 7a:578–580.
107. Bayramoglu G, Tunali Y, Arica MY: Immobilization of [beta]-galactosidase onto magnetic poly(GMA–MMA) beads for hydrolysis of lactose in bed reactor. *Catalysis Communications* 2007, 8(7):1094–1101.
108. Mammarella EJ, Rubiolo AC: Predicting the packed-bed reactor performance with immobilized microbial lactase. *Process Biochemistry* 2006, 41(7):1627.
109. Al-Muftah AE, Abu-Reesh IM: Effects of internal mass transfer and product inhibition on a simulated immobilized enzyme-catalyzed reactor

- for lactose hydrolysis. *Biochemical Engineering Journal* 2005, 23(2):139–153.
110. Al-Muftah AE, Abu-Reesh IM: Effects of simultaneous internal and external mass transfer and product inhibition on immobilized enzyme-catalyzed reactor. *Biochemical Engineering Journal* 2005, 27(2):167–178.
 111. Ozdural AR, Tanyolac D, Boyaci IH, Mutlu M, Webb C: Determination of apparent kinetic parameters for competitive product inhibition in packed-bed immobilized enzyme reactors. *Biochemical Engineering Journal* 2003, 14(1):27–36.
 112. Obon JM, Castellar MR, Iborra JL, Manjon A: [beta]–Galactosidase immobilization for milk lactose hydrolysis: a simple experimental and modelling study of batch and continuous reactors. *Biochemical Education* 2000, 28(3):164–168.
 113. Haider T, Husain Q: Calcium alginate entrapped preparations of *Aspergillus oryzae* [beta] galactosidase: Its stability and applications in the hydrolysis of lactose. *International Journal of Biological Macromolecules* 2007, 41(1):72–80.
 114. Giacomini C, Irazoqui G, Batista-Viera F, Brena BM: Influence of the immobilization chemistry on the properties of immobilized [beta]–galactosidases. *Journal of Molecular Catalysis B: Enzymatic* 2001, 11(4–6):597–606.
 115. Sharma SK, Singhal R, Malhotra BD, Sehgal N, Kumar A: Lactose biosensor based on Langmuir–Blodgett films of poly(3–hexyl thiophene). *Biosensors and Bioelectronics* 2004, 20(3):651.
 116. Zhou QZK, Dong Chen X: Immobilization of [beta]–galactosidase on graphite surface by glutaraldehyde. *Journal of Food Engineering* 2001, 48(1):69–74.
 117. Numanoglu Y, Sungur S: [beta]–Galactosidase from *Kluyveromyces lactis*

- cell disruption and enzyme immobilization using a cellulose–gelatin carrier system. *Process Biochemistry* 2004, 39(6):705–711.
118. Tanriseven A, Dogan S: A novel method for the immobilization of [beta] – galactosidase. *Process Biochemistry* 2002, 38(1):27–30.

저작물 이용 허락서

학 과	화학공학과	학 번	20047643	과 정	박 사
성 명	한글 : 김려화 한문 : 金麗華 영문 : Li-Hua Jin				
주 소	중국 길림성 훈춘시 단결위 11 조 1 단원 308 호				
연락처	E-MAIL : kimlihua@hanmail.net				
논문제목	한글: 단백질체 분석을 통한 metabolic pathway 변화에 대한 연구				
	영문: A study on the metabolic pathway change by the proteomic analysis				

본인이 저작한 위의 저작물에 대하여 다음과 같은 조건아래 조선대학교가 저작물을 이용할 수 있도록 허락하고 동의합니다.

- 다 음 -

1. 저작물의 DB 구축 및 인터넷을 포함한 정보통신망에의 공개를 위한 저작물의 복제, 기억장치에의 저장, 전송 등을 허락함
2. 위의 목적을 위하여 필요한 범위 내에서의 편집·형식상의 변경을 허락함. 다만, 저작물의 내용변경은 금지함.
3. 배포·전송된 저작물의 영리적 목적을 위한 복제, 저장, 전송 등은 금지함.
4. 저작물에 대한 이용기간은 5 년으로 하고, 기간종료 3 개월 이내에 별도의 의사 표시가 없을 경우에는 저작물의 이용기간을 계속 연장함.
5. 해당 저작물의 저작권을 타인에게 양도하거나 또는 출판을 허락을 하였을 경우에는 1 개월 이내에 대학에 이를 통보함.
6. 조선대학교는 저작물의 이용허락 이후 해당 저작물로 인하여 발생하는 타인에 의한 권리 침해에 대하여 일체의 법적 책임을 지지 않음
7. 소속대학의 협정기관에 저작물의 제공 및 인터넷 등 정보통신망을 이용한 저작물의 전송·출력을 허락함.

동의여부 : 동의(●) 반대()

2009 년 2 월

저작자: 김 려 화 (서명 또는 인)

조선대학교 총장 귀하

